TÉCNICO LISBOA

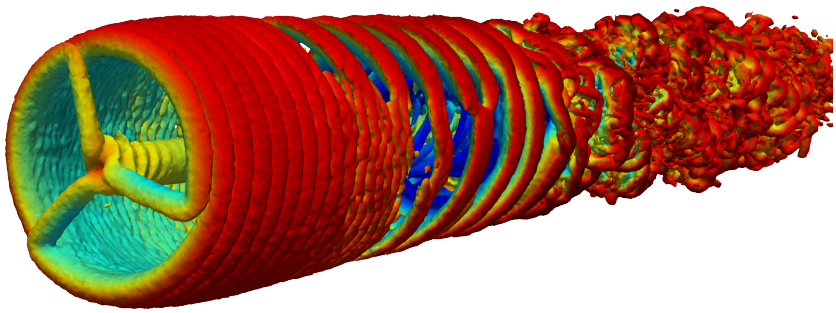

Modeling Wind Turbine Interaction: Large Eddy Simulations for the Verification of Empirical Wind Turbine Wake Models

Valentin Bernard

Thesis to Obtain the Master of Science Degree in

Renewable Energy Engineering and Management

Supervisors: Dr. Ricardo Balbino Dos Santos Pereira, IST
Dr. Pierre Bénard, INSA Rouen

Examination Committee

Chairperson: Prof. Edgar Caetano Fernandes
Supervisor: Prof. Ricardo Balbino Dos Santos Pereira
Member of the Committee: Prof. Luis Rego da Cunha Eça

November 2019

Acknowledgments

I would like to express my gratitude to the people and institutions that made the hereafter presented master thesis possible. I will begin by acknowledging the institutions and universities that accompanied me during the last two years and up to this moment. Thank you to InnoEnergy, the École Polytechnique and the University of Lisbon, for orchestrating an incredible master program that provided immeasurable personal and professional growth. Thank you to the INSA Rouen and the CORIA laboratory for hosting the six month internship during which the presented work was carried out. Thank you to Siemens Gamesa Renewable Energy, the industrial partner of this master thesis, for providing not only financial support, but also the code base on which this projects rests as well as measurement data used in the validation study. Lastly, thank you to the CRIANN research center for allowing me to run massive simulations on their supercomputer-cluster *Myria*.

I also want to personally thank the fantastic people who were involved in the realization of this thesis. Thank you to Ricardo Dos Santos Periera, my academic supervisor in Lisbon, who managed to guide me (remotely) through this journey of discovery, where the route was not always clear. Thank you to Pierre Bénard, my supervisor at the CORIA laboratory, and to the other supervisors of the YALES2 team, Vincent Moureau and Ghislain Lartigue. Their guidance on unfamiliar topics, CFD and others, was fundamental to this thesis. Thank you to Paul Deglaire, head of research at Siemens Gamesa France, who organized this joined master thesis project between research and industry and provided valuable guidance. Thank you to the engineers at Siemens Gamesa, in particular Norbert, Laurent and Bastien, but also Panagiotis, Felix and Boumedyen, who helped me on my first steps in the world of industrial code development. I also want to mention the PhD students I had the pleasure to share an office with, as well as the other PhD students and interns in the CORIA laboratory and at SGRE (Yann, Patricia, Francesco, Felix, Romain, Maxence, Marie, Benoit, Ludovic, Hector, Guillaume, Andrei, Clément, Kevin, Louise and all the rest ...). Thank you for interesting discussions, valuable feedback and sometimes much needed distraction.

Lastly, but perhaps most importantly, I want to thank the people in my personal life who supported me directly of indirectly in the realization of this work. Thank you Vania for your love and your patience. And thank you to my parents for always being there, in spite of the distance, ready to provide advice and support.

Resumo

A energia eólica offshore estabelece-se como um elemento-chave da transicão energética, e as economias de escala pressionam os fabricantes a fornecer turbinas com diâmetro de rotor cada vez maior. Essa evolucão leva a uma necessidade crescente de modelos aerodinâmicos com elevada precisão para prever o nível de fadiga das turbinas e para estimar a producão de energia. Os efeitos observados em parques eólicos, como as esteiras, podem ter um impacto substancial sobre esses resultados e precisam de ser modelados com elevada precisão. A abordagem de *dynamic wake meandering* (DWM), desenvolvida na Universidade Técnica da Dinamarca (DTU), foi recentemente incluida na norma IEC61400 que certifica turbinas eólicas. Esta abordagem promete uma melhor previsão das cargas para turbinas eólicas inseridas em parques eólicos. Nesta tese de mestrado é apresentado um programa que modela a aerodinâmica de parques baseada em DWM, motivando-se as escolhas feitas na sua implementação e descrevendo-se a interface com um código Aero-servo-elástico. A validação é feita utilizando dados reais para uma turbina impactada por uma única esteira, obtendo-se resultados satisfatórios. Além disso, comparou-se o programa com uma caso de referência, gerada usando a biblioteca de simulação LES *YALES2*. As dificuldades encontradas neste processo são descritas, principalmente no que se refere à inclusão de turbulência na simulação LES. Por fim, é derivada uma nova formulação para quantificar a deflexão de esteira de turbinas não alinhadas com o vento. A formulação baseia-se no modelo de deficit de velocidades na esteira usado no programa DWM e é coerente com as hipóteses assumidas no programa. Os resultados da nova formulação são comparados com modelos da literatura e simulações de LES, tendo-se obtido resultados razoáveis.

Palavras-chave: modelos de esteiras, DWM, ALM, guia da esteira

Abstract

Offshore wind energy is establishing itself as a key element of the energy transition, and economies of scale are pushing manufacturers to deliver turbines of ever larger rotor diameter. This evolution leads to an increased necessity for accurate aerodynamic models in order to predict fatigue damage and power production. Farm effects such as wakes can have a substantial impact on these results and need to be modeled accurately. The dynamic wake meandering (DWM) approach developed at Danish Technical University (DTU) was recently added to the IEC61400 standard for wind turbines. The approach promises improved load prediction for wind turbines in farm configurations. In this work, an aerodynamic farm modeling tool based on DWM is presented and the choices made in its implementation, as well as the interface with an aero-servo-elastic solver, are described. Validation with available field data for a turbine impacted by a single wake is carried out, showing satisfactory results. Furthermore, it was attempted to verify the tool by comparison with results for the same case simulated using the large-eddy simulation (LES) library YALES2. The difficulties encountered in this process are described, especially regarding the simulation of atmospheric turbulence in LES. Limited conclusions are drawn from the comparison. Lastly, a new formulation for wake deflection of yawed turbines is derived. The formulation relies on the wake deficit model used in the DWM tool and is coherent with the overall assumptions of the tool. Results of the novel formulation are compared to models from literature and LES simulations, finding fair performance.

Keywords: Wake Modeling, DWM, ALM, Wake Steering

Contents

List of Figures

Nomenclature

Greek symbols

α	Angle of attack.
β	Pitch angle of the blade.
χ	Local tip speed ratio.
δ	Wake offset.
γ	Angle of yaw misalignment.
λ	Turbine tip speed ratio, defined as $\Omega R/u_0$.
μ	Molecular viscosity.
ν	Kinematic viscosity.
Ω	Turbine angular velocity.
ϕ	Angle of incident relative wind.
ρ	Density.
σ	Standard deviation, i.e. width parameter of a gaussian.
τ	Stress tensor.
θ	Wake deflection angle.

Roman symbols

A	Area.
a	Axial induction factor.
a'	Angular induction factor.
B	Number of blades.
B	Number of blades.
b	Wake half width.

C	Centerline wake deficit.
c	Blade section chord length.
C_D	Coefficient of drag.
C_L	Coefficient of lift.
C_P	Coefficient of power.
C_T	Coefficient of thrust.
D	Turbine diameter.
F	Prantel's tip loss factor.
f_c	Cut-off frequency.
I	Turbulence intensity.
k_e	Empirical wake expansion factor.
k_{wt}	Wake turbulence scale factor.
L, D	Lift and drag force.
M	Torque.
N	Number of blades.
P	Mechanical output power.
p	Pressure.
T	Thrust.
m	Flow of mass.
Q_p	Flow of linear momentum.
R	Turbine radius.
t	Time.
$\mathbf{u}$	Velocity vector.
i, j, k	Discretization indices.
r, θ, x	Cylindrical coordinates.
u, v, w	Velocity cartesian components.
x, y, z	Cartesian coordinates.

Glossary

ALM Actuator Line Modeling is an approach to simulating wind turbine in LES without resolving the blade geometry, introduced by Soerensen & Shen in 2012.

BEM Blade Element Momentum theory is a model for the local forces on propellers and wind turbine blades in a free stream.

CFD Computational Fluid Dynamics is a branch of fluid mechanics that uses numerical methods and algorithms to solve problems that involve fluid flows.

DTU Danmarks Tekniske Universitet is the technical university of Denmark that developed many commonly used wind turbine engineering models.

DWM Dynamic Wake Meandering is a semi-stationary wake model developed by researchers at DTU.

EPFL École Polytechnique Fédérale de Lausanne is a Swiss university specialized in science and technology.

IEC The International Electrotechnical Commission prepares and publishes international standards for all electrical, electronic and related technologies.

LES Large Eddy Simulation is an approach to simplify the Navier-Stokes equations by resolving large turbulence explicitly in time and modeling small scale turbulence.

NS Navier Stokes equations, a system of momentum balance equations that govern the flow of fluids.

RANS Reynolds Averaged Navier Stokes is an approach to simplify the Navier Stokes equations by averaging the equations.

SGRE Siemens Gamesa Renewable Energy S.A. is one of the world's largest wind turbine manufacturers and global leader on the offshore wind market.

Chapter 1

Introduction

In the context of global efforts to prevent the catastrophic effects of climate change, electricity production from renewable, CO2-emission-free energy sources such as wind plays a key role [1]. The wind energy sector has experienced rapid growth in recent years, and the evolution of *offshore wind* is particularity outstanding: from being a technological novelty in the early 90's, offshore wind has become a booming sector, doubling deployed capacity every 2.5 years since 2005 [2]. Astounding technological progress has been made since the early years, strikingly showcased by the increase in blade size: while the first 11 offshore turbines installed in Vindeby in 1991 had a blade length of just 17.5 meters, modern offshore turbine blades routinely span over 70 meters, and the most recent blade models reach 100 meters and more [3].

For new turbine models and farms to be reliable and therefore bankable, it is necessary to be able to predict all relevant aspects of their behaviour. Accurate models for energy yield, resistance to extreme wind conditions and fatigue lifetime are fundamental to secure financing of new wind parks and are therefore key to a continued growth of the industry. The present master thesis is framed within the current context of wind turbine aerodynamic modeling, focusing specifically on the simulation of *wake effects*.

1.1 The Relevance of Wind Turbine Wakes

The *wake* of a wind turbine denotes the perturbed wind field downstream of the rotor. It is characterized by decreased velocity and increased turbulence, which lowers the energy production and increases fatigue loading on downstream turbines. Predicting these effects is necessary in order to accurately estimate annual energy production and fatigue life time of turbines. Modeling wake aerodynamics remains a challenge for the wind industry, and while standardized approaches exist [4], their implementation is not necessarily straightforward and accuracy of the models is not guaranteed. This work describes the implementation of a wake simulation tool based on a modelling approach recommended in the IEC61400 standard, the dynamic wake meandering (DWM) approach developed by researchers at DTU [5], and the efforts undertaken to assess the quality of the model. These include code verification, comparison

with a high-fidelity Large Eddy Simulation (LES) as well as validation with field data.

Additionally, the work describes the derivation of a novel formulation to predict the trajectory of the wake of a turbine that is not aligned with the wind. This formulation can be used to model the effectiveness of *wake steering*, and advanced wind farm control strategy where turbines are purposefully misaligned with the wind in order to deflect wakes and limit their overall impact across the wind farm [6].

1.2 Motivation

As wind turbines grow in size and rated power, aerodynamic loads increase and fewer and fewer modeling imprecisions can be tolerated. The DWM approach could be used to generate accurate inflow conditions for numerical simulations of turbines impacted by wakes, leading to more accurate predictions of loads on the turbine. A validated and streamlined implementation of a DWM-based flow field generator would allow to re-simulate configurations which were up to now treated with more conservative approaches. This may lead to the discovery of potential ”fatigue reserves” and points of design improvement: The cost reduction in wind energy is in part driven by such improvements, making such a DWM-based wake modelling tool a valuable asset for the industry.

The attempt to compare the tool to LES, specifically the flow solver ***YALES2*** developed by the CORIA laboratory and associated organizations [7], bares an additional interest. While the use of LES models in the verification of engineering models for wind turbine aerodynamics has become relatively common [8, 9], YALES2 has only recently been equipped with the ability to model wind turbines thanks to the implementation of an Actuator Line Model (ALM) [10]. The successful use of this solver in the verification of an engineering model for wind turbine wakes could pave the way for future research projects and industry collaborations on related topics. The present work represents the first attempt at such a comparison, and is therefore expected to reveal limitations of the current implementation of the ALM-based turbine simulator that must be resolved before the solver can be routinely used for such tasks.

The derivation of a novel wake deflection model was motivated principally by a strive for consistency in the developed wake modeling tool. While wake deflection models from literature exist [8, 9, 11], they are generally based on assumptions about the velocity profile in the wake. No such assumptions are made in the implemented wake modelling tool, making the integration of such models into the tool highly inconsistent. A new formulation for wake deflection, based directly on the velocity profile computed by the tool, is derived and tested against models from literature and against LES results.

1.3 Thesis Outline

Chapter 2 gives an overview of wind turbine models currently employed in the industry, both for rotor aerodynamics and wakes. Chapter 3 gives brief insight in the vast world of computational fluid dynamics (CFD) before describing how these models can be applied to wind energy. The current state of the art in CFD for wind turbines is explored, and the flow solver employed in the present work is introduced. Chapter 4 describes the implementation of a DWM-based wake modeling tool in line with the IEC standard,

able to simulate wake effects for entire wind farms. The underlying assumptions, equations and numerical solution methods are detailed, and use cases and limitations are outlined. Chapter 5 describes the process of verification and validation of the models implemented in the tool, using comparison with measurement data from a large offshore wind farm as well as CFD results. The former are provided by an industry partner, while the latter are obtained using the Actuator Line Methodology (ALM) on the LES solver YALES2. The LES computations are performed on the French supercomputing cluster *Myria* operated by the CRIANN (*Centre Régional Informatique et d'Applications Numériques de Normandie*). The results and limitations of this process are outlined in detail. In chapter 6 a newly derived formulation for wake deflection is presented. The formulation is intended to be added to the wake modeling tool in order to be able to predict the effectiveness of yaw steering on wind farms. Finally, chapter 7 resumes the work performed, draws conclusions and outlines future work.

Chapter 2

Review of Wind Turbine Modeling

In the context of the exceptional growth of the wind industry in recent years, understanding and modeling the behavior of wind turbines has gained increasing importance. New ambitious projects, such as ever larger offshore turbines or floating wind parks, require reliable models to predict the economic performance of new installations and guarantee the life time of the machines. Particular interest lies in modeling the effect of wind turbine wakes on downstream turbines, a topic that is not yet well understood and could have important implications on the collective behavior of wind turbines in farms.

This chapter is intended to serve as a reference for the work presented in subsequent chapters, and will be referred to extensively. It gives an overview of wind turbine models currently employed in the industry, both for rotor and wake aerodynamics. While not aspiring to be comprehensive, a number of commonly used models are explained to the degree of detail that is deemed necessary for comprehension of the present work.

2.1 Rotor Aerodynamics

Rotor aerodynamics are characterized by the interaction between the airfoil-shaped cross-sections of the moving rotor blades and the incoming wind. The phenomenon is most commonly modeled in a discretized manner using the Blade Element Momentum Theory (BEM). Other approaches include formulations based on vorticity (see E. Branlard, 2017 [12]), panel methods or models based on the resolution of the full Navier-Stokes equations (see chapter 3). This section will focus on BEM, as it is currently the *de-facto* industry standard, even though this might change in the coming years. While based on simple physical principles, BEM theory has proven to be incredibly versatile and predictive, even in conditions where its underlying assumptions are violated, thanks to a series of theoretical and empirical corrections that have been developed throughout the years.

The basics of the theory go back to the late 19th century and to pioneers of aerodynamics theory such as W. Froude (1878), W. J. M. Rankine (1865), A. G. Greenhill (1888) and later A. Betz (1919) or H. Glauert (1935) [13, 14, 15]. It combines blade element theory with momentum theory and was originally derived for propellers, even though the application to wind turbines was proposed almost from

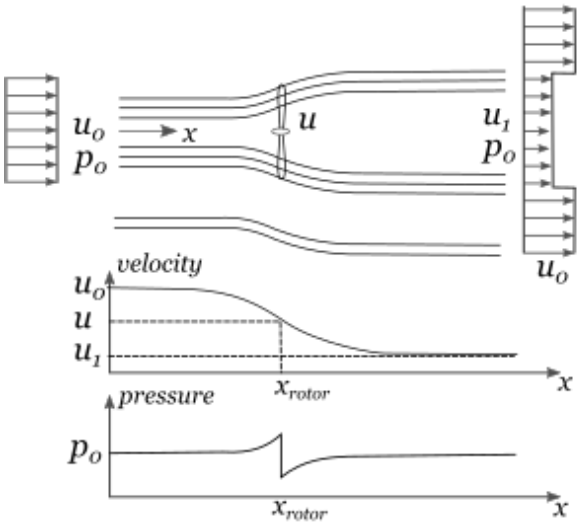

Figure 2.1: Streamlines, velocity and pressure in Momentum Theory for a wind turbine [16].

the start. A detailed description of BEM applied to wind turbines can be found in any standard wind energy textbook. The following summary was mainly sourced from *Aerodynamics of Wind Turbines* by Martin O. L. Hansen [16] and *Wind Energy Explained - Theory, Design and Application* by James F. Manwell [17].

2.1.1 Momentum Theory and the Betz Limit

The Momentum Theory, sometimes denoted Actuator Disk Theory, is a simplified approach to model the extraction or injection of kinetic energy in fluid flows by aerodynamic devices such as propellers or turbines. It is based on a one-dimensional mass and momentum balance along a stream tube and models the aerodynamic device as a permeable disk that exerts a thrust force on the wind. In the case of a wind turbine, this forcing will lead to the wind speed continuously slowing down from u_0 far upstream to u at the rotor and finally u_1 far downstream. Due to mass conservation, this deceleration leads to an expansion of the stream tube. Pressure increases up to the actuator disk, where the thrust force causes a discontinuity in pressure that brings it below atmospheric. The pressure then gradually recovers until returning to atmospheric levels far downstream. The evolution of streamlines, velocity and pressure is illustrated in figure 2.1.

When assuming inviscid, steady and incompressible flow, the Bernoulli energy balance between the inflow and a point right before the turbine can be written, giving:

$$p_0 + \frac{1}{2}\rho u_0^2 = p + \frac{1}{2}\rho u^2 \tag{2.1}$$

while the balance between a point right after the turbine and one far downstream gives:

$$p - \Delta p + \frac{1}{2}\rho u^2 = p_0 + \frac{1}{2}\rho u_1^2 \tag{2.2}$$

The pressure discontinuity Δp can therefore be expressed as:

$$\Delta p = \frac{1}{2}\rho(u_0^2 - u_1^2) \tag{2.3}$$

Momentum balance over a cylindrical control volume of cross-sectional area A that contains the entire stream tube gives:

$$\rho u_1^2 A_1 + \rho u_0^2 (A - A_1) + u_0 m_{side} - \rho u_0^2 A = -T \tag{2.4}$$

where A_1 is the cross sectional area of the stream tube in the far wake and m_{side} the mass flow over the lateral domain boundaries. Mass balance on the same control volume gives:

$$\rho u_1 A_1 + \rho u_0 (A - A_1) + m_{side} - \rho u_0 A = 0 \tag{2.5}$$

Isolating the mass flow leaving from the sides, m_{side}, in the mass balance (eq. 2.5) and inserting it into the momentum balance (eq. 2.4) yields the following expression for the thrust T exerted by the rotor on the fluid:

$$T = \rho A_1 u_1 (u_0 - u_1) = \rho A_{rot} u (u_0 - u_1) \tag{2.6}$$

Combining equations 2.6 and 2.3, and considering the relation $T = A_{rot}\Delta p$ yields:

$$\rho A_{rot} u (u_0 - u_1) = \frac{1}{2} A_{rot} \rho (u_0^2 - u_1^2) \tag{2.7}$$

$$\Rightarrow u = \frac{1}{2}(u_0 + u_1) \tag{2.8}$$

We conclude therefore, that the velocity at the rotor level is equal to the average between the velocities far upstream and far downstream. We define the **axial induction factor** a as:

$$u = (1 - a)u_0 \quad \text{or} \quad u_1 = (1 - 2a)u_0 \tag{2.9}$$

Expressing the thrust as $T = A_{rot}\Delta p$, using eq. 2.3 for Δp and finally substituting u_1 by its expression form eq. 2.9 yields the following relation between the thrust and the axial induction:

$$T = 2\rho u_0^2 a(1 - a) A_{rot} \tag{2.10}$$

To obtain the power extracted by the rotor, equation 2.10 is multiplied by the velocity at the turbine u expressed as a function of the axial induction (eq. 2.9), yielding:

$$P = 2\rho u_0^3 a(1 - a)^2 A_0 \tag{2.11}$$

It is common to express the non-dimensional variables in equations 2.10 and 2.11 as trust and power coefficients C_T and C_P. The dimensional quantities can then be retrieved by multiplying the coefficients

by $\frac{1}{2}\rho u_0^2 A$ or $\frac{1}{2}\rho u_0^3 A$ respectively. The dimensionless coefficients are thus defined as follows:

$$C_T = 4a(1-a); \qquad T = C_T \frac{1}{2}\rho u_0^2 A_{rot} \tag{2.12a}$$

$$C_P = 4a(1-a)^2; \qquad P = C_P \frac{1}{2}\rho u_0^3 A_{rot} \tag{2.12b}$$

The definition of these coefficient is such that their value lies between 0 and 1 during normal wind turbine operation.

The Betz Limit: At this point, a classic result of wind turbine theory known as the *Betz Limit* can be obtained. When maximizing the expression for the extracted power with respect to a, one finds an ideal axial induction of $a = \frac{1}{3}$ for maximum power extraction. Substituting this value, and considering the input power equal to $P_{in} = \frac{1}{2}\rho u_0^3 A_{rot}$ we obtain a theoretical limit for the maximum power coefficient C_P of any device built to mechanically extract power from an unconfined flow:

$$C_{P,max} = \frac{2\rho u_0^3 a(1-a)^2 A_{rot}}{\frac{1}{2}\rho u_0^3 A_{rot}}\Big|_{a=\frac{1}{3}} = \frac{16}{27} \approx \textit{59,26\%} \tag{2.13}$$

2.1.2 Momentum Theory with Rotation

A clear deficit of the presented 1-dimensional theory is that a wind turbine is not a porous disk, but rather a rotating machine. From conservation of angular momentum it is necessary that as the turbine is tangentially accelerated by the flow, the flow also acquires a tangential velocity by interacting with the turbine. We can thus define an angular induction factor a' such that the tangential velocity component of the flow at the rotor plane is equal to:

$$w = 2a'\Omega r \tag{2.14}$$

where Ω is the turbine angular velocity. Conservation of angular momentum is then applied to an annular control volume of width dr. The Euler turbine equation [16] expresses the power extracted in the elemental control volume as:

$$dP = 4\pi\rho u_0 \Omega^2 a'(1-a) r^3 dr \tag{2.15}$$

Dividing by Ω we can obtain a formulation for the infinitesimal torque dM, exerted by the control volume on the fluid,

$$dM = 4\pi\rho u_0 \Omega a'(1-a) r^3 dr \tag{2.16a}$$

while the infinitesimal thrust dT and can direct be derived from equation 2.10 using the infinitesimal area $2\pi r dr$:

$$dT = 4\pi\rho u_0^2 a(1-a) r dr \tag{2.16b}$$

It is possible to establish a connection between the two induction factors considering the local forces on the blade elements. The total induced velocity, sum of angular and axial induction, must be in agreement with the forces at the blade. Under the assumption of inviscid flow over the airfoil profile, the lift force, which is perpendicular to the relative wind, is the only aerodynamic force to consider. Therefore the following geometric relation can be drawn between the axial and angular induction factors:

$$\tan\phi = \frac{u_0(1-a)}{\Omega r(1+a')} \tag{2.17}$$

To obtain the total power and the power coefficient, the expression for dP can be integrated over the actuator disk. The resulting expression can then be optimized using relation 2.17, finding a new limit for rotating energy extraction that is depended on the tip speed ratio $\lambda = \Omega R/u_0$.

2.1.3 Blade Element Theory

Blade Element Theory is based on the subdivision of a rotor blade in elements of length dr along the span, and describing the local lift and drag forces for each element assuming two-dimensional flow. All forces, velocities and angles that appear on the blade element are represented in figure 2.2. The relative wind speed u_R arises as a consequence of incoming wind u_0, axial induction a, rotor rotational speed Ωr and radial induction a'. The angle of the incoming wind, ϕ and the pitch angle β determine the angle of attack α. Elemental lift and drag forces dL and dD arise perpendicular and normal to the incoming wind. Projecting these forces onto the rotor plane normal yields the elemental thrust force dT, while the projection on the rotor plane yields the tangential force dF_{tg} that generates the elemental torque $dM = rdF_{tg}$.

It is assumed that there is a direct relationship between the angle of attack α and the lift and drag force, L and D, described by lift and drag coefficients C_L and C_D. These coefficients vary with the angle of attack α. Neglecting unsteady phenomena, at a given Reynolds number a bijective relation between α and the lift and drag coefficient can be found for a given airfoil geometry, often denoted *(*polars). In a first approximation, the lift and drag characteristics are considered fixed for a given geometry at a given Reynolds number. The lift and drag forces are then computed as follows:

$$L = \frac{1}{2}\rho u_R^2 c C_L(\alpha) \tag{2.18}$$

$$D = \frac{1}{2}\rho u_R^2 c C_D(\alpha) \tag{2.19}$$

where u_R is the relative wind velocity considering induction and c is the chord of the airfoil, defined as the distance between the leading and trailing edge. Through geometric relations, the thrust T and torque M per unit length exchanged between the blade and the flow can be calculated, arriving at the following expression for dT and dM on an annular control volume dr that comprises sections of a number B of blades:

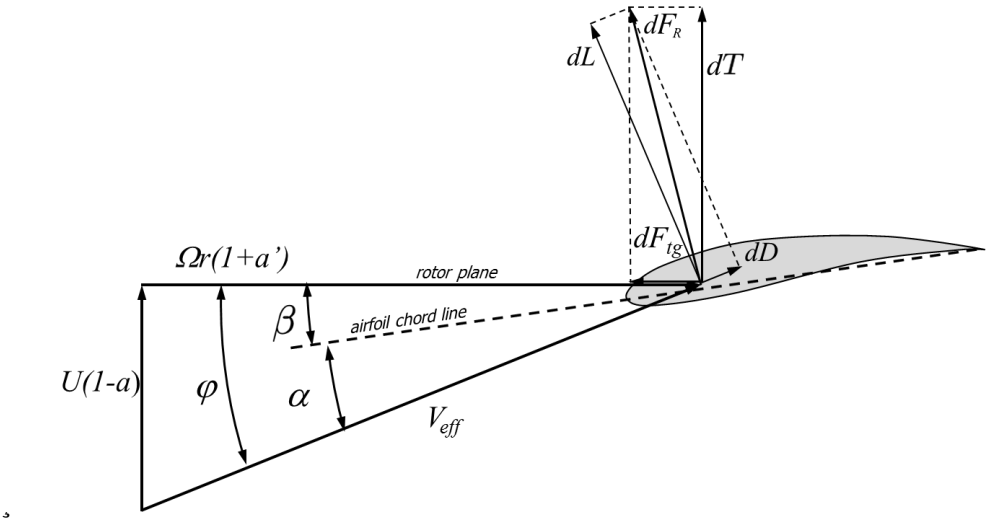

Figure 2.2: Forces, velocities and angles on a blade element [17].

$$dT = \frac{1}{2}\rho B u_R^2 c(C_L \cos\phi + C_D \sin\phi)dr \tag{2.20a}$$

$$dM = \frac{1}{2}\rho B \frac{u_0(1-a)\Omega r(1+a')}{\sin\phi\cos\phi} c(C_L \sin\phi - C_D \cos\phi) r dr \tag{2.20b}$$

It is assumed that all blades give an equal contribution without influencing each other. This approximation is justified, as flow perturbations caused by a blade are rapidly convected away from the rotor plane and do not influence the following blade. The hypotheses of the blade element model are strong and empirical corrections are often introduced to account for them.

2.1.4 Derivation of Blade Element Momentum Theory

Blade Element Momentum theory (BEM) combines momentum theory and blade element theory to obtain a set of equations that can be solved iteratively in order to obtain the local induction, torque, thrust and power for a given blade element. The derivation is based on imposing equality of the expressions for dT and dM derived by the two theories for an annular rotor section. By setting equations 2.16 equal to equations 2.20 one obtains the following relations for linear and angular induction a and a':

$$a = \left(\frac{4\sin^2\phi}{\frac{cB}{2\pi r}(C_L\cos\phi + C_D\sin\phi)} + 1 \right)^{-1} \tag{2.21a}$$

$$a' = \left(\frac{4\sin\phi\cos\phi}{\frac{cB}{2\pi r}(C_L\sin\phi - C_D\cos\phi)} - 1 \right)^{-1} \tag{2.21b}$$

The equation system can be solved iteratively for a given geometry and wind speed. Starting from an initial guess for the induction factors a and a', the following procedure is followed:

1. Calculate ϕ from equation 2.17
2. Obtain the lift and drag coefficient C_L and C_D at the resulting α from characteristic curves

3. Update a and a' through equations 2.21

4. Repeat until reaching convergence

Once convergence is reached, quantities of interest such as torque, thrust or power can be obtained from equations of either Momentum Theory (section 2.1.1) or Blade Element Theory (section 2.1.3).

2.1.5 Limitations and Corrections of BEM

The presented theroy is based on a series of assumptions that limit its applicability if no additional corrections are applied. These assumptions include:

- Steady, uniform inflow conditions and normal incoming wind.
- Inviscid flow in independent annular stream tubes.
- Presence of a blade continuum (infinite blades).
- Axial induction limited to an induction factor of $a = 0.5$.

Several corrections have been introduced to BEM throughout the years in order to overcome limitations caused by these assumptions. One of the earliest among them was the **tip loss correction**, that addresses the assumption of infinite blades. As the rotor blades only cover a small fraction of the rotor area, some air particles will cross the rotor area without being affected by it. Moving closer to the tip, the fraction of rotor area where blades are present decreases, finally bringing the lift at the end of the blade to zero. The most common way to take this into consideration is by through the use of a tip loss correction factor as proposed by Prandtl: Equations 2.16a and 2.16b are multiplied by a tip loss factor F who's value stays close to 1 along most of the blade and continuously drops to 0 towards the tip. The correction factor proposed by Prandtl takes the form:

$$F = \frac{2}{\pi}\cos^{-1}\exp(-f) \quad \text{where} \quad f = \frac{B}{2}\frac{R-r}{r\sin\phi} \tag{2.22}$$

The correction factor is introduced into the BEM formulation, leading to the following modified formulations for the BEM model:

$$a = \left(\frac{4F\sin^2\phi}{\frac{cB}{2\pi r}(C_L\cos\phi + C_D\sin\phi)} + 1\right)^{-1} \tag{2.23a}$$

$$a' = \left(\frac{4F\sin\phi\cos\phi}{\frac{cB}{2\pi r}(C_L\sin\phi - C_D\cos\phi)} - 1\right)^{-1} \tag{2.23b}$$

A phenomenon similar to tip losses is encountered at the blade root, where hub losses ensue. Again a loss factor can be introduced, with a value of 1 along most of the blade and decreasing to 0 towards the root. The final BEM formulation will be equal to expression 2.22, where the correction factor F will consider both tip and root losses.

Another classic correction concerns cases where axial induction is high. Basic momentum theory is not valid for values of induction larger than 0.5, as this implies negative velocities in the wake that cannot occur under the assumptions of BEM. In order to extend the model to cases with high induction, equation 2.16b with empirical relations starting from induction factors of $a \approx 0.4$.

2.1.6 Unsteady Aerodynamic Effects

One of the more unrealistic assumption in classic BEM is uniform, steady and perpendicular incoming wind. This is never the case in reality, as as wind shear and the presence of the tower (*tower shadow*) cause each blade element to see continuous velocity variation during a turbine revolution. Further sources of wind speed fluctuation include ever present turbulence in the atmospheric boundary layer as well as vibrations of the structure of the turbine. At the blade section level, these fluctuations can give rise to quick variations of the perceived angle of attack, leading to unsteady aerodynamic effects that can cause unexpected behavior of the turbine. A second category of unsteady effects are large-scale phenomena, generally related to the inertia of the stream tube when reacting to changes in the induction. These phenomena are observed for example during pitching maneuvers (rotating blades around their main axis). A full description of unsteady effects and their treatment in BEM can be found in [16].

Among the unsteady effects at the blade section level, *dynamic stall* is one of the most influential. Regular stall ensues when the angle of attack α on an airfoil becomes very high and is characterized by boundary layer detachment, a decrease in lift and an increase in drag. The angle of attack at which stall occurs is assumed to be characteristic of the airfoil shape, but for rapid changes in α it actually depends on this rate of change, usually characterized with the reduced frequency k, hence the term dynamic stall. Generally, the stall angle increases if α changes more rapidly. This can lead to dangerous situations when a sudden increase in wind speed, or gust, pushes the angle of attack beyond the critical point. Instead of stalling, the boundary layer stays attached and the lift keeps increasing, leading to larger magnitudes of instantaneous aerodynamic forces.

Another phenomenon that violates some of the basic assumptions of BEM is known as dynamic inflow. In momentum theory, the wind field upstream and downstream of the rotor are assumed to react instantly to changes in the induction, caused for example by pitch control, but in reality, this is not the case. The flow field takes time to adapt to the changes, and therefore the inflow conditions will not be as expected.

Models and corrections exist to deal with these and other effects, and software tools encompassing them are routinely used in the wind industry. The aerodynamic models are often coupled with a structural model for the turbine and a wind turbine controller, leading to complete wind turbine simulators able to deal with unsteady, non-uniform wind fields and transient states such as start-up and stop, yawing or pitch control, all while taking the eventual deformation of the structure into account [18, 19].

2.1.7 Aero-Servo-Elastic Solvers

When coupling an unsteady aerodynamic solver with a structural model for the wind turbine blades and tower as well as a control system that regulates pitch, yaw and generator speed, a compete simulation of the wind turbine behavior becomes possible. These fully unsteady simulation tools, often denoted 'aero-servo-elastic' solvers, are widely used in the wind industry. One such code is the open-source project OpenFAST, forked from NREL's proprietary software FAST (Fatigue, Aerodynamics, Structures and Turbulence), that is developed by NREL and an active open source community [18]. The modular framework of the code allows for replacement and modification of individual sub-models, such as the aerodynamic module or the controller, while OpenFAST acts as a glue code. For this reason, and due to its open-source nature, the code is popular in both research and industry.

Another aero-servo-elastic code is BHawC (Bonus energy Horizontal Axis Wind turbine Code), a commercial tool developed originally by Bonus energy (formerly Danregn) before their acquisition by Siemens AG in December 2004 [19, 20]. The code continues to be developed in-house by Siemens Gamesa Renewable Energy (SGRE), and is constituted by interchangeable modules for aerodynamics, control and structural dynamics. The code is fully unsteady, corrects for 3D effects such as tip and root losses, and is able to take into consideration geometric parameters such as yaw misalignment, tilt and coning as well as non-uniform wind conditions including wind shear, tower shadow and turbulent inflow [19]. The wind conditions in BHawC are set by defining a 3D wind field that is convected across the rotor at the mean ambient wind speed. As there are no constraints on the data contained in the wind field, it is possible to add the wake effects of upstream turbines to this input. As the focus of the present work lies precisely on these wake effects, BHawC will be used as a platform to experiment with the wake models studied in this work.

2.2 Wind Turbine Wake Effects

The wake of a wind turbine is defined as the disturbance in the atmospheric flow caused by the presence of the turbine. It is generally characterized by reduced wind speed and increased turbulence.It is furthermore observed that these wake effects are displaced in an oscillatory manner around the mean wind axis in a phenomenon denoted *wake meandering*. The importance of wakes for the performance of wind farms has been recognized early in the history of modern wind energy, and mathematical models for it have been researched [21]. Focus of most early research was the reduction of wind velocity in the wake, which directly impacts the energy yield of wind farms. The following section will explore some of the models that have been proposed for wake velocity deficits.

2.2.1 The Jensen Wake Model

One of the first to describe the interaction between wind turbines was N. O. Jensen, who published a simple model for turbine wakes in 1983 [21]. The model is today commonly known as both Jensen and Park model. It assumes a uniform, cylindrical velocity deficit, as generated by an ideal actuator disk of

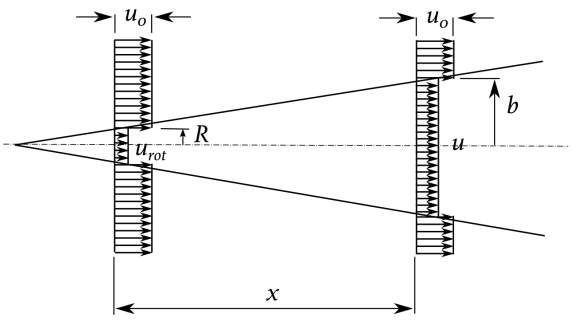

Figure 2.3: Schematic representation of the Jensen wake model [21].

radius R, that expands linearly as shown in figure 2.3. The derived formulation is based exclusively on a mass balance between the rotor plane and plane at the downstream distance of interest, considering axial flow only. This approach yields the following equation:

$$\pi R^2 u_{rot} + \pi(b^2 - R^2)u_0 = \pi b^2 u \tag{2.24}$$

The author himself refers to this equation as *momentum balance* [21], which had lead to the common misconception that the Jensen model uses a momentum balance, while actually only mass conservation is prescribed. The next assumption taken in the model is that the velocity at the rotor u_{rot} assumes the *far downstream* value predicted by classical BEM theory, $u_{rot} = u_0(1 - 2a)$. Using this in the mass balance (eq. 2.24) yields for the velocity in the wake:

$$u = u_0 \left[1 - 2a \left(\frac{R}{R + k_e x} \right)^2 \right] \tag{2.25}$$

where x is the downstream distance and k_e is the linear expansion coefficient of the wake, usually denoted *entrainment constant*. The wake is initially rotor-sized and expands linearly as $b = R + k_e x$. A more common expression can be deduced using the thrust coefficient C_T, that for an ideal turbine is defined according to equation 2.12a as $C_T = 4a(1 - a)$. Using this expression in equation 2.25 yields for the wake deficit [22]:

$$\frac{u_0 - u}{u_0} = \left(1 - \sqrt{1 - C_T)}\right) / \left(1 + \frac{2k_e x}{D}\right)^2 \tag{2.26}$$

Jensen finds that for usual wakes, k_e is approximately 0.1 [21], while more recent authors propose values of 0.04 - 0.05 for offshore and 0.075 for onshore wind turbines [23]. Difference between values proposed for onshore and offshore are due to the turbulence intensity, a main driver for wake expansion, being on average lower offshore. The model, while very basic, allows for a rough estimation of the impact of wakes on power generation in wind parks, including effects of the wakes of multiple upstream turbines. . The formulation remains widely used in industry and has been shown to give good estimates for power production in a variety of studies [24]. However, the top-hat shape of the proposed wake deficit is certainly non-physical, and the sharp change makes the model unsuitable for unsteady BEM calculations in situations of partial wake incidence (half-wake) due to the high gradients. The same holds

true for direct variations of the model such as formulations proposed by Frandsen (1992) [25] or more recently by Luzzatto (2018) [26].

2.2.2 Thebe EPFL Gaussian Wake Deficit Model

In order to overcome the unrealistic shape in the Jensen deficit model, researchers at the École Polytechnique Fédérale de Lausanne (EPFL) propose to assume a Gaussian shape for the deficit, and to impose both mass and momentum conservation [23]. This shape makes intuitive sense as the wake expansion is a diffusive process and is therefore governed by a Laplacian equation, who's characteristic solution is a Gaussian. Wind tunnel and field measurements as well as numerical studies confirm this hypothesis [23].

The assumed wake shaped is mathematically expressed as:

$$\frac{u_0 - u}{u_0} = 1 - C(x)e^{-\frac{r^2}{2\sigma^2}} \tag{2.27}$$

where r is the radial distance from the wake center, σ a parameter for the width of the shape and $C(x)$ the centerline wake velocity at a distance x in wind direction. From mass and momentum conservation, the following equation for $C(x)$ is retrieved:

$$C(x) = 1 - \sqrt{1 - \frac{C_T}{8(\sigma/D)^2}} \tag{2.28}$$

For the wake width parameter σ, a linear expansion as suggested by Jensen [21] is assumed:

$$\frac{\sigma}{D} = k_e \frac{x}{D} + \epsilon \tag{2.29}$$

where the initial wake width ϵ is determined from the initial mass flow deficit caused by the rotor and the expansion rate k_e is determined in the original paper by Large Eddy Simulation (LES), trusting that the results of said simulation are accurate. The final formulation given by the researchers at EPFL reads as follows [23]:

$$\frac{u_0 - u}{u_0} = \left(1 - \sqrt{1 - \frac{C_T}{8(k_e \frac{x}{D} + \epsilon)^2}}\right) \times \exp\left(-\frac{1}{2(k_e \frac{x}{D} + \epsilon)^2}\left\{\left(\frac{z - z_h}{D}\right) + \left(\frac{y}{D}\right)\right\}^2\right) \tag{2.30}$$

where y and $(z - z_h)$ are the radial and vertical coordinates around the wake center and where:

$$\epsilon = 0.25\sqrt{0.5\frac{1 + \sqrt{1 - C_T}}{\sqrt{1 - C_T}}} \tag{2.31}$$

The authors find good agreement of the model with LES studies for the far wake in various test cases [23]. It is stated that a mismatch in the near wake is expected, as the wake velocity profile immediately after the rotor is not Gaussian. The model is considered applicable from a downstream distance of three turbine diameters. In a more recent development of the EPFL wake model the near-wake expansion

and propagation is modeled using a potential core model [9]. This model is described in more detail in section 2.5.2, where its use in the computation of the wake trajectory of a yawed turbine.

2.2.3 The Larsen Wake Model

One of the first to propose a model based based on the fundamental momentum balance that govern fluid flows, *i.e.* Navier-Stokes (NS) equations 3.1 was Gunnar C. Larsen in 1988 [27]. In particular, he proposed the use of an axisymmetric thin-shear-layer approximation of the NS equations that assumes gradients in the radial direction to be significantly larger than in the axial direction. Larsen derived asymptotic analytical solutions for the equations for both first- and second order approximations. The model was refined by the author in 2009, changing the downstream boundary conditions to be derived from full-scale experiments ant thus making it semi-analytical [28]. A detailed derivation of the latest update of this model can be found in [28], while a summary is provided in [29].

2.2.4 The Ainslie Wake Model

Also in 1988, J. F. Ainslie proposed another model based on the thin-shear-layer approximation of the NS equations. In contrast to Larsen however he suggested the use of a numerical solution scheme for the equations instead of finding analytical expressions [30]. Since the wake deficit model implemented in chapter 4 is based on Ainslie's work, a detailed derivation of it is now provided.

Fundamentally, Ainslie proposes a separation of the wake into a near-wake and far-wake region, In the near-wake, up to 2-4 diameters downstream, the flow characteristics are dominated by the relaxation of the pressure gradient created by the turbine as described by momentum theory (section 2.1.1). This causes a reduction of the centerline velocity and an expansion of the wake. After the centerline velocity reaches its minimum it begins to recover. In the far-wake region, at about 3-5 diameters downstream, fluid mixing takes over as the governing phenomenon and the wake becomes fully turbulent. The far-wake profile is assumed to be roughly Gaussian, with the centerline deficit decaying monotonically with a decay rate that increases with the ambient turbulence intensity [30]. Ainslies original formulation was only designed for the far wake, where the pressure-driven wake expansion is concluded. Once the pressure is equalized with the atmospheric level, the pressure gradient term in the equations can be neglected. Assuming furthermore axial symmetry, incompressibility and the dominance of radial gradients ver axial gradients, the thin shear layer incompressible time-averaged NS equations can be obtained [29]:

$$\frac{\partial U}{\partial x} + \frac{1}{r}\frac{\partial}{\partial r}(rV) = 0 \tag{2.32a}$$

$$U\frac{\partial U}{\partial x} + V\frac{\partial U}{\partial r} = -\frac{1}{r}\frac{\partial r\overline{u'v'}}{\partial r} \tag{2.32b}$$

In Ainslie's work, x and r are non-dimensionalized using the turbine diameter. Capital letters U and V mark the steady components of the axial and radial velocity field, while signed minuscules u' and v' mark turbulent velocity fluctuations in the respective direction. The expression $\overline{u'v'}$ denotes a tensor that

describes the momentum transfer caused by turbulence, known as the Reynolds stress tensor. Modeling this term is generally referred to as *turbulence closure.* Ainslie proposes the following closure model:

$$-\overline{u'v'} = \nu_e \frac{\partial U}{\partial r} \tag{2.33}$$

where ν_e, the eddy viscosity, is an empirically determined kinematic diffusion constant that allows to treat turbulent momentum exchange as a viscosity., taking the assumption that the phenomenon of turbulent momentum transfer in the flow is analogous to momentum transfer due to molecular viscosity. The momentum equation 2.32b can therefore be rewritten as [30]:

$$U\frac{\partial U}{\partial x} + V\frac{\partial U}{\partial r} = \frac{\nu_e}{r}\frac{\partial}{\partial r}\left(r\frac{\partial U}{\partial r}\right) \tag{2.34}$$

The effective kinematic viscosity, ν_e, is derived from suitable length- and velocity scales of the fluid phenomenon $l_W(x)$ and $U_W(x)$:

$$\nu_e \approx l_W(x)U_W(x) + \nu_{amb} \tag{2.35}$$

where ν_{amb}, is the ambient turbulence contribution to the effective viscosity taken from the description of the boundary layer and thus derived from the turbine hub height and surface roughness. As length and velocity scales Ainslie proposes the use of the wake width b and the velocity deficit at the wake center U_0U_c. The effective viscosity is modified by multiplying with a blending function in order to account for the build-up of turbulence in the shear layer of the wake:

$$F = \begin{cases} 0.65 + \left(\frac{x-4.5}{23.32}\right)^{\frac{1}{3}} & \text{if } x < 5.5 \\ 1 & \text{if } x > 5.5 \end{cases} \tag{2.36}$$

This leads to Ainslie's final expression for the effective viscosity that is given as follows:

$$\nu_e = F\left[k_1 b(U_0 - U_c) + \nu_{amb}\right] \tag{2.37}$$

The value of k_1 is believed to be a constant property of the shear layer, and good agreement with experiments is found for a value of 0.015, while ν_{amb} includes the effect of the ambient turbulence.

Ainslie envisioned the model to be initialized with a Gaussian-shaped wake deficit at a downstream distance of at least two turbine diameters from the rotor. Later authors propose more elaborate blending functions, tuning the viscosity in the near wake and allowing to initialize the model directly at the rotor [31].

Even though Ainslies model is based on the numerical solution of NS equations, the computational cost remains limited. In the original publication the discretized differential equations are solved using a first order forward difference scheme for the axial advection term, that according to the author "can be performed quickly on a small desktop computer" (in 1988) [30]. Unlike the Jensen model, this model

is able to predict the velocity profile in the wake with reasonable accuracy, as a Gaussian profile has been observed for the far wake in full-scale measurements [32]. The Ainslie model has been refined in subsequent literature, and versions of it are commonly used in industrial applications.

2.3 Wake Meandering

An important phenomenon observed in wind turbine wakes is the so-called wake meandering. The phenomenon consists in a random, large-scale oscillatory motion of the entire wake around the mean wind axis, caused by large-scale turbulent fluctuations in the wind direction [33, 34]. While a model for velocity deficit in the wake allows to give an estimate of the energy harvested by a turbine standing in the wake of another, it is not sufficient to understand the loads that might be caused by a wake. To achieve this, it is important to model the unsteady nature of wakes and therefore the phenomenon of wake meandering. The continuous displacement of the impacting wake causes cyclic loading similar to large-scale turbulence and could therefore be an important factor in fatigue and material life time, constituting a form of apparent turbulence intensity [5]. From a perspective of energy yield meandering also has an impact, as it affects the apparent mean wind speed [33]. Two approaches are possible for modeling meandering: a purely statistical approach that only tries to predict the average wake deficit, and a dynamic approach that allows to use the wake model together with an unsteady aerodynamic turbine model to observe the additional loads caused by the meandering wake.

2.3.1 Statistical Treatment of Wake Meandering

The meandering phenomenon has first been discussed in early work of Ainslie [33], where a statistical treatment of the phenomenon is proposed. In particular, he proposes a reduction of the centerline wake deficit since a stationary observer at the wake center will see different parts of the wake over time. The following expression is given for the reduced centerline wake deficit C [30]:

$$C = C_0 \left[1 + 7.12 \left(\sigma_\theta \frac{x}{b} \right)^2 \right]^{\frac{1}{2}} \tag{2.38}$$

Here C_0 is the centerline wake deficit without meandering, and σ_θ is the standard deviation of the wind direction, measured over the same time period as the averaging but ignoring ”small” fluctuations [33]. Details on the filtering process are however not provided. The meandering correction results in a better estimate of the velocity deficit in the wake compared to measurements.

Larsen et al. [28] identify wake meandering as a main driver of the linear wake expansion that is observed in in wind farms and used as a basis for many static wake models such as Jensen’s model [21] or the Gaussian model by EPFL [23]. This implies that such models take meandering implicitly into account when tuning their parameters to field data.

A statistical approach to meandering is sufficient for power estimates, but does not contribute to understanding the impact of wake meandering on loads, for which dynamic models are necessary.

2.3.2 The Meandering Model of DTU

In the meandering model proposed by researchers at DTU [29], the use of a *passive tracer* assumption is proposed. According to this assumption, the wake can be seen as a "cascade of rotor-sized, disc-shaped, neutrally buoyant balloons" [35] that are emitted from the turbine and advected with the turbulent flothew. Larsen [34] postulates that the wake tracer is advected longitudinally at mean ambient wind speed and transported laterally by large-scale turbulent structures. This pragmatic approach, described and justified in detail in [34], allows for a complete decoupling of the wake deficit and the meandering process. Furthermore, the assumption is made that for small to moderate downstream distances the lateral velocity of the wake tracer is constant and equal to the large-scale turbulent velocity at the rotor at the instance of emission of the tracer. The following equations describe the lateral and vertical position of a wake tracer, emitted at t_0, at time t [31, 4]:

$$\begin{aligned} y(t) &= \tilde{v}(t_0)(t - t_0) \\ z(t) &= \tilde{w}(t_0)(t - t_0) \end{aligned} \tag{2.39}$$

Here $\tilde{v}$ and $\tilde{w}$ denote the lateral and vertical velocities at the rotor, filtered to ignore small-scale fluctuations. This approach requires a precise definition of "large scale" for atmospheric turbulence. Turbulent structures contained in this scale must be at least large enough to justify the assumption that all points of the wake tracer move simultaneously in the same direction [31]. Considering a circular turbulent structure such as a large eddy vortex, its diameter must therefore be at least twice as large as the entire wake tracer, whose size is assumed to be of the order of one turbine diameter D. In a frozen turbulence assumption this leads to a spatial cut-off frequency of $2D$ for the definition of large scale.Considering a frozen turbulence field convected at mean ambient wind speed (Taylor's hypothesis), a length scale L can be translated into a time scale T by dividing through the mean wind speed u_0. Researchers at DTU therefore define a cut-off frequency f_c, that when applied to a turbulent time series of velocities at the rotor yields the wake tracer velocities $\tilde{v}$ and $\tilde{w}$:

$$f_c = \frac{u_0}{2D} \tag{2.40}$$

This filter frequency is applied to a Mann Turbulence spectrum [36], separating between large scale ambient turbulence mainly contributing to wake displacement and small scale turbulence mainly causing dissipative turbulent wake expansion. Even though the distinction is not sharp in reality, this cut-off frequency is considered a logical choice and Larsen finds good agreements with full-scale measurements [31].

2.4 Wake Added Turbulence

A third effect observed in wind turbine wakes is the increase of turbulence intensity in the wake region. A large part of this turbulence originates from the meandering of the incoming wake that generates

apparent large-scale velocity fluctuations for a stationary observer, while a minor contribution is given by small-scale turbulence originating from tip vortices and shear in the wake [5]. Several empirical models for added turbulence have been proposed that mostly attempt to fit the total measured added turbulence without separating meandering. Notable examples are the model by S. Frandsen [37] that is also included in the IEC61400 standard or the model by Crespo and Hernandez [38]. Other models focus exclusively on small-scale fluctuations in the wake caused by shear and vortices [39], and rely on meandering models for the full picture. Such models allow for a dynamic description of the meandering wake while still obtaining the correct turbulence statistics.

2.4.1 Conventional Added Turbulence Models

Many models commonly used in the industry attempt to compute the total apparent turbulence, combining the effect of meandering with smaller effects such as vortices and shear. They generally try to deliver an estimate of the added intensity I_+ such that the total turbulence intensity in the wake I_{wake} can be calculated as [22]:

$$I_{wake} = \sqrt{I_0^2 + I_+^2} \tag{2.41}$$

where I_0 is the ambient turbulence intensity. Among the first to propose such a model were Quarton and Ainslie in 1990, introducing the following formulation based on the thrust coefficient C_T, I_0 and on an estimate of the near wake length x_n [40]:

$$I_+ = 4.8 C_T^{0.7} I_0^{0.68} \left(\frac{x}{x_n}\right)^{-0.57} \tag{2.42}$$

The length of the near wake region x_n is estimated using the following relations:

$$x_n = \frac{\sqrt{0.214 + 0.44m}(1 - \sqrt{0.134 + 0.124m})}{(1 - \sqrt{0.134 + 0.124m})\sqrt{0.2414 + 0.44m}} \frac{r_0}{dr/dx} \tag{2.43}$$

with $m = \frac{1}{\sqrt{1-C_T}}$, $r_0 = D\sqrt{\frac{m+1}{2}}$ and dr/dx defined as follows:

$$dr/dx = \sqrt{\left(\frac{dr}{dx}\right)_a^2 + \left(\frac{dr}{dx}\right)_m^2 + \left(\frac{dr}{dx}\right)_\lambda^2} \tag{2.44}$$

where $\left(\frac{dr}{dx}\right)_a = 2.5 I_0 + 0.005$, $\left(\frac{dr}{dx}\right)_m = \frac{(1-m)\sqrt{1.49+m}}{9.76(1+m)}$ and $\left(\frac{dr}{dx}\right)_\lambda = 0.012 B\lambda$, B being the number of blades and λ the tip speed ratio of the rotor.

This formulation was later modified by Hassan, who proposed the following modification to equation 2.42 in 1993 [41]:

$$I_+ = 5.7 C_T^{0.7} I_0^{0.68} \left(\frac{x}{x_n}\right)^{-0.96} \tag{2.45}$$

A similar model was introduced by Crespo and Hernandez in 1996. Their formulation does not rely on the computation of x_n and is limited in its validity to downstream distances larger than 5 diameters.

The equation reads as follows [38]:

$$I_+ = 0.73a^{0.8325} I_0^{0.0325} \left(\frac{x}{D}\right)^{-0.32} \tag{2.46}$$

Where D is the turbine diameter and a is the induction factor.

A last incarnation of a similar model was proposed by S. Frandsen and reads as follows [42]:

$$I_+ \approx \frac{1}{1.5 + \frac{x}{D}\frac{0.8}{\sqrt{C_T}}} \tag{2.47}$$

This last model has been added to the standard IEC61400 as an option for the treatment of wakes [4], and is therefore commonly employed in the industry. This increased turbulence value is than used to generate inflow for aero-servo-elastic simulations, allowing to estimate the added fatigue loads on all turbine components caused by wakes.

As can be observed in the above presented formulations, these models often are densely packed with empirical constants. This arises from fitting the model to experimental data, but at the same time causes a loss in general applicability of the model. A critical approach is therefore necessary when applying such methods to new cases.

2.4.2 Added Turbulence for Dynamic Wake Meandering

When treating wake meandering in a dynamic way, the added turbulence models described in the previous section can no longer be applied, as they already include the effect of wake meandering on apparent turbulence. New models are required that focus exclusively on the smaller turbulence generated inside the wake. Researchers at DTU describe this as added turbulence "in the meandering frame of reference" [5]. The DWM model by DTU [31], proposed in the 2018 IEC standard as an alternative to Frandsens model [4], includes such a turbulence model.

The added turbulence in the wake is described as an additional, uniform turbulent velocity field with an integral length scale smaller than one rotor diameter [43]. The standard deviation of this velocity field is determined by an empirical factor k_{wt} that is dependent on the velocity deficit and the radial velocity gradient in the meandering wake field [5, 4]:

$$k_{wt}(x,r) = 0.6\left|1 - \frac{U(x,r)}{U_0}\right| + \frac{0.35}{U_0}\left|1 - \frac{\partial U(x,r)}{\partial r}\right| \tag{2.48}$$

The factor is calculated in the meandering frame of reference, and the added turbulence is convected as a passive tracer similar to the wake deficit, as described in section 2.3.2 [31]. In order to obtain the total turbulent velocity field, the added turbulent velocity $\vec{u}_{aw}$ is summed with the ambient velocity field

$\vec{u}'_{amb}$ and the meandering wake deficit $U_0 - U$ component by component [5]:

$$\begin{aligned} u &= u_{amb} + u'_{aw} + U_0 - U \\ v &= v_{amb} + v'_{aw} \\ w &= w_{amb} + w'_{aw} \end{aligned} \tag{2.49}$$

As the wake deficit can be considered purely axial, only the axial component of the total velocity contains a contribution from meandering, resulting in a higher turbulence. This is coherent with experimental results [5].

2.5 Wake Deflection and Steering Models

During steady, normal wind turbine operation, the rotor is kept aligned with the incoming wind in order to maximize energy extraction and avoid unsteady effects related to the radial wind velocity component. This means that the thrust exerted on the flow is aligned with the mean wind direction, causing a deceleration of the flow but no deflection. However, by rotating the turbine about the tower axis and thus voluntarily introducing a yaw error, an off-axis force is exerted on the flow, leading to a deflection of the wake trajectory [8]. Employing a wind farm control strategy based on this mechanism has been shown to significantly improve overall farm performance in situations where the wind direction is aligned with the turbine rows [6]. Several models for wake deflection have been proposed and two of them are detailed below.

2.5.1 Jiménez's Analytical Model

Jiménez derives a model for wake deflection based on momentum conservation assuming a uniform, top-hat shaped wake deficit $u_0 - u$ [8]. Starting from the control volume shown in figure 2.4, the following mass and momentum balances can be written:

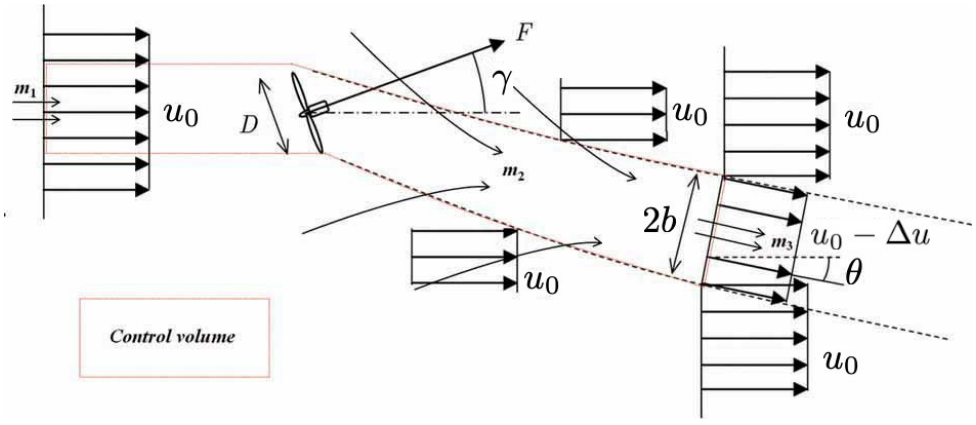

Figure 2.4: Mass flows and velocities in the Jiménez wake deflection model [8].

$$m_1 + m_2 = m_3 \tag{2.50a}$$

$$\vec{F} = m_3(u) - m_1\vec{u_0} - m_2\vec{u_0} \tag{2.50b}$$

Here m denotes a mass flow and $\vec{F}$ the global force exerted by the turbine on the fluid. By projecting the momentum balance in x and y direction, we can link the angle of outflow θ to the total thrust force F exerted by the yawed rotor. Jimenez derives this force from a given thrust coefficient and the normal incident wind (see eq. 2.12a) and projects it on the x and y axis.

$$f_x = -C_T \frac{1}{2}\rho A(u_0 \cos\gamma)^2 \cos\gamma \tag{2.51a}$$

$$f_y = -C_T \frac{1}{2}\rho A(u_0 \cos\gamma)^2 \sin\gamma \tag{2.51b}$$

Inserting this into eq. 2.51b and assuming small deflection angles θ and a small wake deficit $U_0 - U$ leads to the following expression for θ as a function of the wake width $2b$:

$$\theta \approx \left(\frac{D}{2b}\right)^2 \cos^2\gamma \sin\gamma \frac{C_T}{2} \tag{2.52}$$

In an approach similar to the Jensen wake deficit model (see 2.2.1), Jiménez assumes a linear wake expansion starting from the turbine diameter D, therefore $\delta = D + k_e x$, where k_e is a constant expansion coefficient. This yields Jiménez expression for the wake outflow angle θ as a function of x [8]:

$$\theta(x) = \frac{\cos^2\gamma \sin\gamma \frac{C_T}{2}}{\left(1 + k_e \frac{x}{D}\right)^2} \tag{2.53}$$

Integrating the tangent of this function along x leads to the following expression for the lateral deflection δ, that can be evaluated numerically or approximated analytically:

$$\delta = \int_0^x \tan\left(\frac{\cos^2\gamma \sin\gamma \frac{C_T}{2}}{\left(1 + k_e \frac{x}{D}\right)^2}\right) dx \tag{2.54}$$

According to the results of Jiménez, values of the wake growth rate β in the range of 0.09 to 0.125 give results that are most in line with the LES simulations performed in the work, but the parameter should be adapted to each case.

The Jiménez model continues to be applied in both research and industry, but has been shown to overestimate wake deflection in the far wake [9].

2.5.2 The EPFL Model

Researchers at the École Polytechnique Fédérale de Lausanne (EPFL) have questioned the applicability of a top-hat shaped, uniform deficit in yawed turbines [9]. They propose a model based on an asymmetric Gaussian deficit similar to their deficit model (section 2.2.2), considering the elliptic shape of the yawed

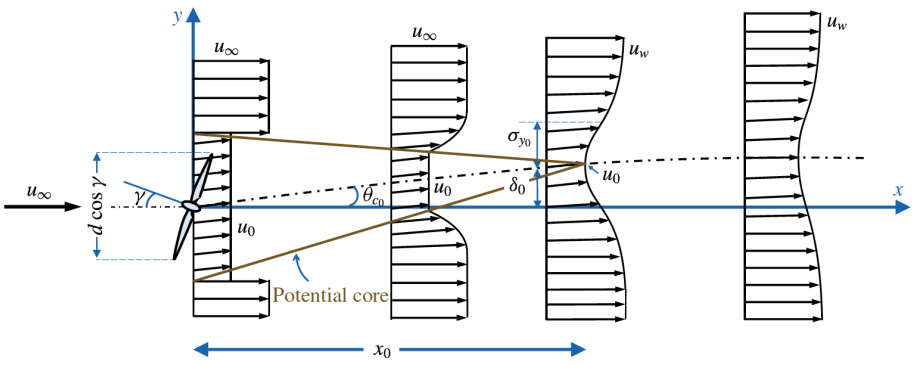

Figure 2.5: Mass flows, velocities and potential core in the EPFL wake deflection model. After the potential core disappears, the deflection angle and deficit shape become Gaussian [9].

turbine. Another addition to the original model is the treatment of the near wake using a ”potential core”. This concept, borrowed from jet theory, denotes a circular area of constant, uniform wake deficit that is emitted from the rotor and maintains its magnitude while shrinking in size until finally disappearing to give rise to a fully Gaussian wake [9], which then proceeds to expand as proposed in the original model [23] in both y and z direction. It is furthermore assumed that the deflection angle α follows a Gaussian behavior similar to the deficit. The model is represented in figure 2.5.

The following equations are assumed to describe the behavior of the deficit and deflection angle in the far wake:

$$\begin{cases} \frac{u_0-u}{u_0} = 1 - C\exp\left(-\frac{(y-\delta)^2}{2\sigma_y^2}\right)\exp\left(-\frac{(z-z_h)^2}{2\sigma_z^2}\right) \\ \frac{\theta}{\theta_m} = \exp\left(-\frac{(y-\delta+\sigma_y)^2}{2\sigma_y^2}\right)\exp\left(-\frac{(z-z_h)^2}{2\sigma_z^2}\right) \end{cases} \tag{2.55}$$

Both expressions describe a tree-dimensional Gaussian with different width in the lateral and vertical direction, σ_y and σ_z. The parameter θ_m describes the wake angle at the center of the deflected wake, δ describes total wake deflection while C is the centerline wake deficit. Applying continuity in the Gaussian region yields for C:

$$C = 1 - \sqrt{1 - \frac{(\sigma_{y_0}\sigma_{z_0})M_0}{(\sigma_y\sigma_z)}} \tag{2.56}$$

where $M_0 = C_0(2-C_0)$ and the subscript $_0$ symbolizes values at the end of the potential core region. By assuming further a linear wake expansion as in equation 2.29 in both x and y direction, an expression for the central deflection angle θ_c can be found:

$$\theta_c = \frac{\theta_{c_0}(\sigma_{y_0}\sigma_{z_0})E_0}{\sigma_y\sigma_z(C^2 - 3e^{1/12}C + 3e^{1/3})} \tag{2.57}$$

where $E_0 = C_0^2 - 3e^{1/12}C + 3e^{1/3}$. Integrating this equation along x gives the total deflection of the wake, and after some algebraic manipulations the paper gives the following final expression [9]:

$$\delta = \delta_0 + \frac{\theta_{c_0}E_0}{5.2}\sqrt{\frac{\sigma_{y_0}\sigma_{z_0}}{k_y k_z M_0}}\ln\left[\frac{(1.6+\sqrt{M_0})\left(1.6\sqrt{\frac{\sigma_y\sigma_z}{\sigma_{y_0}\sigma_{z_0}}} - \sqrt{M_0}\right)}{(1.6-\sqrt{M_0})\left(1.6\sqrt{\frac{\sigma_y\sigma_z}{\sigma_{y_0}\sigma_{z_0}}} + \sqrt{M_0}\right)}\right] \tag{2.58}$$

In order to deduce the values at the end of the potential core, first the value of the potential core deficit C_0 is estimated from Bernoulli's equation as $C_0 = 1 - \sqrt{1 - C_T}$. This deficit is assumed constant in the potential core up to x_0, the end or the potential core region. From a stream-wise momentum balance between the rotor and x_0 one can find the following expression for σ_{z_0} and σ_{y_0}:

$$\frac{\sigma_{z_0}}{D} = \frac{1}{2}\sqrt{\frac{u_R}{u_\infty + u_0}}, \qquad \frac{\sigma_{y_0}}{D} = \frac{\sigma_{z_0}}{D}\cos\gamma. \tag{2.59}$$

Where u_∞ is the unperturbed wind speed and $u_R = u_\infty \frac{C_T \cos\gamma}{2(1-\sqrt{1-C_T\cos\gamma})}$ is the speed at the rotor. Combining the above equations lead to an approximate value of $\frac{\sigma_{z_0}}{D} \approx 1/8$. Finally, the expressions for θ_{c_0} and x_0 are given as [9]:

$$\theta_{c_0} \approx \frac{0.3\gamma}{\cos\gamma}(1 - \sqrt{1 - C_T\cos\gamma}) \tag{2.60}$$

$$\frac{x_0}{D} = \frac{\cos\gamma(1 + \sqrt{1 - C_T})}{\sqrt{2}(4\alpha I + 2\beta(1 - \sqrt{1 - C_T}))} \tag{2.61}$$

where α and β are model parameters to be estimated and I is the ambient turbulence intensity. As the initial deflection angle θ_{c_0} is assumed constant throughout the potential core region, the initial deflection can be simply estimated as $\delta_0 = \theta_{c_0} x_0$. The authors propose values of $4\alpha = 2.32$ and $2\beta = 0.154$, obtaining good agreement with both experiment and numerical results [23], however more recent authors have proposed different values for the parameters [44].

Chapter 3

Computational Fluid Dynamics for Wind Turbines

Computational fluid dynamics (CFD) denotes a branch of fluid mechanics that uses numerical methods to solve the differential equations that govern fluid flow, commonly known as the Navier-Stokes (NS) equations. The field of research is comparatively recent, with earliest work performed at the beginning of the 20th century, and is benefiting greatly from the continued improvement of high-performance computers. The principle of CFD is the subdivision of the fluid of interest into discrete elements, either fixed or moving, and the solution of the discretized NS equations on these elements. The size of fluid phenomena that can be simulated using such an approach depends on the size of said elements, and consequently he number of elements employed in a given problem. Describing the fluid flow in all its details requires a very high number of elements, especially when large fluid domains are of interest. The number of elements is directly related to the computational effort required to solve the system of equations, also referred to as the computational cost. As the name implies, computational cost is indeed a cost, linked to electricity consumption and asset degradation but also to the time required to obtain the desired results.

The case of wind turbines proves to be particularly obnoxious when it comes to its treatment in CFD. Modern wind turbines stand as the largest aerodynamic machines ever built, requiring an enormous fluid domain to be resolved in order to capture their behavior. If the interaction between turbines in a wind farm is to be modeled, domains of several kilometers need to be resolved. At the same time, fluid phenomena that are essential to the behavior of the turbine, such as atmospheric boundary layer turbulence or flow around the airfoil profile of the blades, happen at sub-millimeter scales. Solving the NS equations directly (Direct Numerical Simulation (DNS) approach) for the case of wind turbines remains therefore prohibitively costly. However, approaches such as Reynolds-Averaged NS (RANS) or increasingly Large Eddy Simulations (LES) lower the required grid resolution, making the application of CFD to wind turbines feasible to study phenomena that a more classical BEM approach cannot capture.

This chapter is meant to deliver a brief introduction to the world of CFD, and to present the CFD software package used in the scope of this work, the LES solver YALES2. Much like the previous chapter

it may serve as reference for the work presented in the subsequent chapters, and is most certainly not intended to be comprehensive.

3.1 The Navier-Stokes Equations

As implied by their name, the NS equations were derived by pioneers of fluid mechanics Claude-Louis Navier and George Gabriel Stokes. The equations arise from the application of the second law of motion to fluids. One possible expression of the Navier-Stokes equations, completed with conservation equations for mass and energy, is the following [45]:

$$\frac{\partial \rho}{\partial t} + \nabla \cdot [\rho \boldsymbol{u}] = 0\,, \tag{3.1a}$$

$$\frac{\partial}{\partial t}[\rho \boldsymbol{u}] + \nabla \cdot [\rho \boldsymbol{u}\boldsymbol{u}] = -\nabla p + [\nabla \cdot \boldsymbol{\tau}] + \boldsymbol{f_b}\,, \tag{3.1b}$$

$$\frac{\partial}{\partial t}[\rho e] + \nabla \cdot [\rho \boldsymbol{u} e] = -\nabla \cdot \dot{q}_s - \nabla \cdot [p\boldsymbol{u}] + \nabla \cdot [\boldsymbol{\tau} \cdot \boldsymbol{u}] + \boldsymbol{f_b} \cdot \boldsymbol{u} + \dot{q}_v\,. \tag{3.1c}$$

Equation 3.1a expresses mass conservation in its conservative form, where $\boldsymbol{u}$ is the velocity vector (u, v, w) and ρ is the fluid density. Equation 3.1b expresses conservation of linear momentum, where $\boldsymbol{f}_b$ is a general body force acting on the fluid, p is the pressure and $\boldsymbol{\tau}$ is the viscous stress tensor. Finally, equation 3.1c expresses the conservation of energy as dictated by the first law of thermodynamics, written in terms of specific total energy e, where $\dot{q}_s$ is the rate heat flow across the surface and $\dot{q}_v$ is the rate of heat source or sink within the material volume.

No closed-form solution for the NS equations exists in the general case, therefore numerical methods are necessary to solve the system. The equations are also not closed, requiring a constituent law for the material to relate the stress tensor $\boldsymbol{\tau}$ to the flow variables. For a Newtonian fluid, the stress tensor is given by [45]:

$$\boldsymbol{\tau} = \mu \left[\nabla \boldsymbol{u} + (\nabla \boldsymbol{u})^T\right] + \lambda(\nabla \cdot \boldsymbol{u})\boldsymbol{I} \tag{3.2}$$

where μ is the molecular viscosity, λ is the bulk viscosity and $\boldsymbol{I}$ is the 3×3 identity matrix.

Significant simplifications can be made according to the physical quantities and terms that are significant for a given phenomenon. In the case of wind turbines, the temperature of the flow might ot have a significant influence on the flow, removing the need for equation 3.1c. Furthermore, variations of density are assumed to be negligible, justifying the assumption of incompressible flow [46], that leads to a a significant simplification of the continuity equation 3.1a, that becomes:

$$\nabla \cdot \boldsymbol{u} = 0 \tag{3.3a}$$

and to a simplification of the momentum equation 3.1b that for a Newtonian fluid becomes:

$$\frac{\partial \boldsymbol{u}}{\partial t} + \nabla \cdot [\boldsymbol{u}\boldsymbol{u}] = -\frac{1}{\rho}\nabla p + \nu \nabla^2 \boldsymbol{u} + \frac{\boldsymbol{f_b}}{\rho} \tag{3.3b}$$

where ν is the kinematic viscosity defined as $\nu = \mu/\rho$.

Attempting to discretize and the solve the NS equations directly is difficult, as this requires a grid resolution that is fine enough to resolve all scales of motion that carry significant energy [47]. This approach is called DNS (Direct Numerical Simulation) and is used in specific cases to study turbulence. However, in applications with large domains at high Reynolds numbers use of DNS becomes impossible because of the very wide range between the largest and smallest turbulent scales that cannot be explicitly simulated, even by the most powerful computers [8].

3.2 Reynolds-averaged Navier-Stokes (RANS)

When only a time-averaged solution of the flow field is of interest, such as is sometimes be the case in wind turbine wake studies, the Reynolds-averaged Navier-Stokes (RANS) equations can be used. The velocity and pressure field can be decomposed into a constant average term and a fluctuating term without force term yields:

$$\begin{aligned} \boldsymbol{u} &= \langle \boldsymbol{u} \rangle + \boldsymbol{u}' \\ p &= \langle p \rangle + p' \end{aligned} \tag{3.4}$$

Applying an averaging operation to the incompressible continuity and momentum equation for a Newtonian fluid 3.3a and 3.3b, neglecting additional body forces, yields [45]:

$$\nabla \cdot \langle \boldsymbol{u} \rangle = 0 \tag{3.5a}$$

$$\nabla \cdot [\langle \boldsymbol{u}\boldsymbol{u} \rangle] = -\frac{1}{\rho}\nabla \langle p \rangle + \nu \nabla^2 \langle \boldsymbol{u} \rangle \tag{3.5b}$$

The term $\langle \boldsymbol{u}\boldsymbol{u} \rangle$ is non-linear and can be decomposed using equation 3.4 into:

$$\langle \boldsymbol{u}\boldsymbol{u} \rangle = \langle \boldsymbol{u} \rangle \langle \boldsymbol{u} \rangle + \langle \boldsymbol{u'}\boldsymbol{u'} \rangle \tag{3.6}$$

This introduces a new set of 9 unknowns in the form of the tensor $-\langle \boldsymbol{u'}\boldsymbol{u'} \rangle$, often denominated Reynolds stress tensor $\langle \boldsymbol{\tau} \rangle$. Introducing equation 3.6 into equation 3.5b results in the following expression for the momentum balance in RANS:

$$\nabla \cdot [\langle \boldsymbol{u} \rangle \langle \boldsymbol{u} \rangle] = -\frac{1}{\rho}\nabla \langle p \rangle + \nu \nabla^2 \langle \boldsymbol{u} \rangle + \nabla \cdot \langle \boldsymbol{\tau} \rangle \tag{3.7}$$

The set of incompressible RANS equations is not closed, and additional equations are required to model the Reynolds stress tensor. These turbulence models, or *closure models*, represent a big question in modern CFD, and several approaches have been proposed.

3.2.1 The Boussinesq turbulent viscosity Hypothesis

Most turbulence models are based on the Boussinesq hypothesis, that states that the turbulent stress tensor, analogous to the Newtonian stress tensor, can be expressed as a linear function of the mean velocity gradients. For incompressible flow, the hypothesis is expressed as follows:

$$\langle \boldsymbol{\tau} \rangle = \mu_t \left[\nabla \langle \boldsymbol{u} \rangle + (\nabla \langle \boldsymbol{u} \rangle)^T \right] + \frac{2}{3} \rho k \boldsymbol{I} \tag{3.8}$$

Here μ_t takes the name of *turbulent eddy viscosity*, in analogy to molecular viscosity, and k is the turbulent kinetic energy defined as:

$$k = \frac{1}{2} \langle \boldsymbol{u'} \boldsymbol{u'} \rangle \tag{3.9}$$

Turbulence models based on the Boussinesq hypothesis focus on deriving expressions for the eddy viscosity μ_T. These models are often grouped into four main categories:

- Algebraic (zero-equation) models
- One-equation models
- Two-equation models
- Second-order closing models

One- and two-equations here refers to the number of additional transport equations that have to be solved. Notable turbulence models based on Boussinesq are the $k - \epsilon$ or the $k - \omega$ model, that are part of the two-equation-models.

An alternative to the use of the eddy viscosity concept is given by Reynolds stress equation models.

3.3 Large Eddy Simulations (LES)

Large Eddy Simulations (LES) positions itself between DNS and RANS. Large turbulent structures are numerically resolved, while sub-grid scale (SGS) turbulence is modeled statistically using approaches

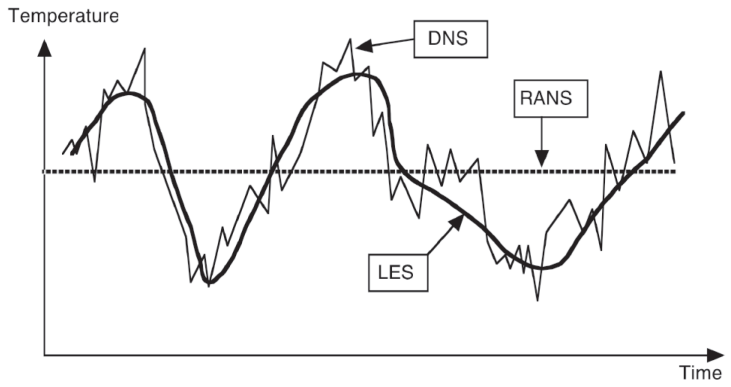

Figure 3.1: Schematic representation of the time evolution of physical quantities using LES, DNS and RANS approach (case of a statistically steady flow). [48].

similar to RANS, as schematically shown in figure 3.1. In order to discriminate between small and large scales, a spatial filter function is applied to the variables in the incompressible NS equations. For a scalar ϕ, the spatial filter is defined as follows [49]:

$$\overline{\phi}(\boldsymbol{x},t) = \int_{\mathbb{R}^3} \phi(\boldsymbol{y},t) G_\Delta(\boldsymbol{y}-\boldsymbol{x}) d\boldsymbol{y} \tag{3.10}$$

where $\overline{\phi}$ denotes the filtered quantity and G_Δ is a filtering kernel associated to the scale Δ. Due to its integral nature, the filtering operation is commutative with respect to summation and derivation. The filtered variable can be written as the sum of a function evolving at a scale larger than Δ, denoted as $\overline{\phi}$, and smaller than Δ, denoted as ϕ'':

$$\phi = \overline{\phi} + \phi'' \tag{3.11}$$

The analogy with the Reynolds-average decomposition in equation 3.4 is striking, however the term $\overline{\phi}$ is not constant in time. Furthermore, the mathematical properties of the filtering operation are quite distinct from the average, as it is not idempotent and for distribution over multiplication it holds that:

$$\overline{\boldsymbol{u}\boldsymbol{u}} = \overline{\overline{\boldsymbol{u}}\,\overline{\boldsymbol{u}}} + 2\overline{\boldsymbol{u}'\overline{\boldsymbol{u}}} + \overline{\boldsymbol{u}'\boldsymbol{u}'} \tag{3.12}$$

Applying the filter to the incompressible NS equations results in an expression analogous to the RANS equations, but with a transient term in the momentum equation:

$$\nabla \cdot \overline{\boldsymbol{u}} = 0 \tag{3.13a}$$

$$\frac{\partial \overline{\boldsymbol{u}}}{\partial t} + \nabla \cdot [\overline{\boldsymbol{u}\boldsymbol{u}}] = -\frac{1}{\rho}\nabla \overline{p} + \nu \nabla^2 \overline{\boldsymbol{u}} \tag{3.13b}$$

Again a non-linear term emerges, $\overline{\boldsymbol{u}\boldsymbol{u}}$. In order to separate an equation for the filtered variables, the following expansion of the non-linear term is used:

$$\overline{\boldsymbol{u}\boldsymbol{u}} = \overline{\boldsymbol{u}}\,\overline{\boldsymbol{u}} + \underbrace{\overline{\boldsymbol{u}\boldsymbol{u}} - \overline{\boldsymbol{u}}\,\overline{\boldsymbol{u}}}_{(1)} \tag{3.14}$$

The term (1) can be seen as a tensor that incorporates the effects of turbulent motion smaller than the filter scale Δ, denoted $\overline{\tau}$. This leads finally to a formulation of the LES momentum balance that is analogous to equation 3.7:

$$\frac{\partial \overline{\boldsymbol{u}}}{\partial t} + \nabla \cdot [\overline{\boldsymbol{u}}\,\overline{\boldsymbol{u}}] = -\frac{1}{\rho}\nabla \overline{p} + \nu \nabla^2 \overline{\boldsymbol{u}} + \nabla \cdot \overline{\boldsymbol{\tau}} \tag{3.15}$$

The use of an LES formulation rather than a RANS formulation for modeling turbulent flows brings two major advantages. Most importantly, the presence of the transient term allows for the simulation of transient phenomena and time the evolution of parameters. This allows for example to observe the helical vortex structures in the wake of a rotating turbine. A second advantage lies in the treatment of turbulence. Since large-scale turbulent motions are numerically resolved, the Reynolds stress tensor only

needs to account for small-scale turbulence, notably the sub-grid scale on a discretized domain. Small-scale turbulence lends itself much better to statistical treatment, since it is generally more isotropic. Therefore, it may be possible to characterize it with simpler models than what is used in RANS without committing large errors. Turbulence closure models for LES are usually algebraic, such as the Smagorinsky or Dynamic Smagorinsky models. A relatively recent model for SGS turbulence is the SIGMA model proposed by Nicoud et al. (2011) [50]. Nonetheless, LES simulations remain computationally much more expensive than RANS simulations, and their application in industrial contexts remains relatively rare.

3.4 Actuator Line Modeling

The treatment of Wind Turbines in CFD has long been supposed to be computationally too expensive due to the large range of scales involved. Indeed, as the scales of interest reach from fractions of a millimeter for the smallest turbulent eddies up to several kilometers of spacing between turbines, the application of a DNS approach will remain impossible for years to come. In addition, meshing the geometry of the moving turbine requires dynamic re-meshing, increasing the, computational complexity further. This can be circumvented by solving the equations in a rotating frame of reference, which in turn makes it impossible to model the static parts of the turbine, in particular tower effects. Due to these difficulties, CFD is still a long way from replacing engineering models like BEM (cf. section 2.1) in wind turbine design. However, over the years CFD has been employed successfully in restricted domains and as quasi-analytical solution for the verification of engineering models for turbine aerodynamics or wakes [8, 51, 10].

In most CFD applications to wind turbines, simplified models for the rotor are employed in order to circumvent the need for meshing the geometry. These approaches include actuator disk models (ADM) where the rotor is treated as a permeable disk exerting a body force on the flow and actuator line models (ALM), where the rotating blades are modeled as lines of point forces that act on the fluid. The actuator disk approach is used in RANS models, as they are steady in nature and can therefore not model blade movement. The actuator line approach has first been proposed in 2002 by Sørensen and Shen [51]. The magnitude of the point forces in an ALM model can either be prescribed directly directly for a given case by running an BEM simulation and extracting the forces or computed from lift and drag characteristics and the local flow velocity determined during the simulation. These point forces are applied to the flow by spreading them over the closest grid points through a mollification kernel that transforms a point force into a distributed volume force, as described by figure 3.2. The forcing term enters into the NS momentum equation that is solved on the grid points, mimicking the effect of the turbine blade on the flow without the need to mesh the blades themselves or resolve the airfoil boundary layer. The ALM can only be employed in LES, as it requires the dynamic treatment of the motion of the blade. ALM studies allow to study unsteady effects such as the helical vortex structure behind a blade, as shown in figure 3.3. The approach was designed to study wind turbine wakes, but good results for local bending moments and output power have been obtained using the model [51, 10].

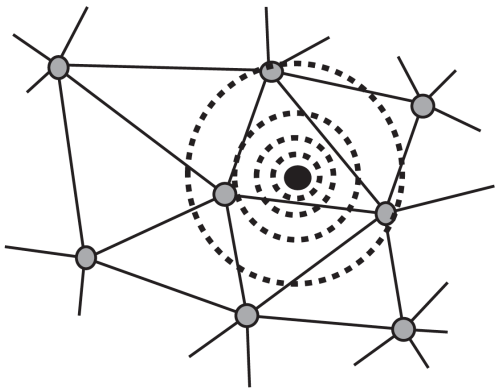

Figure 3.2: Mollification of a point force on an unstructured grid [10].

In general, the main purpose of the development of LES models for wind turbines is the study of wakes [51]. While BEM models (section 2.1) with unsteady corrections continue to prove effective for rotor aerodynamics, and vortex-based tools such as panel-method codes with even higher precision might enter the market soon, neither of them allow for a precise modeling of the wake of the turbine at large downstream distances. Engineering models such as the ones presented in sections 2.2 to 2.3 are being proposed and refined, however a clear standard on the treatment of wakes has yet to be established in the industry. The IEC61400 standard for wind turbines proposes several alternative ways of dealing with wakes, including not dealing with them at all [4]. LES models could become a standard tool for wakes if great progress is made on high-performance computation, but so far they remain too expensive to use extensively. What is however already feasible the use of LES model based on the AD or AL framework in the verification of lower-order wake models, a practice that is common among researchers [9, 35, 8].

3.5 YALES2: A Massively Parallel Low-Mach Number CFD Library

In the course of the present master thesis, LES computations for wind turbines with an ALM approach have been performed using the massively parallel multi-scale multi-physics low-Mach CFD simulation library YALES2. The software package was developed originally 2003 by V. Moureau and is maintained principally by the CORIA laboratory under the supervision of V. Moureau, G. Lartigue and P. Bénard [7, 10].

The code is designed for efficient parallelization on large computation clusters and uses a double-domain decomposition to create an even distribution of the work load on all processors while minimizing intra-processor communication [7]. While originally designed for combustion problems, the library now encompasses solvers for incompressible, variable density, and compressible flows, chemical reactions, heat transfer, sprays, granular flow and more [52]. The code is able to auto-generate structured grids but accepts unstructured grids generated by external mesh generators. Furthermore, it is capable of automatic mesh refinement for any given mesh, as well as dynamic mesh adaptation during execution [53].

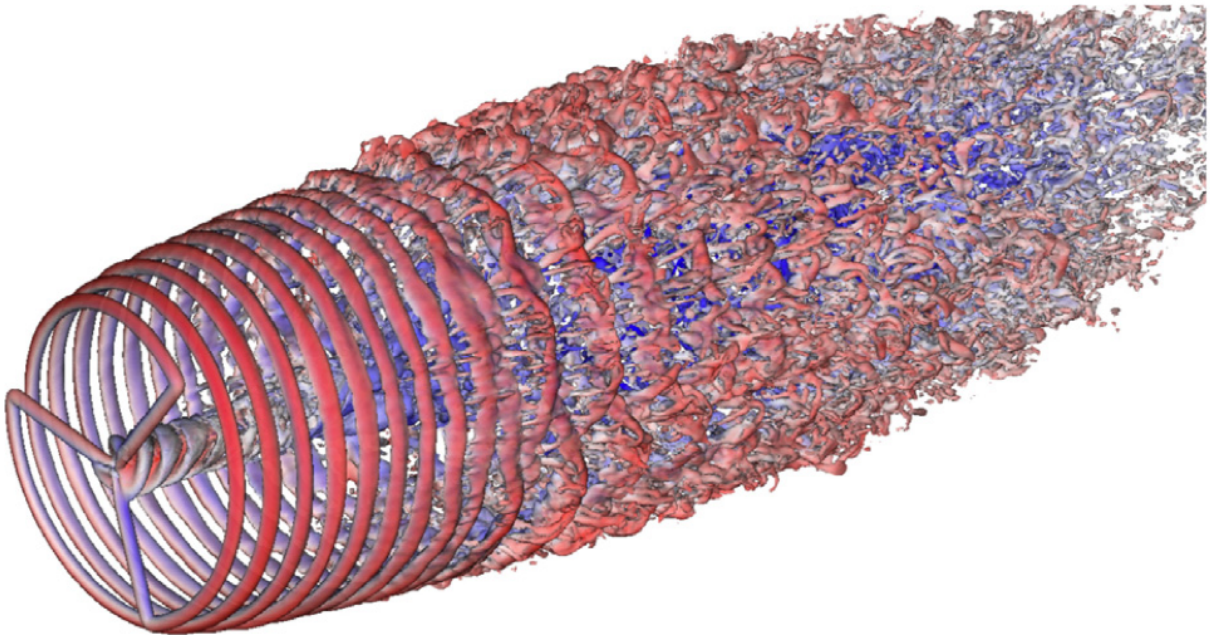

Figure 3.3: Iso-vorticity surface at TSR = λ = 7.07 using an ALM approach [10]. The results show helical tip vortices being generated, expanding, destabilizing as the vortices start to mutually interact and finally collapsing, causing a fully turbulent wake farther downstream.

For spatial integration of momentum, the library uses 2nd- or 4th-order central finite volume schemes, while time integration is performed using either a Runge-Kutta (RK) scheme (up to 4 steps), or a novel TFV4A scheme, that constitutes a blend between RK and the Taylor–Galerkin finite element scheme (TTG4A, [54]). Finally, several linear solvers for solving the generic system $A\boldsymbol{x} = \boldsymbol{b}$ are available in the library, and the Deflated Preconditioned Conjugate Gradient (DPCG) solver is used in the context of this work.

Recently, tools for simulating wind turbines using an ALM approach have been added to YALES2. The implementation is able to handle both direct force inputs and lift-and drag characteristics [10]. Results of the model are shown in figure 3.3, where an iso-vorticity profile unveils helical structures of the wake flow field that destabilize after a few turbine diameters to yield a fully turbulent flow. Simulations have been performed with and without inclusion of tower and ground effect, and without upstream turbulence injection. The researchers comment that a future addition of dynamic mesh adaptation, a feature already available in the code, could lead to improved results at a lower computational cost.

Chapter 4

Implementation of a Wake Modeling Tool Based on the Dynamic Wake Meandering Model

In the following chapter, the implementation a wake modeling tool for wind farms based on the dynamic wake meandering model developed at DTU [29] is described. The work has been carried out at Siemens Gamesa Renewable Energy (SGRE), and part of the pre-existing code base from the industrial partner has been used in the implemented tool after verification. This includes notably the Ainslie wake deficit model.

The model is implemented as described in annex E.2 *Dynamic Wake Meandering* of the international standard IEC61400-1 ED4 (2018) [4]. This approach to wake modeling was first proposed by Larsen et al. in 2007 [31] and later refined and calibrated by Madsen et al. in 2010 [5]. It encompasses models for the three phenomena observed in wind turbine wakes introduced in sections 2.2 to 2.4, using a refined Ainslie model for the velocity deficit (section 2.2.4), a dynamic model based on a passive tracer assumption for wake meandering (section 2.3.2) and a model for added turbulence that complements the apparent turbulence from meandering (section 2.4.2).

The modeling tool described in this chapter is intended to be integrated into the SGRE code environment, notably relying on free stream turbulence data provided by a turbulence generator and creating input files for the aero-servo-elastic simulation tool BHawC that was introduced in section 2.1.7.

In conceptual order, the chapter will first describe the implementation of the velocity deficit model for the wake of a single, unperturbed (rank one) turbine. Then it will go over how the deficit result is used to compute the added turbulence inside the steady wake. Subsequently, it describes how a meandering time series for the wake is obtained from a given ambient turbulent velocity field. Finally it explains how these results are used to dto compute the wind conditions at wake-impacted turbines based on a given wind farm layout and wind direction. This allows to calculate in turn the wakes wakes of these turbines, and their impact on the third rank. The process can be repeated up to the last turbine rank, adding the

effects of multiple wakes. The interface between the wake model and the aero-servo-elastic simulation software BHawC is described before concluding with a brief overview over the capabilities and limitations of the model.

The development results in a wake modeling tool able to generate turbulent, sheared inflow containing the effects of multiple meandering wakes for every turbine in a given park layout, at any given wind condition.

4.1 Wake Deficit

In order to compute the velocity deficit in a steady wake, a model based on the thin-shear-layer NS equations is used [31]. The model is based on the work of Ainslie [30] presented in section 2.2.4, and parametrized as prescribed by the IEC61400 standard [4]. A pre-existing implementation of the wake model by Krumm, H. [55] was taken as the basis of this work.

4.1.1 Governing Equations

We recall the rotationally symmetric thin-shear-layer approximation of the Navier-Stokes equations in their simplified form using an eddy-viscosity ν_e to model turbulence [31]

$$\frac{\partial U}{\partial x} + \frac{1}{r}\frac{\partial}{\partial r}(rV) = 0 \tag{4.1a}$$

$$U\frac{\partial U}{\partial x} + V\frac{\partial U}{\partial r} = \frac{\nu_e}{r}\frac{\partial}{\partial r}\left(r\frac{\partial U}{\partial r}\right) \tag{4.1b}$$

where U and V describe the axial and radial velocities while x and r describe the axial and radial coordinate centered at the rotor hub. In this implementation it was chosen to non-dimensionalize equations 4.1a and 4.1b using the dimensionless quantities $\tilde{U} = U/U_0$, $\tilde{V} = U/U_0$, $\tilde{x} = 2x/D$ and $\tilde{r} = 2r/D$. The substitution is straightforward and leads to the following expressions:

$$\frac{\partial \tilde{U}}{\partial \tilde{x}} + \frac{1}{\tilde{r}}\frac{\partial}{\partial \tilde{r}}(\tilde{r}\tilde{V}) = 0 \tag{4.2a}$$

$$\tilde{U}\frac{\partial \tilde{U}}{\partial \tilde{x}} + \tilde{V}\frac{\partial \tilde{U}}{\partial \tilde{r}} = \frac{2\nu_e}{DU_0}\frac{1}{\tilde{r}}\frac{\partial}{\partial \tilde{r}}\left(\tilde{r}\frac{\partial \tilde{U}}{\partial \tilde{r}}\right) \tag{4.2b}$$

The non-dimensional eddy viscosity $\tilde{\nu_e} = \frac{2\nu_e}{DU_0}$ is assumed to be a direct function of the wake deficit, ambient turbulence intensity and downstream distance to the turbine according to empirical relations taken from the standard [4]:

$$\tilde{\nu_e} = 0.023F_1(I_{amb})^{0.3} + 0.016F_2\frac{b}{D}\left(1 - \frac{U_{min}}{U_0}\right) \tag{4.3}$$

where I_{amb} is the incoming ambient turbulence intensity, U_{min} is the minimum velocity in the wake and b is the wake radius, defined in this case as the radial position at which the velocity value U attains

99.99% of the incoming wind speed U_0. The filter functions F_1 and F_2 are function of the non-dimensional downstream distance $\tilde{x}$ and are defined as follows:

$$F_1 = \begin{cases} \left(\frac{\tilde{x}}{8}\right)^{\frac{3}{2}} - \frac{\sin\left(2\pi(\tilde{x}/8)^{\frac{3}{2}}\right)}{2\pi} & \text{if } \tilde{x} \leq 8 \\ 1 & \text{if } \tilde{x} > 8 \end{cases} \tag{4.4a}$$

$$F_2 = \begin{cases} 0.0625 & \text{if } \tilde{x} \leq 4 \\ 0.025\tilde{x} - 0.0375 & \text{if } 4 \leq \tilde{x} < 12 \\ 0.00105(\tilde{x} - 12)^3 + 0.025\tilde{x} - 0.0375 & \text{if } 12 \leq \tilde{x} < 20 \\ 1 & \text{if } \tilde{x} > 20 \end{cases} \tag{4.4b}$$

4.1.2 Numerical Solution Method

In order to solve the equation system, the governing equations are discretized on a two-dimensional Cartesian grid and numerically solved at the nodes of the grid. A 4th order central finite difference scheme is used to approximate the radial derivatives $\partial/\partial r$ and $\partial^2/\partial r^2$, while a first order backward differences scheme is used for axial derivatives $\partial/\partial x$. The use of backwards differences makes it possible to propagate the solution explicitly along the axial direction, since only data from upstream points is used in the scheme. The stencil of the numerical scheme is shown schematically in figure 4.1.

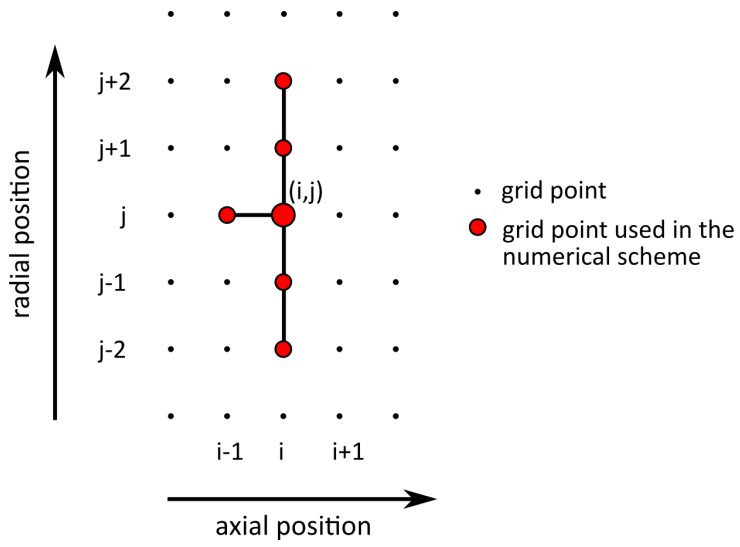

Figure 4.1: Points involved in the discretization of the continuity and momentum equation at the point (i, j)

Using a nomenclature where i denotes the discretized axial position and j the discretized radial position, the 4th order finite difference scheme for radial derivatives for a generic function ϕ, $\partial\phi/\partial r$ and $\partial^2\phi/\partial r^2$, on an arbitrarily spaced grid read as follows [56]:

$$\frac{\partial \phi^j}{\partial r} = \frac{\frac{1}{12}\phi^{j-2} - \frac{1}{12}\phi^{j+2} + \frac{2}{3}\phi^{j+1} - \frac{2}{3}\phi^{j-1}}{\frac{1}{2}(r^{j+1} - r^{j-1})} \tag{4.5a}$$

$$\frac{\partial^2 \phi^j}{\partial r^2} = \frac{\frac{4}{3}\phi^{j-1} + \frac{4}{3}\phi^{j+1} - \frac{5}{2}\phi^j - \frac{1}{12}\phi^{j+2} - \frac{1}{12}\phi^{j-2}}{\frac{1}{4}(r^{j+1} - r^{j-1})^2} \tag{4.5b}$$

while the first-order upwind scheme for the derivative $\partial\phi/\partial x$ reads:

$$\frac{\partial \phi^i}{\partial x} = \frac{\phi^i - \phi^{i-1}}{\Delta x} \tag{4.5c}$$

Inserting these finite difference equations into the momentum and continuity equations 4.2b and 4.2a yields a system that can be solved numerically if values at all points of the stencil are defined. The following process is applied for each axial position i:

- A first guess for $\tilde{U}$ at all radial points is made, initializing all values to the values at the previous upstream positions $i-1$.

- Values for $\tilde{V}$ are obtained by integrating equation 4.2a numerically. The analytical expression of the integral reads as follows:

$$\tilde{V}(\tilde{r}) = -\frac{1}{\tilde{r}} \int_0^{\tilde{r}} \frac{\partial \tilde{U}}{\partial \tilde{x}} \tilde{r} d\tilde{r} \tag{4.6}$$

  Using equation 4.5c for the derivative and a piecewise linear numerical quadrature scheme, the integral can be approximated by the expression:

$$\tilde{V}^{(i,j)} = \frac{1}{\tilde{r}^j} \sum_{k=1}^{j} \frac{\tilde{r}^k(\tilde{U}^{(i,k)} - \tilde{U}^{(i-1,k)}) + \tilde{r}^{k-1}(\tilde{U}^{(i,k-1)} - \tilde{U}^{(i-1,k-1)})}{2\Delta\tilde{x}} \Delta\tilde{r} \tag{4.7}$$

- Using the available data for $\tilde{V}$ and $\tilde{U}$, an estimate for all terms of the discretized momentum equation is known. As the terms will not perfectly sum up to 0, a momentum flow deficit ΔQ_p is obtained:

$$\begin{aligned}
\Delta Q_p^{(i,j)} = {} & \tilde{U}^{(i,j)} \frac{\tilde{U}^{(i,j)} - \tilde{U}^{(i-1,j)}}{\Delta\tilde{x}} + \tilde{V}^{(i,j)} \frac{\frac{1}{12}\tilde{U}^{(i,j-2)} - \frac{1}{12}\tilde{U}^{(i,j+2)} + \frac{2}{3}\tilde{U}^{(i,j+1)} - \frac{2}{3}\tilde{U}^{(i,j-1)}}{\frac{1}{2}(\tilde{r}^{j+1} - \tilde{r}^{j-1})} \\
& - \frac{\tilde{\nu_e}^i}{\tilde{r}^i} \left(\frac{\frac{1}{12}\tilde{U}^{(i,j-2)} - \frac{1}{12}\tilde{U}^{(i,j+2)} + \frac{2}{3}\tilde{U}^{(i,j+1)} - \frac{2}{3}\tilde{U}^{(i,j-1)}}{\frac{1}{2}(\tilde{r}^{j+1} - \tilde{r}^{j-1})} \right. \\
& \left. + \tilde{r}^j \frac{\frac{4}{3}\tilde{U}^{(i,j-1)} + \frac{4}{3}\tilde{U}^{(i,j+1)} - \frac{5}{2}\tilde{U}^{(i,j)} - \frac{1}{12}\tilde{U}^{(i,j+2)} - \frac{1}{12}\tilde{U}^{(i,j-2)}}{\frac{1}{4}(\tilde{r}^{j+1} - \tilde{r}^{j-1})^2} \right)
\end{aligned} \tag{4.8}$$

- By multiplying the equation 4.8 by $\Delta x/U^{(\tilde{i},j)}$, we obtain a term $\tilde{U}^{(i,j)} - \tilde{U}^{(i-1,j)}$ that we denote q, the velocity correction. All other terms of the equation are only function of values at the current axial position i. We can therefore seek a value q that, when inserted in the equation, yields a momentum deficit $\Delta Q = \Delta Q_p \Delta x/\tilde{U}$ equal and opposite in sign to the deficit found by equation 4.8. A value q at each radial point is therefore sought such that:

$$-Jq = \Delta Q \tag{4.9}$$

where the matrix J is a square matrix describing along the diagonal how a velocity perturbation q around $\tilde{U}$ would affect the momentum balance at the point, considering all influencing neighboring point. The goal is to find for each point a velocity modification that would cause the observed momentum deficit $\Delta Q = \Delta Q_p \frac{\Delta x}{\tilde{U}}$ and correct the velocity estimate accordingly. The matrix elements of J are therefore defined as follows:

$$
\begin{aligned}
J(j,j-2) &= -\frac{1}{12}\frac{\Delta\tilde{x}}{\tilde{U}_j}\frac{\tilde{\nu_e}}{\tilde{r}_j\Delta\tilde{r}} - \frac{1}{12}\frac{\Delta\tilde{x}}{\tilde{U}_j}\frac{\tilde{\nu_e}}{\Delta\tilde{r}^2} - \frac{1}{12}\frac{\Delta\tilde{x}}{\tilde{U}_j}\frac{\tilde{V}(\tilde{r})}{\Delta\tilde{r}} \\
J(j,j-1) &= \frac{2}{3}\frac{\Delta\tilde{x}}{\tilde{U}_j}\frac{\tilde{\nu_e}}{\tilde{r}_j\Delta\tilde{r}} + \frac{4}{3}\frac{\Delta\tilde{x}}{\tilde{U}_j}\frac{\tilde{\nu_e}}{\Delta\tilde{r}^2} - \frac{2}{3}\frac{\Delta\tilde{x}}{\tilde{U}_j}\frac{\tilde{V}(\tilde{r})}{\Delta\tilde{r}} \\
J(j,j) &= -\frac{\Delta\tilde{x}}{\tilde{U}_j^2}\frac{\tilde{\nu_e}}{\tilde{r}_j}\frac{\partial\tilde{U}}{\partial\tilde{r}} - \frac{\Delta\tilde{x}}{\tilde{U}_j^2}\tilde{\nu_e}\frac{\partial^2\tilde{U}}{\partial\tilde{r}^2} + \frac{\Delta\tilde{x}}{\tilde{U}_j}\frac{\partial\tilde{U}}{\partial\tilde{r}}\tilde{V}(\tilde{r}) + \frac{\Delta\tilde{r}}{2\tilde{U}_j}\frac{\partial\tilde{U}}{\partial\tilde{r}} - 1 \\
J(j,j+1) &= -\frac{2}{3}\frac{\Delta\tilde{x}}{\tilde{U}_j}\frac{\tilde{\nu_e}}{\tilde{r}_j\Delta\tilde{r}} + \frac{4}{3}\frac{\Delta\tilde{x}}{\tilde{U}_j}\frac{\tilde{\nu_e}}{\Delta\tilde{r}^2} + \frac{2}{3}\frac{\Delta\tilde{x}}{\tilde{U}_j}\frac{\tilde{V}(\tilde{r})}{\Delta\tilde{r}} \\
J(j,j+2) &= \frac{1}{12}\frac{\Delta\tilde{x}}{\tilde{U}_j}\frac{\tilde{\nu_e}}{\tilde{r}_j\Delta\tilde{r}} - \frac{1}{12}\frac{\Delta\tilde{x}}{\tilde{U}_j}\frac{\tilde{\nu_e}}{\Delta\tilde{r}^2} + \frac{1}{12}\frac{\Delta\tilde{x}}{\tilde{U}_j}\frac{\tilde{V}(\tilde{r})}{\Delta\tilde{r}}
\end{aligned}
\tag{4.10}
$$

- Using q, a new guess for the axial velocity at position i is computed using:

$$\tilde{U}^i_{n+1} = \tilde{U}^i_n + q \tag{4.11}$$

- The process is iterated until a convergence criterion is reached. The implemented criterion on the velocity correction q is set to $\max(q) < 10^{-3}$. This is considered a good balance between precision and speed, and later chapters will show that the criterion is sufficient to guarantee mass and momentum conservation to a reasonable extent. The convergence of the iteration process is rapid, both for points in the immediate near wake and in the far wake, as shown in figure 4.2. Intuitively, convergence takes more steps in the near wake as gradients involved are high and the solution evolves more rapidly, however this difference is only of a single iteration.

This procedure is performed up to the user-specified downstream distance, and the entire 2D velocity data is stored in a data structure. This is not optimal for performance, but has the advantage that the result can be re-used for all cases up to the maximum distance. The code is therefore in practice only run once for each velocity U_0 with available BEM data and for a range of turbulence intensities I. From this result, a Matlab linear interpolation object is created, that is able to interpolate the wake deficit at any location, for any wind speed and at any turbulence intensity in a fraction of the time it would take to execute the numerical model. While the model computes the wake field up to 20 diameters downstream in a few seconds, the interpolation of the pre-computed wake deficit is almost immediate. The interpolation object can further more be stored and later loaded, allowing the numerical solver for the boundary layer equations to be run only once for a given turbine type.

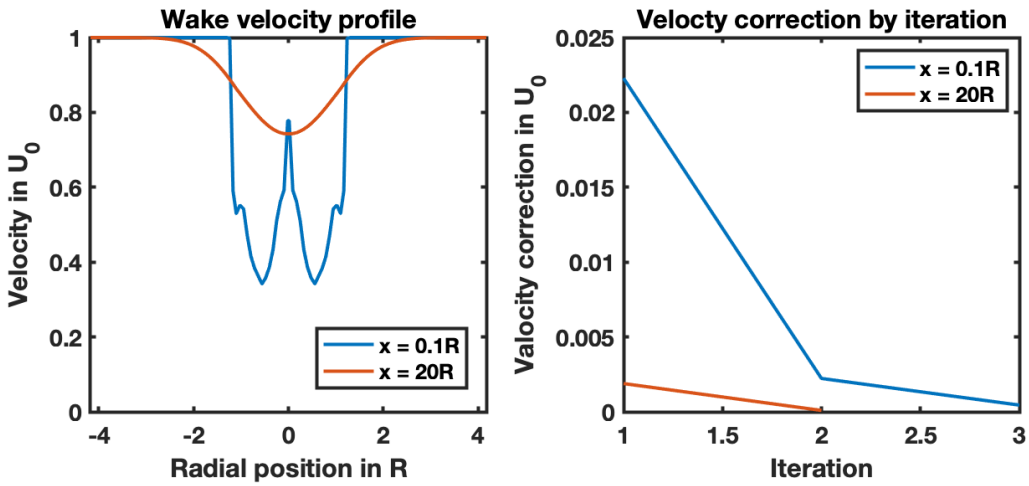

Figure 4.2: Velocity profile and convergence of the numerical scheme for an axial slice in the immediate near wake and one in the far wake.

4.1.3 Boundary Conditions

In order to close the differential equation system, boundary conditions must be provided at the limits of the domain. Velocity at the inlet is prescribed based on the local induction factor $a(r)$ of the rotor, pre-calculated by a BEM model as described in section 2.1 for a range of velocities. Since the employed Ainslie-type deficit model neglects the pressure term in the NS equations, it cannot simulate the wake expansion in the near wake characterized by pressure equilibration. The approach used instead is to assume that the velocity reaches the far-wake value predicted by momentum theory (section 2.1.1), $U = U_0(1-2a)$, immediately after the rotor. While this is not exact, the distance from the rotor to where the air velocity reaches this minimum is typically assumed to be small (order of 1 diameter) [9], and the assumption is used in several wake models [31, 21, 9]. In addition, errors introduced by this assumption are supposedly mitigated by the definition of the eddy viscosity in the near-wake though the functions shown in equation 4.4a and 4.4b. Madsen et al. are able to get good agreement with experimental data for downstream distances larger than 3 turbine diameters and at moderate ambient turbulence [5].

The boundary conditions at the inlet of the domain are hence defined as a prescribed velocity (Dirichlet boundary condition) for U, with the following prescribed values:

$$\tilde{U}^{(1,j)} = \begin{cases} 1 & \text{if } \tilde{r}^j > \tilde{r}_w \\ 1-2a(\tilde{r}_0^j) & \text{if } \tilde{r}^j \leq \tilde{r}_w \end{cases} \tag{4.12}$$

where $a(r_0^j)$ is the local induction factor at the blade section with radius r_0^j corresponding to the non-expanded radial position from BEM data. As mass continuity requires a wake expansion to reduce de velocity from $(1-a)$ to $(1-2a)$, the radial positions r_0^j are expanded to take this into account. The following formulation is used to obtain the expanded radial positions r^j at which to apply the induction calculated by the BEM model for the radial position r_0^j:

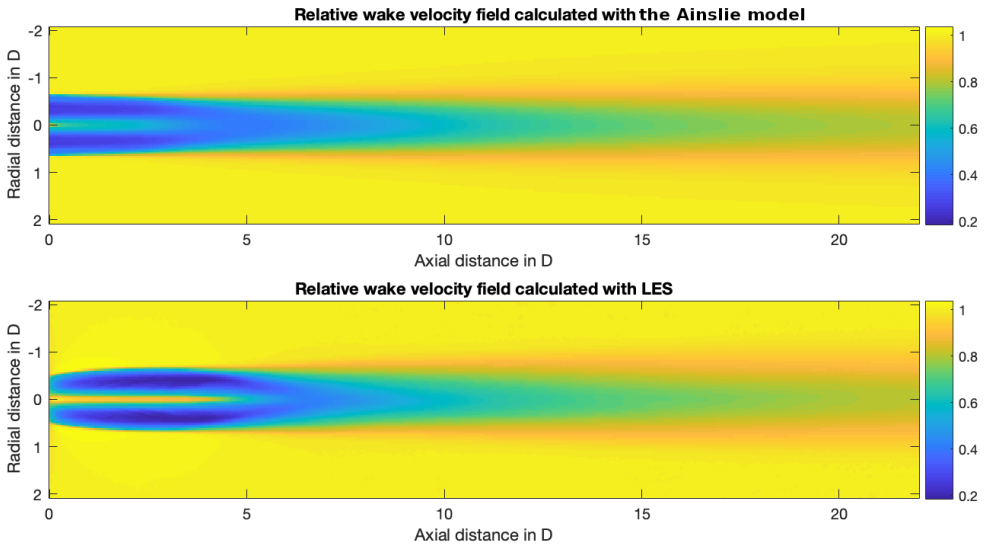

Figure 4.3: Comparison of the wake velocity field calculated using the DWM wake deficit model and LES, showing the difference in wake shape in the immediate near wake region.

$$
\begin{aligned}
r^1 &= r_0^1 \\
\tilde{r}^{j+1} &= (1 - 0.45\langle a \rangle^2)\sqrt{\frac{1-a_i}{1-2a_i}\left((\tilde{r}_0^{j+1})^2 - (\tilde{r}_0^{j})^2\right) + (\tilde{r}^{j})^2}
\end{aligned}
\tag{4.13}
$$

where $\langle a \rangle$ denotes the mean induction across the rotor. The assumption of immediate wake expansion leads to a non-physical wake shape in the immediate near wake, as the real wake slows down and expands gradually. This can be clearly seen in a comparison with LES results as shown in figure 4.3. Details of the LES simulation are given in chapter 5.

The remaining boundary conditions are chosen in order to simplify the implementation of the chosen numerical scheme. For the radial boundary far from the rotor, a Dirichlet condition is used, fixing the velocity to the unperturbed wind speed U_0. This choice is expected to introduce small errors as it adds momentum to the wake as soon as the expanding wake meets the boundary. These confinement effects can however be limited if the domain is chosen sufficiently large. A domain of 4 diameters from the rotor center was chosen and the choice is confirmed in chapter 5. The radial boundary at the rotor axis in an axisymmetric model should be chosen as a Neumann boundary conditions, imposing zero gradient normal to the wall, however another solution was adopted to simplify the implementation: The entire domain is mirrored, and a Dirichlet condition is imposed again far from the rotor, eliminating the need to implement gradient boundary conditions. The choice comes at a computational cost, however the symmetry of the domain can be used when creating the solution matrix J (equation 4.10), resulting in a time loss much lower than factor 2. This trade off was considered acceptable, as the total execution time of the model remains relatively short. As described in the closing words of section 4.1.2, during use the deficits calculation procedure is more often than not substituted by a linear interpolation of pre-calculated results, reducing the impact of this choice further.

In the long run, especially if the model is expected to see increased use, a re-implementation of the

numerical solution system is proposed, using a more efficient programming language, a finite volume approach to guarantee conservation of mass and momentum and the implementation of more efficient and physically more accurate boundary conditions.

4.2 Added Wake Turbulence

Added turbulence, as seen by a stationary observer in the wake of a turbine, is composed of velocity fluctuation due to wake meandering and increased velocity fluctuation inside the wake. As the presented simulation tool models wake meandering explicitly in time, the added wake model has to yield only the added turbulence that an observer "in the meandering frame of reference" would see [39]. The added wake turbulence model described in 2.4.2 is therefore used, as recommended in the standard [4]. This model proposes to compute added turbulent velocity components in the meandering frame of reference by scaling a uniform velocity field with standard deviation $\sigma = 1m/s$ locally by an empirical scale factor that is derived from the results of the deficit model. As was the case for the wake deficit, the velocity scale factor is only calculated once for each turbine type, and stored in an Matlab interpolation object together with the wake velocity deficit.

In the implementation, a field of turbulence data with mean 0 is loaded from a library of turbulence data generated according to a Mann-spectrum, and all 3 turbulent velocity components are scaled to obtain $\sigma_{x,y,z} = 1$. At every data point of this loaded turbulent field, the velocity scale factor k_{wt} is calculated according to equation 2.48, taking into consideration the meandering offset of the wake with respect to the centerline of the field. The locally scaled turbulent velocity field is then added component by component to the ambient turbulence field, as suggested by equation 2.49. Assuming the two turbulence fields have are statistically independent and have mean value zero, this results in a new turbulence field with variance equal to the sum of the variances of the original variables. The result is hence guaranteed to have increased turbulence intensity.

4.3 Wake Meandering

A meandering model based the DTU model presented in section 2.3.2 is implemented, and a time series for the wake position at a given downstream distance is computed. As described in the theory section, the time series is extracted from a turbulent velocity field by means of a low-pass filter with cut-off frequency $U_0/2D$. The turbulence data is taken from *turbulence boxes*, pre-generated files that contain 3-dimensional Mann spectrum turbulence.

The lateral and vertical velocity components of the turbulence at the center of a turbulent box are extracted. This spatial signal is then filtered using an order 1 digital IIR filter at a cut-of frequency equal to $U_0/2D$. The filter can be mathematically expressed as follows [57]:

$$\hat{v}_k = \alpha_f \hat{v}_{k-1} + (1 - \alpha_f) v_k \tag{4.14}$$

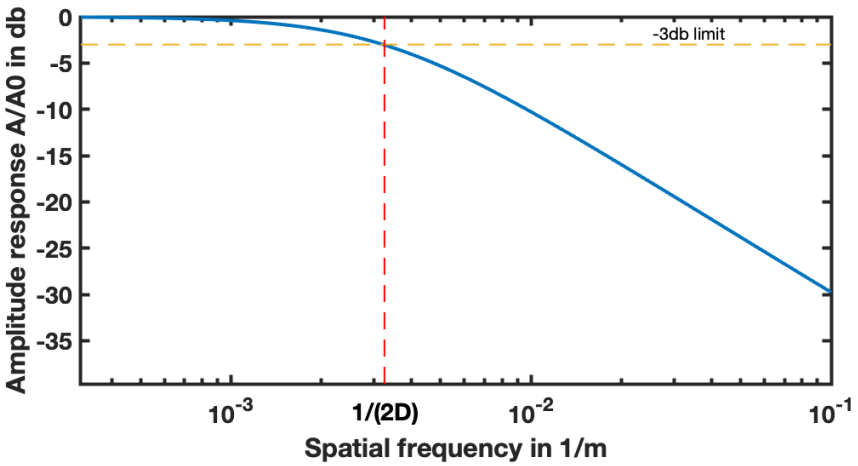

Figure 4.4: Frequency response of the 1st order IIR filter used to obtain the meandering time series. The cut-off frequency $1/(2D)$ and the -3 decibel level are pointed out.

where $\hat{v}_k$ is the filtered velocity at the discrete sampling point k, and α_f is the filter constant that defines the cut-off frequency. The following link can be drawn between this digital filter constant and the digital cut-off frequency f_c [57]:

$$f_c = \frac{-f_s \log(\alpha_f)}{2\pi} \tag{4.15}$$

where f_s is the digital sampling frequency. In a frozen turbulence hypothesis, a temporal turbulence signal and filter can be transformed into a spatial one and vice versa, considering frozen convection at mean wind speed. This allows to streamline the implementation, filtering the spatial series extracted from the box directly. The desired filter frequency in space becomes $f_{c*} = 1/2D$, and the link between filter constant and cut-off frequency reads as:

$$f_c^* = \frac{-\frac{1}{\Delta x} \log(\alpha_f)}{2\pi} \tag{4.16}$$

Where Δx is the sampling distance in longitudinal direction. From equation 4.16 one can obtain an expression for α_f to obtain the desired cut-off:

$$\alpha_f = \frac{1}{1 + \frac{\pi \Delta x}{D}} \tag{4.17}$$

The frequency response together with the spatial cut-off frequency and the -3 decibel threshold (expected gain for a 1st order filter at the cut-off) is shown in figure 4.4.

The filtered velocity signal is multiplied with the time to reach the downstream distance of interest x as suggested by equation 2.39. Convection of the wake at the ambient wind speed U_0 is assumed to obtain this time, leading to the expression:

$$\delta_{y,z}(t) = \hat{v}_{y,z}(t) \frac{x}{U_0} \tag{4.18}$$

where δ_y and δ_z are the meandering offset in lateral and vertical direction of the wake emitted at the rotor at time t when it reaches the downstream position x.

The assumptions taken in the meandering model are questionable. The constant lateral velocity might lead to an overestimation of the meandering offsets for large distances, as the function linearly diverges. Another strong assumption is uniform advection of the wake, as the wind shear across large rotors leads to substantial differences in the unperturbed wind speed between at the top and the bottom of the wake. In addition, research has concluded that the entire wake is advected at a lower speed than the unperturbed ambient wind speed [58]. In recent research, De Maré [35] derives an improved dynamic model for wakes that could be integrated easily into the modular structure of the implemented modeling tool.

4.4 Higher Ranked Turbines and Wake Superposition

While the treatment of rank 1 turbines is prescribed precisely in the IEC61400 standard [4], instructions on the treatment of higher-rank turbines impacted by one or several wakes is not as clear. The wake models take as an input only two scalar parameters: the mean ambient velocity and the mean ambient turbulence intensity. In order to treat higher-rank turbines it is therefore necessary to break the effects of all incoming wakes down to these parameters. The turbines will experience a lower mean velocity and a higher turbulence intensity, and their wakes will change accordingly.

In order to deliver an estimate for the mean velocity at a turbine in the wake it is necessary to consider meandering, as the Ainslie-type velocity deficit model does not take this into account [30]. Since in the case of a Dynamic wake meandering model the meandering time series is explicitly computed, it can be used directly, avoiding the use of additional models such as proposed by Ainslie (cf. section 2.3.1). For the mean velocity deficit, the following approach is therefore used:

1. The target turbine is discretized by a number of P points with corresponding numerical quadrature weights w_p.

2. The meandering offset time series for an impacting wake at the location of the target turbine is computed, resulting in T offset values in lateral and vertical direction.

3. For each quadrature point p and each meandering time step t, the location of p relative to the incoming meandered wake is computed.

4. For the $P \times T$ resulting points, the wake deficit is computed through interpolation of pre-calculated results from the wake deficit model, yielding a velocity deficit time series of the length of the offset time series for each point p.

5. The deficit at each quadrature point p is time averaged, and by using the quadrature weights w_p the average velocity deficit across the rotor is computed.

6. The process is repeated for all N wakes that impact the target turbine, adding the wake deficits under the assumption of linear wake superposition

Using a nomenclature where $\Delta U(n,p,t)$ denotes the deficit caused by turbine n at the location p at the time step t, the procedure described above can be summarized in the following equation:

$$\langle \Delta U \rangle = \sum_{n=1}^{N} \sum_{p=1}^{P} \frac{\sum_{t=1}^{T} \Delta U(n,p,t)}{T} w_p \tag{4.19}$$

It is worth noting that due to the commutative property of summation, this formulation is mathematically equivalent to one where the time-averaged values at each quadrature point for each incoming wake are added before performing the numerical quadrature over the rotor.

Finally, the average velocity at the rotor is computed considering both the computed average deficit and the shear profile at the rotor, using the same numerical quadrature used for the deficit also for the shear. The final equation for the average wake velocity of a turbine impacted by wakes reads therefore:

$$U_w = \sum_{p=1}^{P} U_{shear}(p) w_p - \langle \Delta U \rangle \tag{4.20}$$

Delivering an estimate for the turbulence intensity on a rotor impacted by wakes is more complex, as several factors contribute to this turbulence. Firstly, there is a base turbulence level in the flow that is experienced by every turbine in the farm. Secondly, the meandering of the wake causes velocity fluctuations on the rotor. And finally, every time a point finds himself hit by the meandering wake it experiences locally increases turbulence. In the implementation, all three of these phenomena are considered independently, and linear summation of the added turbulent variances σ^2 is assumed.

For turbulence caused by meandering, a similar approach to the one used for the velocity deficit is used. However, in step 5 instead of computing the average deficit over time, the variance of the deficit at each point is computed. The expression used for the average variance across the rotor caused by wake meandering σ^2_{wm} is as follows:

$$\langle \sigma^2_{wm} \rangle = \sum_{n=1}^{N} \sum_{p=1}^{P} \frac{\sum_{t=1}^{T} \left(\Delta U(n,p,t) - \langle \Delta U(n,p) \rangle_T \right)^2}{T} w_p \tag{4.21}$$

where $\langle * \rangle_T$ is the time average of the argument.

Added variance from the increased turbulence in the wake is computed separately, but again in a similar fashion. Instead of computing the wake deficit at every point and time step, the velocity scaling factor k_{wt} according to equation 2.48 is computed. The scaling factor is meant to be applied to a velocity field u_σ of standard deviation equal to 1 m/s in order to obtain the added turbulent velocity field. In order to compute the average variance at each point, it is assumed that the meandering position varies slowly, in which case we can write for variance caused at the point p by wake added turbulence generated from turbine n as:

$$\langle \sigma^2_{wt}(p,n) \rangle_T = \frac{\sum_{t=1}^{T} \left(k_w u_\sigma(n,p,t) - \langle k_{wt} u_\sigma(n,p,t) \rangle_T \right)^2}{T} = \frac{\sum_{t=1}^{T} k_w^2}{T} \tag{4.22}$$

Equation 4.22 is valid if the time interval T can be split into smaller intervals $T1$, T_2, ..., T_k such that

on each interval the meandering position and therefore k_w is approximately constant, but the standard deviation of u_σ remains unchanged. Under the assumption that meandering happens at a slower time scale than turbulence, it is reasonable to assume that such a decomposition is possible. This allows us to compute a total rotor-averaged added variance caused by the added turbulence in the meandering wake σ^2_{wt} as:

$$\langle \sigma^2_{wt} \rangle = \sum_{n=1}^{N} \sum_{p=1}^{P} \frac{\sum_{t=1}^{T} k^2_{wt}}{T} w_p \tag{4.23}$$

As all three causes of velocity fluctuation in the wake (ambient turbulence, deficit meandering and wake turbulence) are considered statistically independent, their variances can be added linearly to obtain the total variance of the velocity field seen by a wind turbine effected by wakes:

$$\langle \sigma^2_{tot} \rangle = \langle \sigma^2_{wm} \rangle + \langle \sigma^2_{wt} \rangle + \sigma^2_{amb} \tag{4.24}$$

The ambient turbulent standard deviation σ_{amb} is considered an input of the problem, and can for example be deducted from models such as the Normal Turbulence Model (*ntm*) that can be found in the standard [4], or from site-specific measurements. The turbulence intensity including wake effects I_w is finally computed from the total variance by normalizing with the mean velocity calculated previously, using the equation:

$$I_w = \frac{\sqrt{\langle \sigma^2_{tot} \rangle}}{U_w} \tag{4.25}$$

It may be noted that the added wake turbulence is only taken from the turbulence in the axial direction. This follows the suggestions by the researchers from DTU that developed the model, arguing that turbulence in the main wind direction is the most important for wind turbine operation [5]. The computed average velocity U_w and average turbulence intensity I_w are used in term to compute the wake deficit and wake added turbulence for higher order turbines, mowing from rank one all the way to the last rank of the farm.

4.5 Generating Input for an Aeroelastic Solver

The output of this wake modeling tool is intended for the SGRE in-house developed aero-servo-elastic solver BHawC. The solver deals with turbulent inflow by loading pre-calculated turbulent velocity fields as input. These files, denoted *tubulence boxes*, describe the turbulent velocity component of a 3D wind field discretized on a box of a certain size and resolution depending on the diameter of the target turbine. The height and width of the box contain the full rotor disk, while the length is such that running through the box at mean ambient wind speed takes as long as the simulation. Turbulence boxes are generated by an external generation tool only for one standard deviation, and are scaled by BHawC in order to obtain the desired turbulence intensity. The mean wind speed as well as the shear are normally added during the execution of the solver.

To use the implemented dynamic wake meandering model in the aero-servo-elastic solver, no code modifications have to be applied. Instead, the turbulence boxes are used as a way to inject the wake

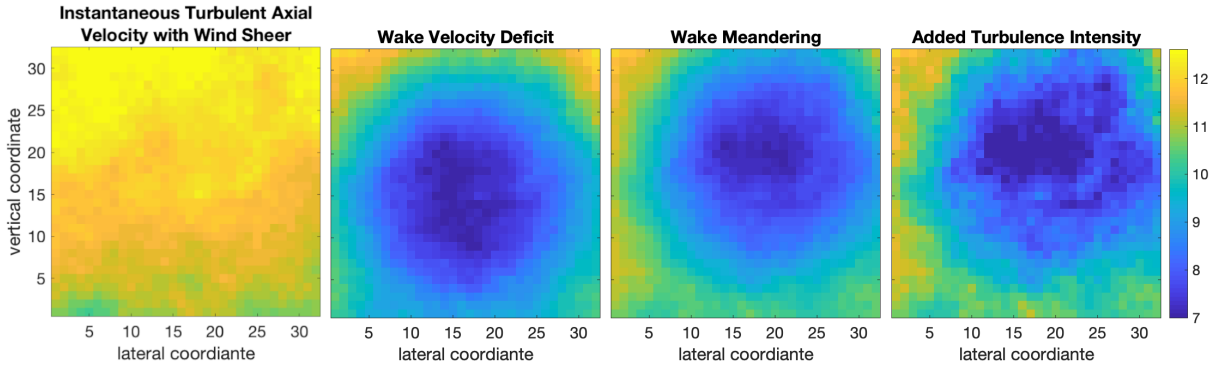

Figure 4.5: 2D sheared turbulent wind field, discretized on a 32x32 grid, successively showing the impacts of added wake effects.

velocity field directly into the solver. BHawC is simply instructed to leave the input turbulence box unscaled and to only add the mean wind speed. Figure 4.5 shows the evolution of a 2D cross section of the turbulence box as effects are successively added. The developed tool takes care of scaling the boxes to the desired ambient turbulence, adds the effect of shear and finally adds the described local wake effects to the wind field. Turbulence boxes can be exported for any turbine in any given wind farm. This allows to test the effect of wakes on power and loads directly in an aero-servo-elastic code without the need for any further development.

4.6 Use Cases and Limitations of the Implemented Tool

The implemented wake modeling tool represents a complete interpretation of one of the most advanced engineering models for wakes, the Dynamic Wake Meandering model developed by DTU [29]. The tool can be used in combination with an aero-servo-elastic solver to study the effects of placing a wind turbine downstream of another turbine, both looking at power and loads. Turbine placement and wind direction can be freely chosen, so the implemented tool also allows to study cases of half-wake, where one side of the rotor is impacted by a wake while the other is not. Analyzing this situation in an aeroelastic solver is of great interest since it might reveal high cyclic loads or unexpected turbine behavior. The tool allows further to analyze the effect of multiple wakes on a turbine, allowing to give an estimation of the wind conditions deep inside a farm that up to this day remain little understood. Accurate engineering models for interaction across entire wind farms will increase our ability to predict differences in behavior and component lifetime between ”internal” and ”external” turbines, and the DWM modelling approach represents an important step in this direction.

However, due to strong assumptions taken in the constituent models, the implemented DWM tool has to be used with care as its applicability has certain limitations.

Firstly, due to the nature of the boundary conditions in the deficit model the tool is not able to give a correct estimation of the wake effects in the near wake. The assumption of instantaneous wake expansion implies that the near-wake result is non physical, and all results at less than 3-5 diameters downstream distance cannot be expected to be accurate. This means that turbine configurations with

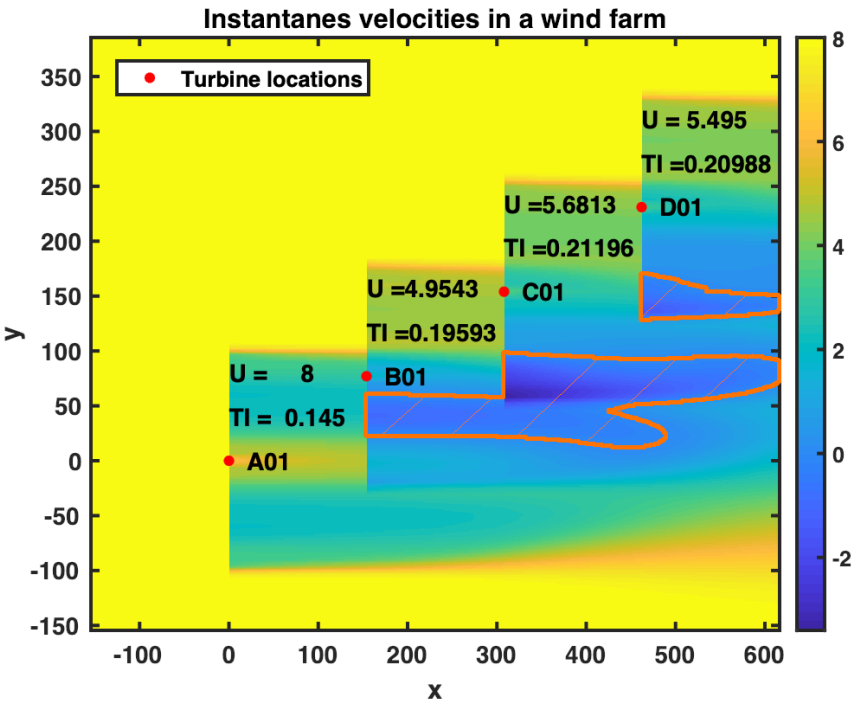

Figure 4.6: Velocity field in a closely spaces wind farm, indicating mean rotor velocities and turbulence intensities. Areas where linear superposition of wake effects predicts a negative wake velocity are shown in orange. This demonstrates the limits of the linearity assumption for wake effects.

close spacing cannot be simulated accurately by the model. This is however a rare occurrence do to the associated high wake losses.

Another limitation concerns very large inter-turbine distances due to the assumptions taken in the meandering model. The model assumes that the meandering velocity of each wake tracer is assigned at emission and stays constant over time, leading to a linear growth the meandering offset. Apart from being highly unintuitive, this does not respect assumption of ”passive scalar transport” of the wake. Under this assumption the velocity of each tracer would actually change over time according as the tracer moves through the filtered turbulence field. No conclusion on the maximum distance for which the model is valid has been reached, but it is expected that a limit exists. It is however questionable if wake deficit values at such high distances are still relevant. Alternative meandering models recently introduced use assumptions under which the meandering offset is limited. uch alternative models could be easily be implemented in the developed tool due to the modular structure of the code.

A third limitation is the validity of the assumption of linear superposition of wake effects. As the underlying physics of fluid flow are highly non-linear, it is unlikely that this approximation holds true in all cases. A clear example of this is the fact that negative average velocities can be achieved locally in the wake of turbines that are exposed to multiple wakes, as demonstrated in figure 4.6. This phenomenon is caused in part also by basing the axial induction purely on the mean wind speed across the entire rotor, neglecting local differences. While these negative velocities almost never impact a downstream rotor in realistic farm layouts, they show that the model is indeed not simulating the true physics of the flow field.

4.6.1 Use of Alternative Wake Models

In addition to the use of the wake model described above, the modular structure of the code allows further another use that might be of interest: As the models used to calculate the wake effects can easily be switched out or individually deactivated, different wake models can be compared directly. It is of great interest to understand if the dynamic wake meandering model really increases accuracy of power predictions compared to the commonly used Jensen model, or if the computed total added turbulence ileads to better estimates of loads than the commonly used Frandsen model. With the tool that was implemented, such comparative studies can be performed easily and without the need of any modification in the tool chain.

One last use case to be pointed out is the possible addition of wake steering models as described in section 2.5. The steering offset can be implemented as an addition to the meandering offset, and several steering models could be tested against each other.

The only limitation to the integration of alternative models is that the presented implementation is intrinsically built on the assumption of an axisymmetric wake deficit, making the tool currently unfit to deal with wake models that predict a distortion of the wake shape, which is the case in some yaw deflection models.

Chapter 5

Verification and Validation of the Wake Modeling Tool

In order to assess the quantitative accuracy of a numerical modeling tool, the steps of Verification and Validation (V&V) are of great importance. While similar in scope, the definitions of the two terms are very clear and distinct [59]:

- **Verification** deals with the correctness of the implementation, trying to answer the question ”Does the simulation tool correctly solve the underlying equations?” The numerical methods employed in the solution of the equations are checked for convergence and compliance of the results with the equations is assessed. If available, the model is tested against benchmark numerical solutions or analytical solutions for simplified problems.
- **Validation** deals with the physical accuracy of the model, trying to answer the question ”Does the simulation tool reflect the underlying reality?” Validation is generally carried out by comparison with experimental data, ideally acquired in validation experiments carried out explicitly for the purpose.

In this chapter, a validation and verification of the wake modeling tool introduced in chapter 4 is presented. Validation is focused on the Ainslie-type wake deficit model, as it encompasses the solution of simplified Navier-Stokes equations and is therefore most susceptible to numerical errors, non-convergence of the solution and mistakes in the implementation. Validation is carried out using a set of data from field measurements provided by the industry partner. The comparison aims to validate the complete tool, as data for the individual models cannot be retrieved from the 10 min average samples collected in the field.

Finally, a second route of verification is explored: comparison with a benchmark solution for the wake field generated with a high-fidelity LES solver using an ALM framework (see section 3.4) and an incompressible flow solver. This verification route has to be handled with care, as the ALM tool itself still lacks validation with experimental data for wakes. However, the underlying flow solver has been verified and validated in a number of cases, including cases of atmospheric flow [7] and is therefore assumed to give a quasi-analytical estimate of the solution of the incompressible Naiver-Stokes equations for the

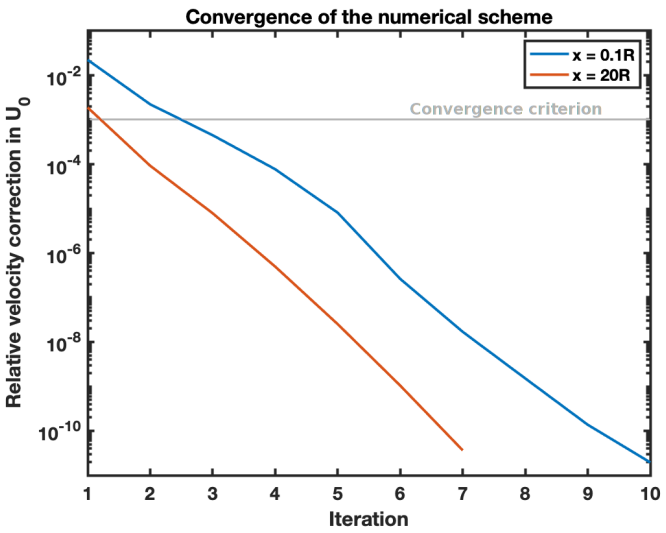

Figure 5.1: Convergence of the numerical scheme for a point in the near wake and a point in the far wake, showing the velocity correction obtained by solving equation 4.9. The chosen convergence criterion is indicated.

given case, i.e. a wake field behind a turbine. Verification of the Ainslie model by comparison with the LES result is attempted.

5.1 Verification of the Wake Deficit Solver

The wind farm wake velocity deficit model is based on a solver for the rotationally symmetric thin-shear-layer approximation of the Navier-Stokes equations. The implementation is not trivial, and doubts can emerge on whether the equations are solved correctly. In order to asses this it is necessary to test whether the results converge, and whether they comply with the governing equations of fluid flow.

5.1.1 Convergence of the numerical scheme

In order to evaluate the implemented flow solver it has to be verified if the solution actually converges. This test has been performed and it was found that the chosen numerical scheme converges quickly and reliably, as shown in figure 5.1. Convergence is shown up to a mass residual 10^{-10}, however in the implementation is set to 10^{-3}. Results indicate that the residual decreases by one order of magnitude per iteration step over a wide range.

5.1.2 Conservation of Mass and Axial Momentum

The governing equations of all fluid problems are based on the fundamental principles of conservation of mass, momentum and energy. However in the present model no state variable for energy such as temperature is considered, making energy conservation impossible to asses. The two remaining principles of conservation are therefore:

- **Conservation of mass:** Mass is neither destroyed nor created in any fluid domain. Therefore, the mass flow across the boundary of any given control volume must be balanced by the change in density integrated over the volume at all times. In integral form this reads:

$$\iiint_V \frac{\partial \rho}{\partial t} dV + \oiint_A \vec{u} \cdot \vec{n} dA = 0 \tag{5.1a}$$

- **Conservation of linear momentum:** Newton's second law of motion applied to a fluid control volume implies that the variation of linear momentum inside a control volume is equal to the integral of all forces acting on the fluid and the momentum outflow over the surface. If only pressure and viscous forces at the boundary are present, the law reads in integral form:

$$\iiint_V \frac{\partial \rho \vec{u}}{\partial t} dV + \oiint_A \vec{u}^T \vec{u} \cdot \vec{n} dA = - \oiint_A p \vec{n} dA + \oiint \mu (\nabla \vec{u}) \cdot \vec{n} dA \tag{5.1b}$$

In this verification step, the compliance of the solution found by the implemented flow solver with the described conservation equations is assessed. As only a time-averaged solution is found, the transient terms $\partial / \partial t$ in the equations can be ignored. Furthermore, by choosing a control volume such that the pressure at the boundary is atmospheric and the velocity gradients are negligible, both the pressure and viscous term can be neglected leading to the following simplified expressions:

$$\oiint_A \langle \vec{u} \rangle \cdot \vec{n} dA = 0 \tag{5.2a}$$

$$\oiint_A \langle \vec{u}^T \rangle \langle \vec{u} \rangle \cdot \vec{n} dA = 0 \tag{5.2b}$$

If the result of the implemented flow solver respects these laws, the implementation of the equations and the approximations made to derive them can be considered accurate. In order to test this assumption, the wake deficit has been calculated for a range of velocities and turbulence intensities. The flow field is computed in a cylindrical coordinate system, therefore the conservation expressions have to be evaluated on an annular extrapolation of a given 2D area in the solution plane. While equations 5.1a and 5.1b should be invalided for any control volume, it is easiest to test the conservation laws on a cylindrical control volume. This avoids numerical integration over more complex annular surfaces that could potentially lead to interpolation errors. Furthermore, it is advantageous to choose a control volume that passes through existing radial and axial grid point in order to limit the use of interpolation.

A cylindrical control volume with radius r_k corresponding to the outermost radial grid point or the domain is chosen. Here, radial gradients of velocity are low and pressure is atmospheric, allowing the assessment of conservation of mass and momentum through the simplified conservation equations 5.2a and 5.2b. When the length of the cylinder is chosen as x_n corresponding to the n$^{\text{th}}$ axial point, the following numerical approximation of the integral form of the simplified conservation equation can be

used to compute mass and axial momentum flow imbalance:

$$\Delta Q_m = -2\pi \sum_{j=1}^{k} r_j U_{i=1,j} + 2\pi \sum_{j=1}^{k} r_j U_{i=n,j} + 2\pi r_k \sum_{i=1}^{n} V_{i,j=k} \tag{5.3a}$$

$$\Delta Q_p = \underbrace{-2\pi \sum_{j=1}^{k} r_j U_{i=1,j}^2}_{\textit{Inflow at Rotor}} + \underbrace{2\pi \sum_{j=1}^{k} r_j U_{i=n,j}^2}_{\textit{Outflow over Base}} + \underbrace{2\pi r_k \sum_{i=1}^{n} V_{i,j=k} U_{i,j=k}}_{\textit{Outflow over Side}} \tag{5.3b}$$

This computation has been performed on a discrete series of cylindrical control volumes of radius equal to 4 turbine diameters (the domain size) and increasing length. Furthermore, the computation was performed for several wind conditions in order to assess conservation across the entire input space. The result of this computation, seen in figure 5.2 shows the total mass and momentum deficit in the resulting wake flow field, calculated for all relevant wind speeds and for the wind speed of 8 m/s at a range of relevant turbulence intensities. The study has been performed using a grid resolution of 0.075 turbine radii in radial direction and 0.1 turbine radii in axial direction. The resolution was fixed after showing that a further doubling of the resolution did not lead to significant change in the results.

The figures show that the relative mass and momentum deficit remains small for all control volumes, with relative values never reaching more than 0.1% for mass conservation and 1% for momentum conservation. The order of magnitude of the imbalance corresponds to the order of magnitude of the convergence criterion that was set to 10^{-3} m/s for the velocity correction term, as indicated in figure 5.1. This confirms that the implemented numerical model is indeed solving the underlying equations correctly.

It can be observed that the momentum deficit for very high turbulence intensities at large downstream distances diverges. This reflects the fact that an improper boundary condition was chosen to simplify the implementation. At high turbulence intensities, the wake diffuses faster since the modeled eddy viscosity is directly proportional to the turbulence intensity. When the expanding wake hits the boundary, the Dirichlet condition forces the velocity to the free stream value, effectively adding linear momentum to the system in an unphysical way. This affects the the momentum flow error ΔQ_p noticeably, but the relative error still remains low. The effect is interesting to observe, but unlikely to have an impact on cases with realistic, and therefore more moderate, turbulence intensity. It can be concluded that the choice of boundary conditions will not compromise the results obtained from the wake modeling tool in most relevant cases. The wake deficit model can therefore be considered verified.

5.2 Validation with Experimental Data

Usually, and certainly in the present case, the goal of a numerical simulation is to accurately predict physical processes. In order to assess whether this is the case, comparison with experimental data is essential. For the wake modelling tool presented here, field data from an offshore wind park was provided by the industrial partner in order to validate the tool.

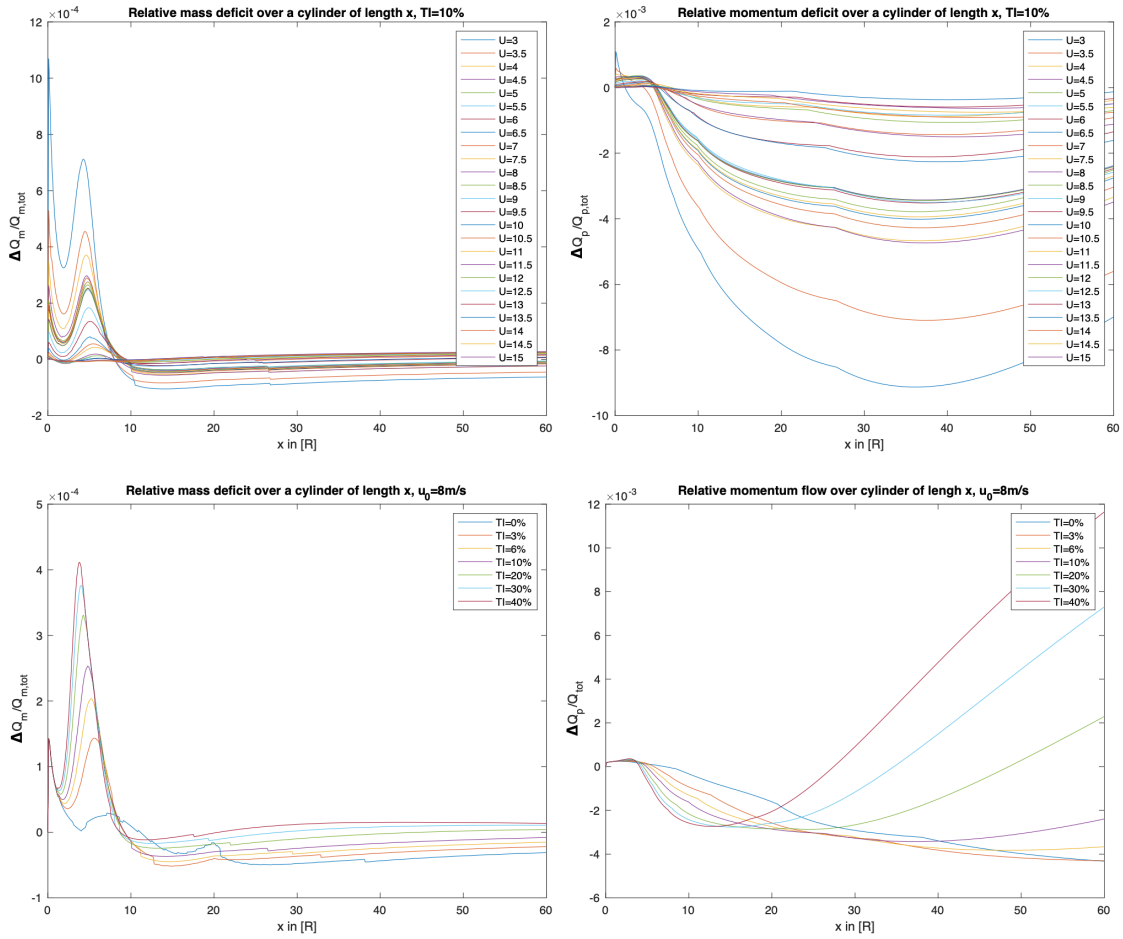

Figure 5.2: Relative mass and momentum flow deficit over a cylinder of Radius 4D and length x, normalized by the total flow over the inlet. Results for a range of relevant velocities and turbulence intensities are shown.

Data for velocity and turbulence inside a wind farm has been collected over an extensive period of time. Velocity is estimated from power curves, while wind fluctuation, *ie.* turbulence, is estimated from the standard deviation in measured loads over 10 minute intervals. The exact estimation procedure is not disclosed for confidentiality reasons. As is standard practice for wind turbines, the collected data takes the form of 10-minute statistics. Each turbine records relevant variables (notably wind speeds, power and bending moments) at a relative high sampling rate, however only 10 minute averages and standard deviations are stored. This makes it impossible to use field data to validate the individual models of the wake modeling tool independently. Velocity measurements can be used to validate the combined meandering and deficit tool, while accuracy on turbulence would indicate the correctness of the combined DWM model, as all models contribute to the velocity fluctuations in the wake.

5.2.1 Velocity Deficit Comparison

In order to assess accuracy of the combined velocity deficit and meandering model, only data of a turbine affected by a single wake has been selected from the available data set. Comparisons for cases with superimposed wakes are left to be performed in follow-up studies. From a large dataset

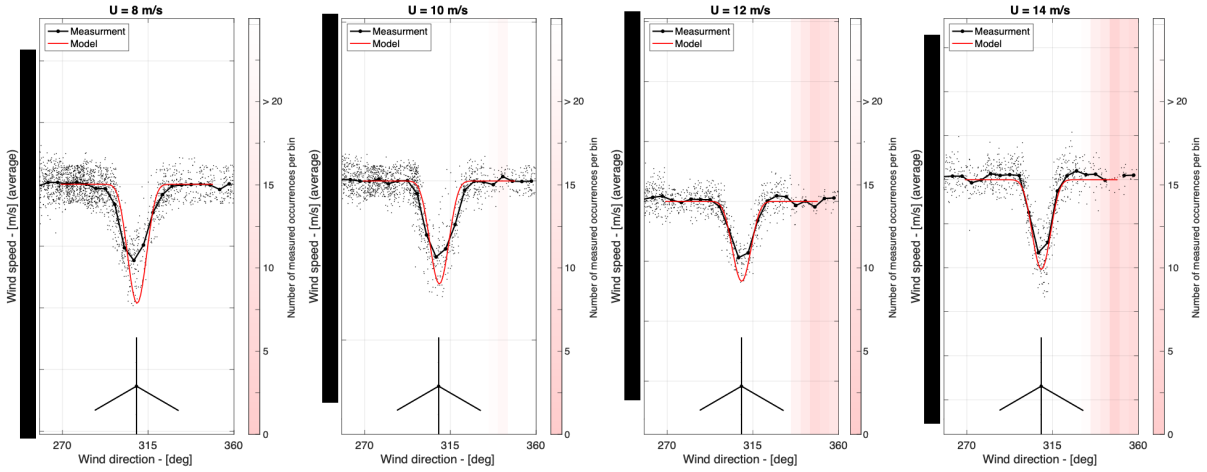

Figure 5.3: Comparison of the model results for average wind speed with data for different unperturbed wind speeds (1 m/s bins) at different inflow angles. Black dots represent average values over 5 degree bins. Model results have been obtained using the average undisturbed ambient turbulence. Pink shading indicates angular bins with limited data points.

of 2 years, engineers at the industrial partner extracted data for the wind speed at the turbine hub at different unperturbed wind conditions and different wind directions. The simulation tool has been run, emulating the farm layout and wind conditions, and the average wind speed at the target turbine has been computed as described in section 4.4. Both simulated and measured values (data points and binned averages) for a given unperturbed wind speed have been plotted for relevant angles around the angle of alignment between the turbines (305 degrees). The results obtained for 4 selected unperturbed velocities are shown in figure 5.3.

5.2.2 Added Wake Turbulence Comparison

The comparison of turbulence predictions with measurement could potentially result in a validation of the full model, as added turbulence is caused both by the meandering wake deficit and by the added turbulence within the wake. Such a comparison has been performed, following the same approach that was presented in the previous section for the velocity deficit. Turbulence was computed at the turbine following the procedure described in 4.4. Experimental data for added turbulence at a given angle of incident wind is compared with the model result. The results of this comparison are shown in figure 5.4.

5.2.3 Conclusion of the Experimental Validation

The results show an overall good agreement between the model and measurements. The velocity predicted by the model is lower than the average of the measured data, especially at low wind speeds. This might indicate that the wake deficit is calibrated for around-rated wind speed, which makes sense as this is where the highest loads are expected to occur. On the other hand the estimated turbulence is generally lower than what measurements show, especially at high wind speeds, and the base of the predicted ”bell shape” is too narrow. This seems to indicate a problem in the added turbulence model, since at high wind speeds (14 m/s) the velocity deficit, resulting from the deficit and meandering

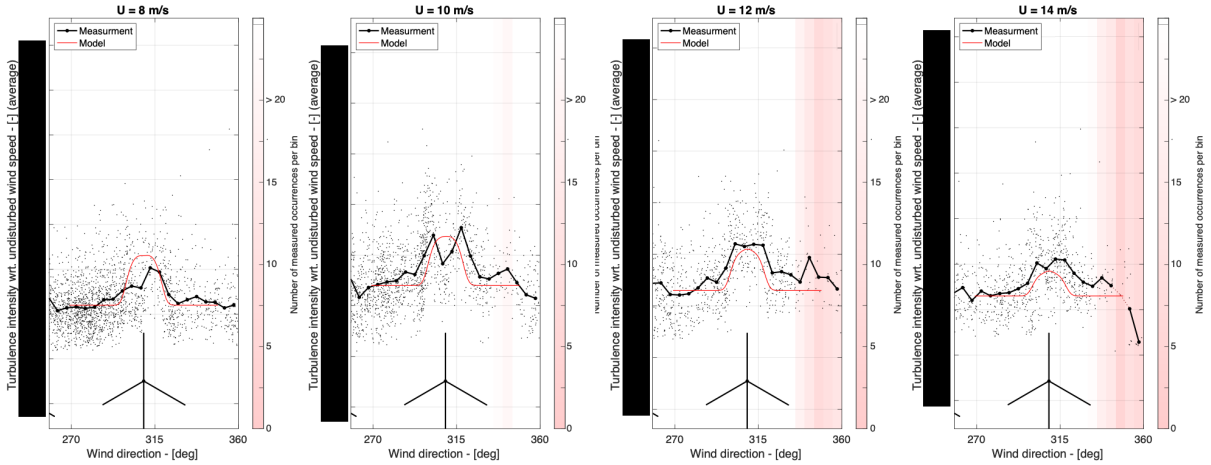

Figure 5.4: Comparison of the model results for turbulence with data for different unperturbed wind speeds (1 m/s bins) at different inflow angles. Black dots represent average values over 5 degree bins. Model results have been obtained using the average unperturbed ambient turbulence. Pink shading indicates angular bins with limited data points.

model, matches well with measurements. The model results have to be handled with some caution, as they were all obtained at the same undisturbed ambient turbulence for a given wind speed, while the actual ambient turbulence varies widely. Direct comparisons for specific data triplets of direction, unperturbed wind speed and ambient turbulence intensity could help to better understand the behavior of the model. Overall it can be concluded that the modeled curves are contained entirely inside the cloud of measurement points, but fail to accurately predict the average in some instances.

The experimental validation performed in the course of this work was limited in scope due to the lack of field-measurable quantities that can be directly compared with model results. As data is only measured in 10 min averages, the direct validation of the meandering model is not possible. Furthermore, measurement data only provides a single velocity value at the rotor hub, making it impossible to validate the predicted wake shape and velocity distribution across an impacted rotor. Full 3D wind field measurements with LIDAR technology could be used to validate the complete wind filed predicted by the DWM model. However, the technology has not been extensively used in the field, and no LIDAR data from wind farms was available for the present validation. The comparisons that could be performed using the available data have not been exhaustively explored, notably lacking individual comparisons for single data points that could help to understand the influence of ambient turbulence. Furthermore, measurement data is available for local turbine loads from strain gages. Predicting these loads is one of the ultimate goals of this simulation tool. It is therefore of interest to use the tool to generate wind field input data for an aeroelastic solver, obtaining simulated results for loads to compare with measurements.

5.3 Verification with a High-Fidelity Flow Solver

A way to verify a model that employs numerical methods to solve a system of equations is the comparison with an analytical solution in cases where such a solution can be obtained. In the case of the wake behind a wind turbine, no analytical solution for the Naiver-Stokes equations can be found. However, a

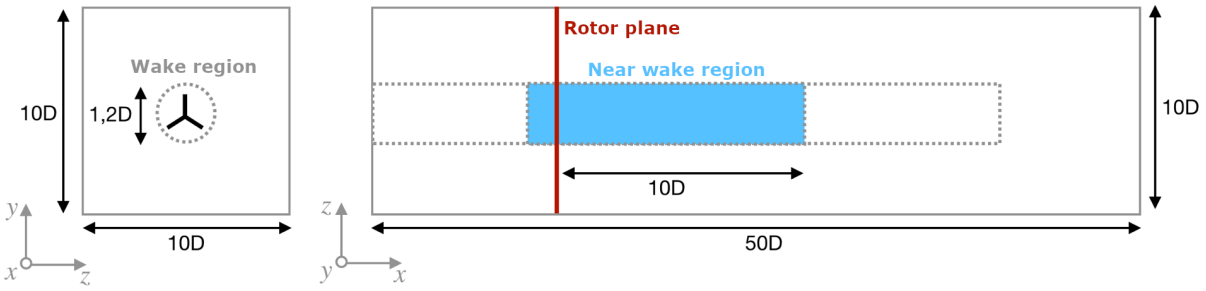

Figure 5.5: Simulation domain of the LES computation, with dimensions in turbine diameters D. The dotted outline denotes a region of local grid refinement, while in the blue area the grid is refined even further.

higher-order numerical model is sometimes used as a quasi-analytical benchmark to the same end. In wind energy, this approach is often used to extract parameters for low-order engineering models from CFD results. In this section, results of the implemented wake modeling tool are compared to LES results computed with the computational fluid dynamics library YALES2 introduced in section 3.5. The results are obtained using ALM and the incompressible flow solver available in YALES2. This approach for treating wind turbines in CFD is introduced in more in detail in section 3.4.

5.3.1 Methodology

The focus of this verification process is the comparison of the time-averaged flow field in the wake of a wind turbine without yaw error between a LES-ALM model and the implemented Ainslie-type wake deficit model described in section 4.1. The LES calculations are performed on the massively parallelized flow solver YALES2 on an unstructured 71.1 million cell grid, locally refined in a cylindrical region around the rotor and wake. The dimensions and refinement regions of the domain are shown in figure 5.5. An initial flow field is first computed on a 9 million element grid of the same dimensions.

The simulation is performed without the presence of the static components of the turbine such as nacelle or tower, and no ground effects are considered. These simplifications serve to make the result comparable with the Ainslie deficit model, where the approximation of radial symmetry does not allow to introduce these elements. It is however known that the addition of these effects in ALM can have a noticeable impact over the entire 3D flow field in the wake of the rotor [10].

Wake results are obtained at a single wind speed due to restrictions on the available turbine data explained in the following section. Furthermore, the simulations are run without ambient turbulence as the LES tool does not dispose of a way to generate realistic atmospheric turbulence in the flow field. Minimal random velocity fluctuation of standard deviation equal to 1% of the wind speed are added at the domain inlet, however this ”turbulence” only serves to destabilize laminar flow that could lead to phenomena that are never observed in the real atmospheric boundary layer. This procedure was introduced after an initial study on grid convergence showed that a further grid refinement caused a significant change in the results. With the injection of destabilization turbulence, the effects of a further grid refinement disappeared almost completely.

After an initial pre-run on the low-resolution grid and a second run on the fine grid to fully establish

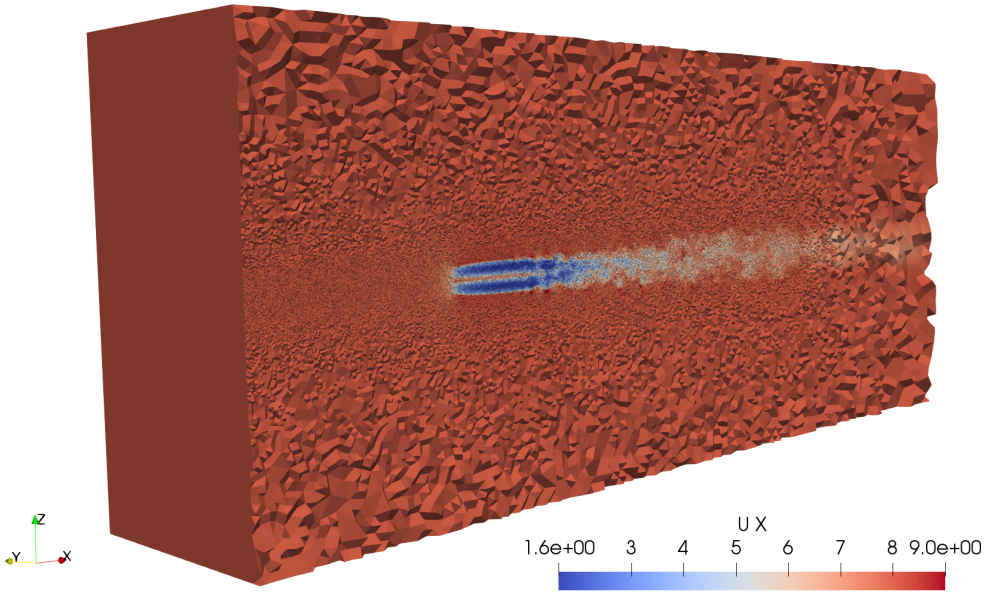

Figure 5.6: Illustration of the computational domain coloured according to the instantaneous axial velocity and sectioned along the plane $y = 0$ along grid boundaries. The figures gives an impression of the unstructured grid cell size and of the overall dimensions of the computational domain.

the wake, simulation data has been acquired during a final run, collecting statists only from a flow field that is assumed to have reached a stable condition. No methodical studies have been performed on the time requirements for convergence to a stable wake state, but a visual inspection of the time evolution of mean values showed that they had reached a stable value and were no longer changing during the acquisition run. The physical time simulated in the pre-runs is of approximately 2 hours, including roughly 1:30 of initialization on the unrefined 9 million element grid. The data acquisition time is of 38 minutes, corresponding to roughly 350 full rotations. A cross-section of the domain showing the final computation result for instantaneous axial velocity can be seen in figure 5.6.

From the acquisition run, data is exported on a vertical plane through the center of the wake at various time steps used mainly for affirming that a stable state was reached, while the whole flow field is exported at the last time step. The acquired dataset contains statistics on the velocity that will be the basis of comparison with the steady-state model developed in chapter 4. Mean velocity data is extracted from an axial slice of the final LES result to be compared with the flow field computed by the Ainslie-type wake deficit model. Extracting data from both a horizontal and a vertical plane in the simulation shows that the mean velocity result computed by LES is indeed axisymmetric, as can be seen in figure 5.7. It was finally decided to extract data from the vertical plane only, however averaging multiple planes could have been a more valid approach.

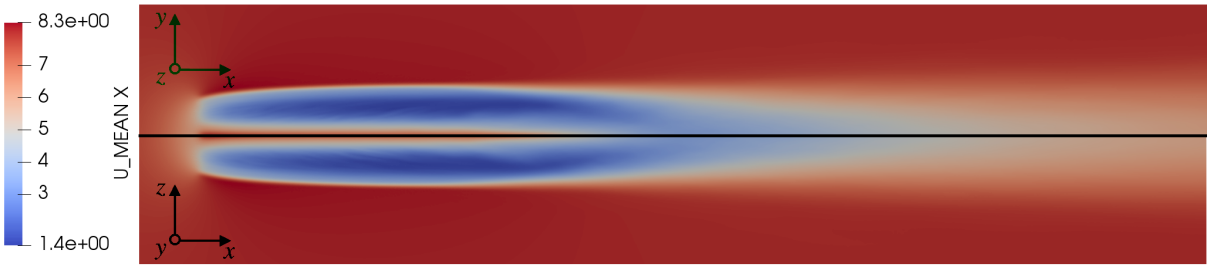

Figure 5.7: LES result for average axial velocity in the xy and xz plane, demonstrating the radial symmetry of the result.

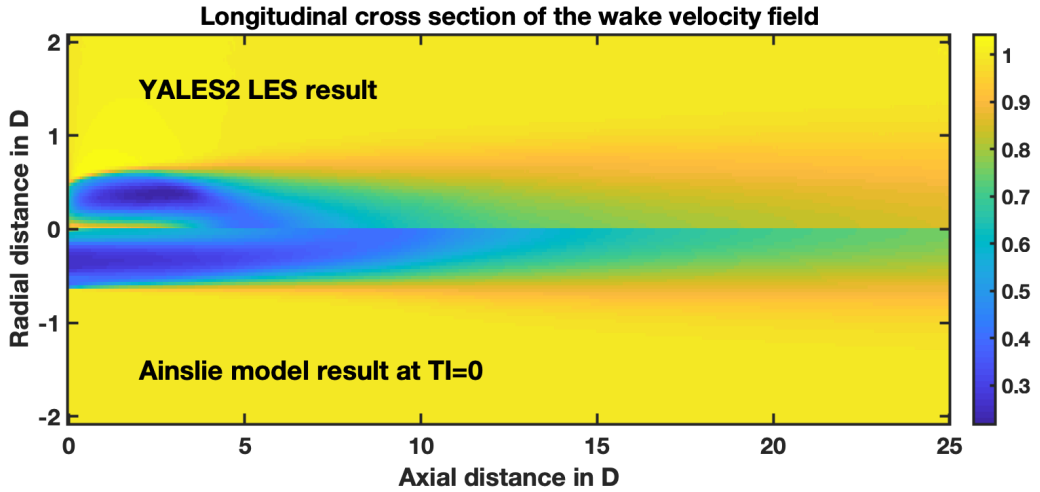

Figure 5.8: Comparison of the velocity field in the wake between the LES result (top) and the implemented wake deficit model (bottom) at 0% ambient turbulence

5.3.2 Results

A series of comparisons has been performed between the data extracted from LES and the Ainslie model results. Firstly, a visual comparison is proposed by plotting the two wake results next to each other on the same scale (figure 5.8). Visual comparison shows that the wake simulated in YALES2 recovers significantly faster than the wake computed using the Ainslie model. The most plausible reason for this is that the Ainslie model is calibrated using measurements in atmospheric turbulence conditions and is therefore not necessarily expected to match a numerical case with no turbulence. The estimation of the eddy viscosity parameter ν_e that controls the turbulent diffusion is based on the ambient turbulence and on fitted parameters, as seen in equations 4.3 and 4.14, and can therefore not be expected to be correct at zero turbulence.

This said, the results do appear to be in line with the observation in the previous section, where at low wind speeds the Ainslie model overestimate the wake deficit compared to measurement. This might again be due to calibration, as the empirical relations for the eddy viscosity do not depend on velocity, a strong assumption that could potentially be wrong.

In figure 5.9 the velocity at the centerline of the wake obtained from YALES2 is shown together with results from the Ainslie model at various turbulence intensities. While the difference in the near wake

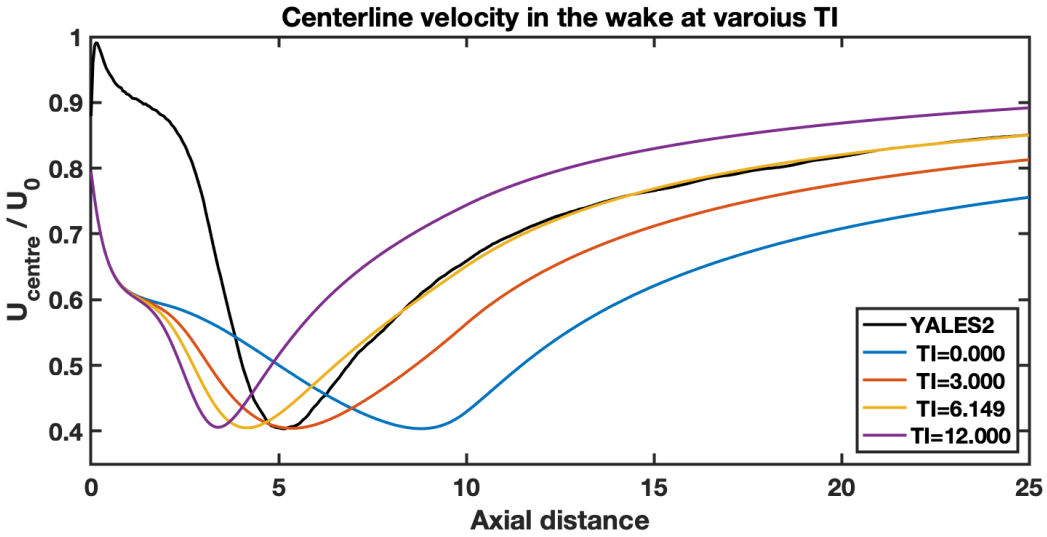

Figure 5.9: Comparison of the wake centerline velocity between the LES result and the implemented wake deficit model at various values of ambient turbulence TI. By fitting the ambient turbulence, an excellent match can be achieved in the far wake.

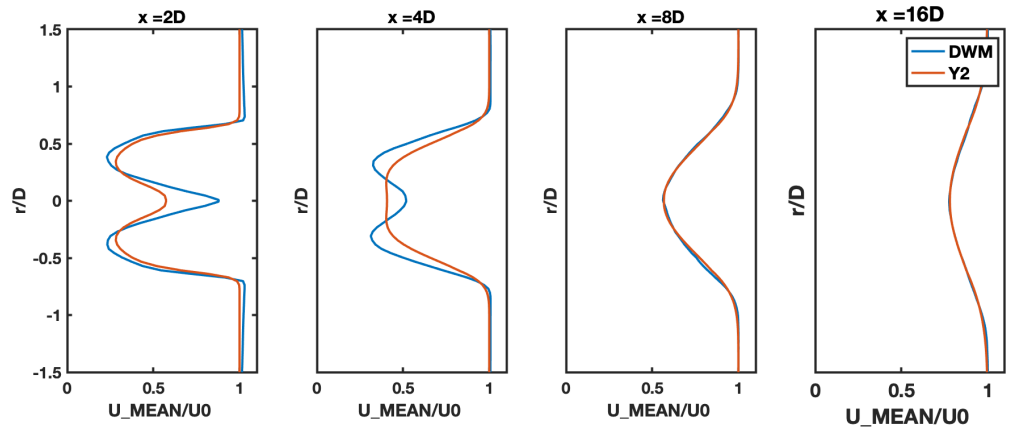

Figure 5.10: Comparison of the velocity profile in the wake at various downstream distances between the LES result and the implemented wake deficit model at the fitted ambient turbulence, 6.15%.

is expected given the inlet boundary conditions described in section 4.1.3, in the far wake the Ainslie model at 0% turbulence underestimates the velocity strongly. By increasing the turbulence intensity in the Ainslie model however, the result of the model can be tuned to fit the LES results. When inputting a value of 0.615 in the turbulence intensity parameter of the Ainslie model, the resulting centerline velocity deficit matches the LES result in the far wake. This proves that a calibration of the eddy viscosity parameters in equations 4.3 and 4.14 could eliminate the difference observed between the two models. This can also be seen in figure 5.10, where the velocity profiles from LES and the Ainslie model are plotted at various downstream distances. The fitted model is not only able to predict the centerline, but also the velocity profile. A more striking representation of the same result can be seen in the flow fields in figure 5.11, where the results of the Ainslie and LES-ALM model are virtually indistinguishable in the far wake.

The excellent match achieved by fitting the ambient TI shows that the implemented model can be

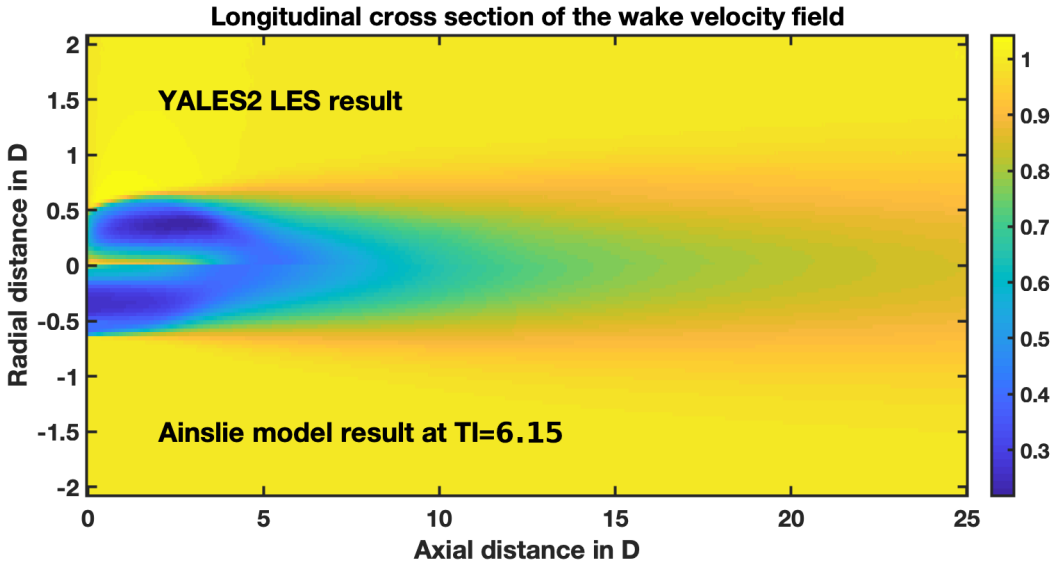

Figure 5.11: Comparison of the velocity field in the wake between the LES result (top) and the implemented wake deficit model (bottom) at the fitted ambient turbulence, 6.15%.

calibrated to estimate both the wake centerline deficit and deficit shape as precisely as an LES simulation. It is however not advised to modify the parameters in the implementation (equations 4.4a and 4.4a) in order to fit the available LES data. The case of 0% turbulence does not have any practical interest and the parameters recommended in the IEC61400 standard for wind turbines [4] have been validated more thoroughly.

Even though the model was shown to be unable to predict the wake field at the limit case of 0% turbulence, this results can be viewed as a successful verification step, proving that the underlying equations are solved correctly even though the empirical relations that prescribe the eddy viscosity are not calibrated for the attempted case. Furthermore, the results validate some of the underlying assumptions of the model. As shown earlier in figure 5.7, the wake appears to be axisymmetric as proposed by the model, as long as tower and shear are not considered and the wind turbine is aligned with the mean wind direction.

5.3.3 Conclusions and Limitations of the Actuator Line Method

The AL method by Sørensen and Shen [51] is a formidable approach to modeling the interaction of blades with an incoming flow, able to resolve phenomena such as tip and root vortices and therefore likely to give a much more realistic result of the near wake than the concurrent actuator disc approach. However, the methodology bears some considerable difficulties that were encountered in the course of the present verification study. A few of them are listed below:

Deformation of the Blade

In turbines with large diameters, such as is the case in offshore turbines of nominal power greater than 5MW, the aerodynamic forces cause large deformations of the blade [60]. Bending of the blade, often by

several meters, generally causes a coupled twisting of the cross section that changes the aerodynamic behaviour of the blade in a given wind. The shape of the actuator line and twist angle β of blade sections become a function of the operation conditions of the turbine. Since no structural coupling is implemented in the YALES2 ALM models, the deformed geometry needs to be generated externally for each given configuration. This includes technically each wind speed as well as each yaw angle, rotor speed and pitch setting, as the deformation of the blade is affected by these control parameters. No automatic process for this exists so far, but implementing it is necessary if YALES2 is to be used more extensively in the verification of engineering models for turbine aerodynamics. For the simulations performed in this work, only one blade deformed geometry for one wind speed in a no-yaw configuration was available. The verification study was therefore limited in its scope.

Turbulence Injection

As mentioned above, in the course of this work it was not possible to set the ambient turbulence on the rotor in the ALM model to a desired level. This would require in fact a realistic simulation of the atmospheric boundary layer (ABL), that might require taking into consideration atmospheric stability, shear and temperature gradients [61]. This makes it possible to create realistic, stable turbulence that is comparable to the real ABL. Such simulations have never been performed with the utilized LES solver, however they are technically possible. In future work, a methodology for generating realistic turbulent inflow conditions for the ALM model based on ABL simulations could be proposed.

Computational Cost

The biggest downside of the treatment of wakes in LES is the enormous computational cost of the simulations compared to simplified engineering models. Obtaining the wake results presented above, even using a state-of-the-art LES solver on 280 cores on a supercomputer cluster, took over 48 hours. The computational cost was of 12.079 processor hours, and the simulation consumed a total of roughly 500kWh of electricity according to data provided by the supercomputer log files. Extrapolating this result, the analysis of a single turbine at all relevant wind speeds, turbulence intensities and yaw conditions would bear a cost of 840 MWh. If the cost is further extrapolated to the analysis of a full wind farm, the use of LES to evaluate a farm of 50 turbines at all possible wind directions would rise to 7.5 **TWh**. This is equivalent to the entire production of the farm in its first seven and a half years of life [1]. The financial implications of this are clearly beyond reasonable, but for the sake of completeness, at an average wholesale price of 60 euros per MWh the simulations would check in at a whopping 450 million euros. The use of LES is therefore very costly in every sense of the word, and the tool should only be used to simulate reference cases to fit computationally cheaper engineering models.

[1] The estimation assumes simulation at wind speeds from 3 to 20 m/s and yaw angles from -30 to 30 degrees and at **3** levels of turbulence intensity, using a 1 m/s resolution for wind speed (**18**) and a 2° resolution for wind directions (**31**). The extrapolation to a farm simulation was performed by multiplying the total cost by the number of turbine (**50**) and simulating the farm for all possible wind directions, again with a 2°. The total number of simulations is therefore $3 \times 31 \times 18 \times 50 \times 180 \approx 15 \times 10^9$ The estimate of annual production was made by assuming 6MW turbines at a capacity factor of 40% (1.05 TWh/y)

Chapter 6

A Novel Wake Steering Model Based on an Ainslie-Type Deficit Model

In the context of wind farm optimization, wake steering through yaw control is sliding into the focus of academic and industrial research alike [6]. First studies on the phenomenon have been performed over a decade ago, however deriving and validating numerical models has proven difficult [6], especially due to the difficulty of performing validation experiments at scale. Jiménez, Crespo and Migoya studied the phenomenon using LES in 2010 [8] and proposed the first analytical model for wake deflection in yawed turbines. The *Jiménez deflection model* is based a top-hat shaped wake wake velocity profile as proposed by Jensen [21] combined with a lateral momentum balance. The model has been used extensively, however it is known to over-predict wake deflection consistently [9, 11]. In 2016, Bastankhah and Porté-Agel proposed a new model based on a Gaussian wake velocity profile in the far wake, using a potential core model for the near wake [9]. The Gaussian model has been used and improved in a series of recent publications, that proposed new values for the model parameters [11] as well as the use of the deflection *angle*, rather than just the offset, to generate inflow for downstream turbines [44]. Details of these models can be found in section 2.5. More complex wake deflection models based on vortex theory have been proposed [62], but are rarely used for wind turbines.

For the wind farm wake modelling tool developed in the context of this work, the addition of a wake deflection model for yawed turbines is an interesting prospect. Such an addition will allow to use the tool to investigate the effects of wake steering control strategies on the farm both in terms of power and turbine loads. The use of models from literature, such as the Jimenez model [8] or the Gaussian model by Bastankhah&Porté-Agel [9] is possible. However, these models are based on an assumption of the velocity profile in the wake, and their use is therefore conceptually inconsistent with the implemented Ainslie-type wake deficit model that explicitly computes the velocity profile in the wake. It is therefore logical to use the computed wake shape, rather than an assumption, in a formulation for wake steering. Such a formulation is proposed in the following.

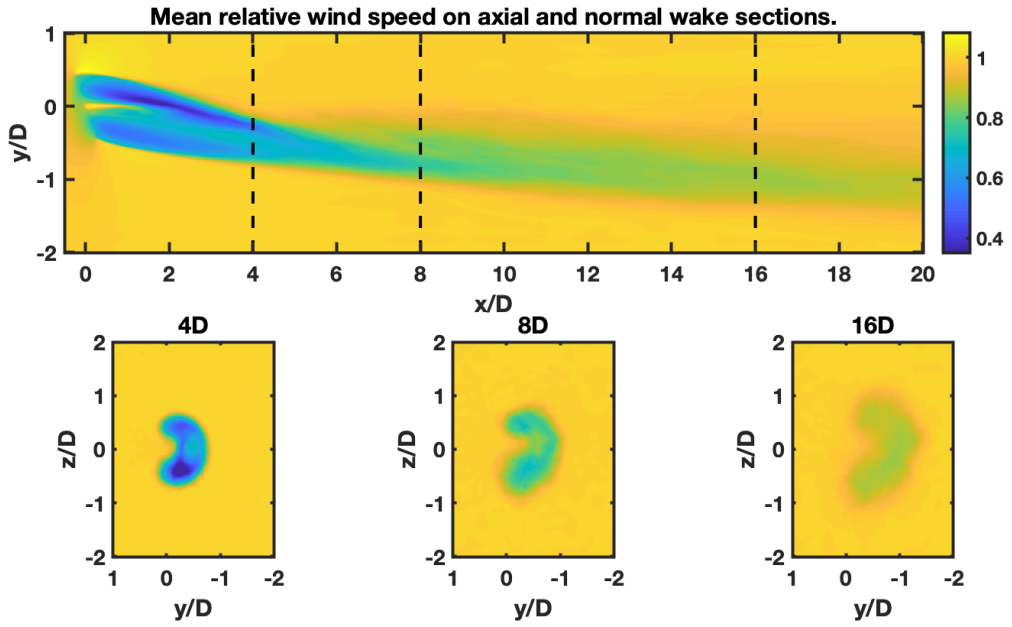

Figure 6.1: Radial and axial cross sections through the velocity field in the wake of a turbine in 30° yaw. Radial sections at 4, 8 and 16 diameters downstream of the turbine, from LES-ALM simulations.

6.1 Model Assumptions

The proposed wake deflection model is based on the Ainslie deficit model [30], in particular on the implementation of described in section 4.1, and therefore inherits its underlying assumptions. This includes the assumption of radial symmetry of the wake around the wake centerline. It is known from both field measurements and LES studies that this does not accurately reflect realty in yawed cases [9]. As confirmed by LES calculations performed using the set-up described in section 5.3, the wake deficit of a yawed turbine assumes a characteristic kidney shape in the far wake, as can be seen in figure 6.1. The assumption of an axisymmetric wake is however considered acceptable in literature as long as yaw angles remain small [8] and will therefore also be used in the new formulation. The wake deflection model is used to obtain a horizontal offset by which the wake centerline is displaced from the rotor axis. This assumption is similar to the passive tracer assumption for wake meandering, and is therefore considered in line with the general model assumptions. Furthermore, the addition of such a yaw steering offset to the implemented wake modelling tool is straightforward, as the computed deflection can directly be added to the existing meandering time series.

6.2 Model Derivation

Under the described assumption, a simple model for wake deflection can be derived. Much like in the derivation of the Jiménez model [8] described in section 2.5.1, a momentum balance is written for a stream tube as depicted in figure 6.2. The following expression is obtained:

$$\vec{F} = \vec{Q}_{p,3} - Q_{m,1}\vec{u_0} - Q_{m,2}\vec{u_0} \tag{6.1}$$

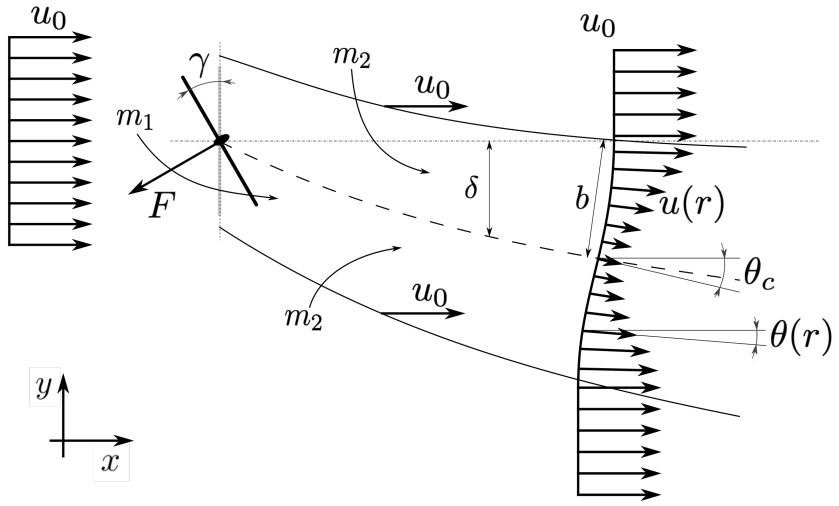

Figure 6.2: Schematic representation of the proposed wake steering model based on an Ainslie-type wake deficit model. The velocity in the wake $u(r)$ is taken from the deficit model at a given downstream distance, while the central deflection angle θ_c is retrieved from a momentum balance over the wake stream tube.

In this equation $\vec{Q}_{p,3}$ denotes the momentum flux over the outlet of the stream tube, $Q_{m,1}$ is the mass flux over the domain inlet, $Q_{m,2}$ the entrained mass flux and $\vec{F}$ the total body force excreted by the wind turbine on the flow. This force can be directly deduced from local induction $a(r)$, a parameter also required as input for the Ainslie wake deficit model and therefore available in the existing framework. It is obtained by integrating the local thrust given by momentum theory over the rotor plane (see eq. 2.16b) :

$$F = \int_0^R 4\pi\rho(u_0 \cos\gamma)^2 a(r)(1-a(r))rdr \tag{6.2}$$

The momentum flux in both axial and lateral direction over the outlet of the stream tube of radius b can be computed considering the wake skew angle $\theta(r)$ and the wake velocity $u(r)$:

$$Q_{p,3,x} = \int_0^b 4\pi\rho u(r)^2 \cos\theta(r) rdr \tag{6.3a}$$

$$Q_{p,3,y} = \int_0^b 4\pi\rho u(r)^2 \sin\theta(r) rdr \tag{6.3b}$$

It is worth noticing that both the momentum flux at the inlet and the entrained momentum flux only have an axial component, as the velocity field outside the wake steam tube is assumed to be uniform and directed in mean wind direction. Projecting the momentum balance on the axial and lateral directions x and y yields therefore:

$$F\cos\gamma = Q_{p,3,x} - Q_{m,1}u_0 + Q_{m,2}u_0 \tag{6.4a}$$

$$F\sin\gamma = Q_{p,3,y} \tag{6.4b}$$

A further simplifying assumption is made in order to obtain an expression for the wake deflection directly from the lateral momentum balance 6.4b. The wake skew angle $\theta(r)$ is assumed to follow the same distribution as the velocity deficit according to the expression:

$$\theta(r) = \theta_c \frac{\Delta u(r)}{\Delta u_c} \tag{6.5}$$

where θ_c and Δu_c are the centerline wake deflection angle and velocity deficit respectively. This assumption is similar to what is proposed in the deflection model developed by Bastankhah et al. [23], where it is assumed that the skew angle follows the same Gaussian behavior as the velocity deficit.

Combining the presented equations and assuming small wake deflection angles finally yields the following, simplified expression for the centerline wake deflection θ_c:

$$\theta_c \approx \frac{\cos^2\gamma \sin\gamma \int_0^R a(r)(1-a(r))rdr}{\int_0^b \left(1 - \frac{\Delta u(r)}{u_0}\right)^2 \frac{\Delta u(r)}{\Delta u_c} rdr} \tag{6.6}$$

This integral can only be solved numerically, as the centerline and local wake deficit Δu_c and Δu, are only known on a discrete radial grid from the Ainslie model. The integration is performed using a piecewise constant constant numerical quadrature, as this was found to be sufficient due to the high regularity in the behaviour of the integrand. Integrating the tangent of θ_c numerically along x finally gives the deflection δ of the wake centerline at any given downstream distance.

6.3 Comparisons to other Deflection Models

Results of the newly developed approach are compared with models commonly employed in wind turbine research and industry, the model by Jiménez [8] and the Gaussian model by Bastankhah and Porté-Agel [9]. The Jiménez model was parametrized according to standard literature, while the Gaussian model was parametrized according to recent work of Altun [44]. The parameters used in both models are summarized in table 6.1.

Furthermore, simulations with a yaw error were run in the LES set-up described in section 5.3. The LES result cannot be considered a perfect benchmark, as the ALM framework that is used does not take into account the correct deformation of the blades in yawed conditions, and the issue with ambient turbulence explained in the discussion in section 5.3 also must be considered for this validation. However, comparison to these LES result can give a first indication that the model results are realistic. Figure 6.3 shows how the Gaussian and Jiménez deflection models perform compared to the LES result and to the new model. It is found that the Jiménez model tends to overestimate the wake deflection in

	k_e (k_σ)	α	β
Jiménez	0.04		
Gaussian	0.039 I_{amb} +0.006	3.0782	0.0213

Table 6.1: Parameters of the steering models used in the validation

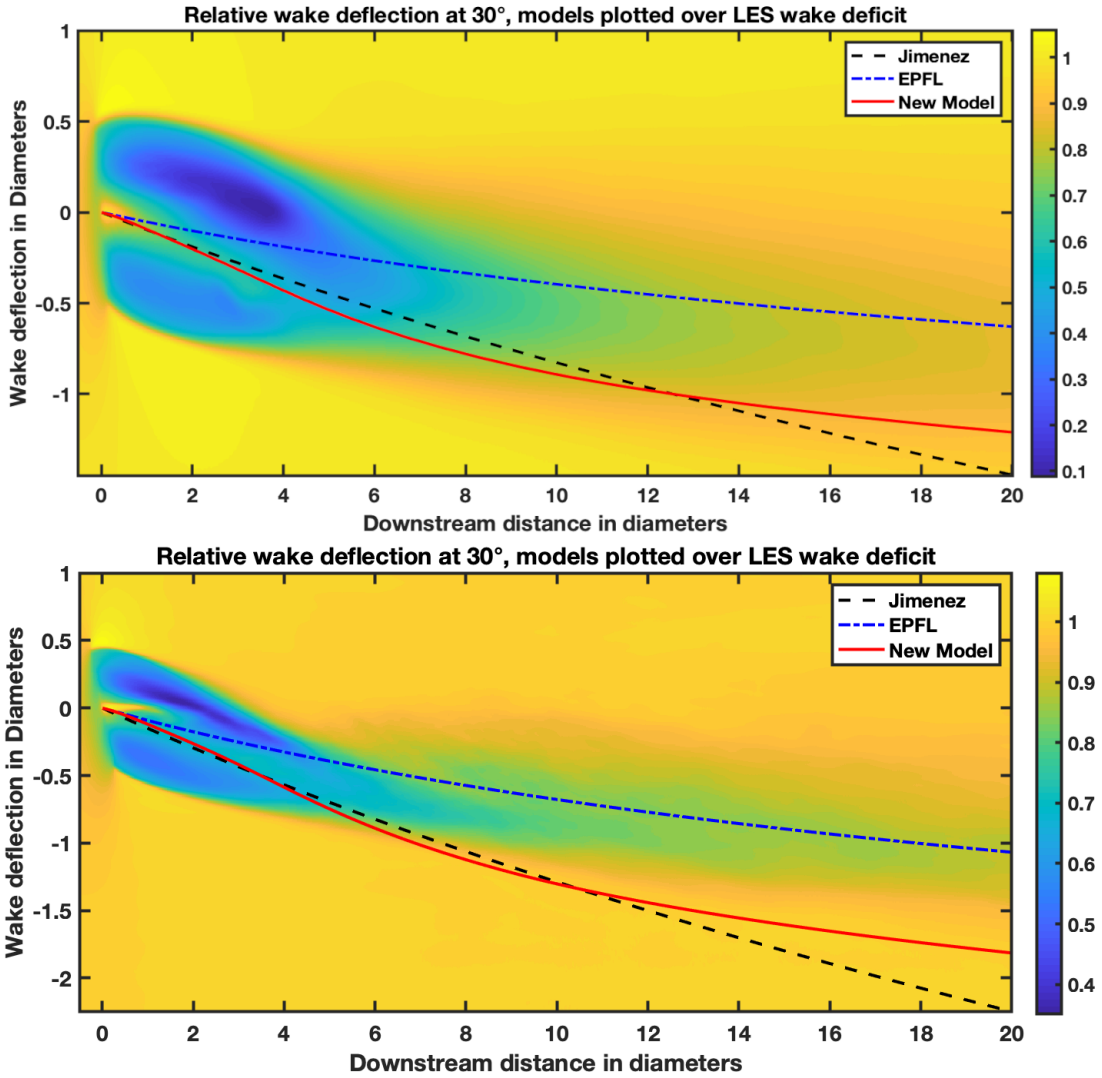

Figure 6.3: Comparison of the wake deflection models from literature and the new deflection model. Centerline deflection plotted on top of results from an LES-ALM simulation. Cases at 15 and 30 degree yaw misalignment.

the far wake while the Gaussian model appears more in line with the LES result, confirming the results from Bastankhah & Porté-Agel [9]. Results of the new model appear to be similar to the Jimenez model, but appear not to diverge in the far wake.

6.4 Discussion

Unlike other models found in literature, the newly proposed formulation does not rely on additional calibration parameters other than those of the Ainslie deficit model itself, eliminating a source of uncertainty. Furthermore, there is no longer a need to distinguish between a near and far wake model, as the deficit model provides velocity data to calculate the deflection in both wake regions. For these reasons, the proposed deflection model is perfectly adapted to be implemented alongside a full dynamic wake meandering (DWM) model as proposed in the IEC61400 standard [4].

It has been proven that the novel formulation for wake deflection can easily be implemented and that the obtained results compare well with with LES simulations. The model seems however to overestimate wake deflection, especially at higher yaw angles. A well-fitted Gaussian model outperforms the new formulation in the treated cases, while the classic Jensen model gives very similar results. It is possible that the model could be fitted with additional parameters to match the LES data, but it is not recommended because it would compromise one of the main advantages of the present model, the lack of additional fitting parameters. However, the assumption that wake recovery in yawed cases is governed by the same empirical eddy viscosity as the non-yawed must be critically reviewed.

In its simplicity, the presented model suffers from a series of limitations that could be addressed. As mentioned above, the assumption of radial symmetry in the deflected wake does not hold, however this model is only used to derive the wake deflection and not the wake shape. The impact of the deformation on the centerline deflection is not straightforward to understand, and modeling it would require a more physical approach such as 3D RANS or LES. Given that the assumption of an axisymmetric wake deficit is inherent to DWM, it is consistent to use this assumption in the deflection model as well. Another limitation of the model lies in the wake width b. As the radial computational domain is finite, the wake quickly grows to attain the limits of this domain. Hereafter, the parameter b remains constant, leading to an offset in the computed momentum flow. However, as the deficit and hence the skew angle at the outskirts of the domain is almost negligible, the magnitude of this effect is assumed to be small.

It has been shown that in multi-turbine configurations, added wake turbulence has a large impact on wake deflection [44]. While such effects cannot be implemented in a Jiménez approach, and have to be implemented explicitly in the case of a Gaussian model, the here-presented model takes these effects into account intrinsically since an added turbulence is already part of the wake modeling tool. No validation steps on multiple-turbine configurations have been performed so far, however fair performance of this model is expected.

Chapter 7

Conclusion

The presented work describes the efforts undertaken to implement, verify and validate a wholistic wind farm aerodynamics modeling tool. hese efforts includes the verification of an Ainslie-type wake deficit model, the creation of a wind park model able to predict velocity and turbulence intensity across a farm based on the DWM model, the creation of an interface between this farm model and an aero-servo-elastic solver and the proposition of a novel wake steering model that is conceptually in line with the wake defect model.

Additionally the goal was to carry out numerical validation experiments using the LES solver YALES2 and to compare model results with real field measurements provided by the industry partner. Furthermore, a new wake steering model was proposed, implemented and tested, mostly out of the desire to create a fully coherent wind park model that computes all wake effects based on a consistent set of assumptions.

All points of the scope have been addressed during the 6 month project. Several of them have been brought to a satisfying conclusion, while for others preliminary results have been obtained and further work is necessary to draw definitive conclusions. This chapter will recapitulate what was achieved during this work and what is left to be done in the future.

7.1 Results of the Work

7.1.1 Conclusions on the Implemented Wake Modeling Tool

The first task carried out in the course of this work was the verification of an existing implementation of the Ainslie-type wake deficit model recommended in the IEC standard to be used in the dynamic wake meandering model. After studying grid convergence, numerical convergence of the schemes and mass- and momentum conservation, it was concluded that the implementation correctly solves the underlying equation, *i.e.* the incompressible, time averaged, axisymmetric thin shear layer Navier-Stokes equations with Eddy viscosity turbulence closure.

An added turbulence model according to the IEC standard was added to the aerodynamic calculation code, while a meandering model was already present. This results in a complete implementation of the

DWM model by DTU described in the IEC61400 [4].

Next, the velocity deficit, meandering and added turbulence model were combined with a linear superposition method into a complete farm modeling tool. The tool is able to compute the average wind speed and turbulence intensity at each turbine for any farm layout at any wind condition, using velocity-dependent axial induction data to compute wake deficits and turbulence generated according to a Mann spectrum for wake meandering. Superposition of wake effects is considered linear, a choice that leads to unphysical results in tight-spaced turbine configurations. As these cases have no practical relevance, this is accepted.

In the same framework, an interface between the wake models and an unsteady aero-servo-elastic wind turbine simulator was created. A 3D turbulent wind field, containing the effects of multiple, superimposed wakes, is generated in a format that can be used directly as input to the turbine simulator. This enables the use the developed tool without any modifications to the aero-servo-elastic code.

Lastly, wake steering models were added to the code, creating a complete farm modeling tool able to consider most of the effects that have been observed inside wind farm environments. The classic Jimenez deflection model as well as the Gaussian deflection model proposed by Bastankhah & Porté-Agel were implemented.

7.1.2 Validation and Verification Results

In order to assess the accuracy of the implemented, two approaches were followed: comparison with measurement data for wind speed and turbulence intensity as described in section 5.2 and comparison with LES simulations performed specifically for the purpose using the flow solver YALES2 and an ALM frame work.

The comparison with measured data shows good agreement for the average velocity and turbulence intensity on a turbine affected by a single wake. A slight but persistent estimation of the velocity is observed, while the turbulence intensity is over-or underestimated depending on the wind speed. Further comparison studies will be necessary to understand the behavior of the model, but the results are encouraging.

The comparison with LES simulations ran into a series of problems related mainly to the addition of turbulence, but also to the lack of a way to treat blade deformation. At the considerable dimensions of the offshore turbines studied in this work, large blade deformation may occur. As such, the spatial coordinates of the collocation points that the ALM model uses to apply the forces change for every wind condition and yaw configuration. Unfortunately, blade deformation data was available only at one wind speed. In the presented study LES simulations were therefore only performed at one wind speed.

Regarding turbulence, the lack of an established way to model atmospheric boundary layer turbulence in the LES solver made it impossible to design a One-to-One numerical validation experiment. It was therefore decided to treat only the case of 0% turbulence in LES. While this case not necessarily representative of real conditions as measured ambient turbulence rarely drops below 5% (see figure 5.4), it was still possible to use the results to deduce that the deficit model can be tuned to perfectly

fit the LES model in the far wake. This serves as a further proof that the implemented Ainslie deficit model does indeed solve the correct equations, but opens some questions on the calibration of the eddy viscosity.

The deflection models were also tested against LES simulations. Good agreement was found for the Gaussian model, while the Jiménez model tends to overestimate the deflection, as is expected from literature.

7.1.3 Implementation of a Novel Wake Steering Model

In addition to the work previously mentioned, a novel wake deflection model based on the Ainslie wake deficit was derived. This avoids the need for additional parametrization that arises from the use of empirical models. The newly proposed model enforces momentum conservation and assumes that the deflection angle follows the deficit profile. Reasonable result are found, but tends to overestimate deflection similarly to the Jiménez model. The comparison with the LES results presented in chapter 6 however has to be treated with care, namely because it is possible that the addition of more realistic turbulence in the LES model could change the outcome.

7.2 Future Work

Some validation work still needs to be done before the implemented wake modeling tool can be used in an industrial set-up. While the expressions recommended in the standard were correctly implemented, it is unclear whether the parametric values proposed by the IEC are applicable over the full range of wind conditions and turbine types.

The proposed next step in the validation process would be to further exploit the measurement data. As stated in section 5.2, the measurement points were not binned by upstream turbulence intensity, a factor that is crucial for the wake deficit model. A recommended approach would be to perform a comparisons of single 10 minute average measurement data points with 10 minute aero-servo-elastic simulations, using the developed interface to feed wake effects to the turbine solver (One-to-one approach). This would allow for a much more precise comparison, considering the correct ambient turbulence intensity for each data point.

A further possible use of the available data would be to validate the wake superposition model of the developed tool. Such a study could quickly be performed using the average wind farm modeling tool, but again a One-to-One approach using the aero-servo-elastic solver would be the preferred option.

Regarding the employed ALM-LES tool, work remains to be done before it can be used to generate quasi-analytical result for the verification of lower-order wake models. One important step would be the addition of a wind turbine rotor deformation model, possibly through coupling with an existing aero-servo-elastic solver. This would allow to perform simulations at different wind speeds without the constraint of assuming rigid numerical blades. Furthermore, as ambient turbulence plays a vital role in the presented wake modeling tool, a standard procedure for injecting and modeling ambient turbulence

must be introduced.

Bibliography

[1] M. Allen et al. Technical summary: Global warming of 1.5 c. an ipcc special report on the impacts of global warming of 1.5 c above pre-industrial levels and related global greenhouse gas emission pathways, in the context of strengthening the global response to the threat of climate change, sustainable development, and efforts to eradicate poverty. Technical report, Intergovernmental Panel on Climate Change, 2019.

[2] Global figures - offshore wind, September 2019. URL `https://gwec.net/global-figures/global-offshore/`.

[3] R. Thresher, M. Robinsion, and P. Veers. Wind energy technology: current status and r&d future. Technical report, National Renewable Energy Lab.(NREL), Golden, CO (United States), 2008.

[4] IEC TC 88. Wind energy generation systems - part 1: Design requirements. Technical Report IEC 61400, The International Electrotechnical Commission, Denmark, 2018.

[5] H. A. Madsen, G. C. Larsen, T. J. Larsen, N. Troldborg, and R. Mikkelsen. Calibration and validation of the dynamic wake meandering model for implementation in an aeroelastic code. *Journal of Solar Energy Engineering*, 132(4):041014, 2010.

[6] M. F. Howland, S. K. Lele, and J. O. Dabiri. Wind farm power optimization through wake steering. *Proceedings of the National Academy of Sciences*, 116(29):14495–14500, 2019. ISSN 0027-8424. doi: 10.1073/pnas.1903680116. URL `https://www.pnas.org/content/116/29/14495`.

[7] V. Moureau, P. Domingo, and L. Vervisch. Design of a massively parallel cfd code for complex geometries. *Comptes Rendus Mécanique*, 339(2-3):141–148, 2011.

[8] Á. Jiménez, A. Crespo, and E. Migoya. Application of a les technique to characterize the wake deflection of a wind turbine in yaw. *Wind energy*, 13(6):559–572, 2010.

[9] M. Bastankhah and F. Porté-Agel. Experimental and theoretical study of wind turbine wakes in yawed conditions. *Journal of Fluid Mechanics*, 806:506–541, 2016.

[10] P. Benard, A. Viré, V. Moureau, G. Lartigue, L. Beaudet, P. Deglaire, and L. Bricteux. Large-eddy simulation of wind turbines wakes including geometrical effects. *Computers & Fluids*, 173:133–139, 2018.

[11] G.-W. Qian and T. Ishihara. A new analytical wake model for yawed wind turbines. *Energies*, 11(3): 665, 2018.

[12] E. Branlard. *Wind turbine aerodynamics and vorticity-based methods*. Springer, 2017.

[13] W. J. M. Rankine. On the mechanical principles of the action of propellers. *Transactions of the Institution of Naval Architects*, 6, 1865.

[14] A. Betz. Schraubenpropeller mit geringstem energieverlust. *Gottinger Nachrichten*, pages 193–213, 1919.

[15] H. Glauert. Airplane propellers. In *Aerodynamic theory*, pages 169–360. Springer, 1935.

[16] M. O. L. Hansen. *Aerodynamics of wind turbines*. Routledge, 2008.

[17] J. F. Manwell, J. G. McGowan, and A. L. Rogers. *Wind energy explained: theory, design and application*. John Wiley & Sons, 2010.

[18] Openfast. `https://github.com/openfast`, August 2019.

[19] L. Savenije, T. Ashuri, G. Bussel, and J. Staerdahl. Dynamic modeling of a spar-type floating offshore wind turbine. In *Scientific Proceedings European Wind Energy Conference & Exhibition*, 2010.

[20] Siemens AG. 2004 annual report. `https://sie.ag/2KN17Df`, December 2004.

[21] N. Jensen. A note on wind turbine interaction. *Risø National Laboratory, Roskilde, Denmark, Technical Report No. M-2411*, 1983.

[22] A. Niayifar and F. Porté-Agel. A new analytical model for wind farm power prediction. In *Journal of physics: conference series*, volume 625, page 012039. IOP Publishing, 2015.

[23] M. Bastankhah and F. Porté-Agel. A new analytical model for wind-turbine wakes. *Renewable Energy*, 70:116–123, 2014.

[24] M. Gaumond, P.-E. Réthoré, A. Bechmann, S. Ott, G. C. Larsen, A. P. Diaz, and K. S. Hansen. Benchmarking of wind turbine wake models in large offshore windfarms. In *The science of Making Torque from Wind 2012: 4th scientific conference*, 2012.

[25] S. Frandsen. On the wind speed reduction in the center of large clusters of wind turbines. *Journal of Wind Engineering and Industrial Aerodynamics*, 39(1-3):251–265, 1992.

[26] P. Luzzatto-Fegiz. A one-parameter model for turbine wakes from the entrainment hypothesis. In *Journal of Physics: Conference Series*, volume 1037, page 072019. IOP Publishing, 2018.

[27] G. C. Larsen. *A simple wake calculation procedure*. Risø National Laboratory, 1988.

[28] G. C. Larsen. A simple stationary semi-analytical wake model. 2009.

[29] T. Göçmen, P. Van der Laan, P.-E. Réthoré, A. P. Diaz, G. C. Larsen, and S. Ott. Wind turbine wake models developed at the technical university of denmark: A review. *Renewable and Sustainable Energy Reviews*, 60:752–769, 2016.

[30] J. F. Ainslie. Calculating the flowfield in the wake of wind turbines. *Journal of Wind Engineering and Industrial Aerodynamics*, 27(1-3):213–224, 1988.

[31] G. C. Larsen et al. Dynamic wake meandering modeling. 2007.

[32] R. J. Barthelmie, G. Larsen, S. Frandsen, L. Folkerts, K. Rados, S. Pryor, B. Lange, and G. Schepers. Comparison of wake model simulations with offshore wind turbine wake profiles measured by sodar. *Journal of atmospheric and oceanic technology*, 23(7):888–901, 2006.

[33] J. F. Ainslie. Wake modelling and the prediction of turbulence properties. *Proceedings of the Eighth British Wind energy Association Conference, Cambridge, Mar*, pages 19–21, 1986.

[34] G. C. Larsen, H. A. Madsen, K. Thomsen, and T. J. Larsen. Wake meandering: a pragmatic approach. *Wind Energy: An International Journal for Progress and Applications in Wind Power Conversion Technology*, 11(4):377–395, 2008.

[35] M. T. de Maré. *Wake dynamics in offshore wind farms*. PhD thesis, DTU, 09 2016. PhD Thesis.

[36] J. Mann. The spatial structure of neutral atmospheric surface-layer turbulence. *Journal of fluid mechanics*, 273:141–168, 1994.

[37] S. Frandsen and M. L. Thøgersen. Integrated fatigue loading for wind turbines in wind farms by combining ambient turbulence and wakes. *Wind Engineering*, pages 327–339, 1999.

[38] A. Crespo, J. Herna, et al. Turbulence characteristics in wind-turbine wakes. *Journal of wind engineering and industrial aerodynamics*, 61(1):71–85, 1996.

[39] H. A. Madsen, G. C. Larsen, and K. Thomsen. Wake flow characteristics in low ambient turbulence conditions. *Proceedings of the Copenhagen Offshore Wind*, 2005.

[40] D. Quarton and J. Ainslie. Turbulence in wind turbine wakes. *Wind Engineering*, pages 15–23, 1990.

[41] U. Hassan. *A wind tunnel investigation of the wake structure within small wind turbine farms*. Harwell Laboratory, Energy Technology Support Unit, 1993.

[42] S. T. Frandsen. *Turbulence and turbulence-generated structural loading in wind turbine clusters*. Risø National Laboratory, 2007.

[43] H. M. Aagaard, G. C. Larsen, T. J. Larsen, R. Mikkelsen, and N. Troldborg. Wake deficit-and turbulence simulated with two models compared with inflow measurements on a 2mw turbine in wake conditions. In *2008 European Wind Energy Conference and Exhibition*. European Wind Energy Conference and Exhibition, 2008.

[44] S. B. Altun. Modeling the effects of yaw-based wake steering on the downstream and cross-wind neighboring wind turbines. Master's thesis, DTU, 3 2019. Master Thesis.

[45] F. Moukalled, L. Mangani, M. Darwish, et al. *The finite volume method in computational fluid dynamics*. Springer, 2016.

[46] J. G. Leishman. Challenges in modelling the unsteady aerodynamics of wind turbines. *Wind Energy: An International Journal for Progress and Applications in Wind Power Conversion Technology*, 5(2-3):85–132, 2002.

[47] M. Klein, A. Sadiki, and J. Janicka. A digital filter based generation of inflow data for spatially developing direct numerical or large eddy simulations. *Journal of computational Physics*, 186(2): 652–665, 2003.

[48] P. Bénard. *Analyse et amélioration d'une chambre de combustion centimétrique par simulations aux grandes échelles*. PhD thesis, Rouen, INSA, 2015.

[49] N. Legrand. *Numerical and modeling methods for multi-level large eddy simulations of turbulent flows in complex geometries*. PhD thesis, Normandie Université, 2017.

[50] F. Nicoud, H. B. Toda, O. Cabrit, S. Bose, and J. Lee. Using singular values to build a subgrid-scale model for large eddy simulations. *Physics of Fluids*, 23(8):085106, 2011.

[51] J. N. Sørensen and W. Z. Shen. Numerical modeling of wind turbine wakes. *Journal of fluids engineering*, 124(2):393–399, 2002.

[52] CORIA laboratory. YALES2 private wiki. `https://yales2.coria-cfd.fr/`, August 2019.

[53] P. Benard, G. Balarac, V. Moureau, C. Dobrzynski, G. Lartigue, and Y. d'Angelo. Mesh adaptation for large-eddy simulations in complex geometries. *International journal for numerical methods in fluids*, 81(12):719–740, 2016.

[54] M. Kraushaar. *Application of the compressible and low-Mach number approaches to Large-Eddy Simulation of turbulent flows in aero-engines*. PhD thesis, INPT, 2011.

[55] H. Krumm. Wind turbine design load impact from wake effects. Master's thesis, TU Braunschweig, 4 2016. Master Thesis.

[56] B. Fornberg. Generation of finite difference formulas on arbitrarily spaced grids. *Mathematics of computation*, 51(184):699–706, 1988.

[57] J. Arzi. Tutorial on a very simple yet useful filter: the first order iir filter. http://www.tsdconseil.fr/tutos/tuto-iir1-en.pdf, 2016.

[58] E. Bossanyi. Combining induction control and wake steering for wind farm energy and fatigue loads optimisation. In *Journal of Physics: Conference Series*, volume 1037-A3, page 032011. IOP Publishing, 2018.

[59] W. L. Oberkampf and C. J. Roy. *Verification and validation in scientific computing*. Cambridge University Press, 2010.

[60] F. L. Ponta, A. D. Otero, L. I. Lago, and A. Rajan. Effects of rotor deformation in wind-turbine performance: the dynamic rotor deformation blade element momentum model (drd–bem). *Renewable Energy*, 92:157–170, 2016.

[61] F. Porté-Agel, Y.-T. Wu, H. Lu, and R. J. Conzemius. Large-eddy simulation of atmospheric boundary layer flow through wind turbines and wind farms. *Journal of Wind Engineering and Industrial Aerodynamics*, 99(4):154–168, 2011.

[62] M. K. Rwigema. Propeller blade element momentum theory with vortex wake deflection. In *Proceedings of the 27th Congress of the International Council of the Aeronautical Sciences, Nice, France, September*, pages 19–24, 2010.